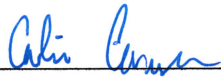


Design and Integration of a High-Powered Model Rocket-I

A Major Qualifying Project Report
Submitted to the Faculty of the
WORCESTER POLYTECHNIC INSTITUTE
in Partial Fulfillment of the Requirements for the
Degree of Bachelor of Science
in Aerospace Engineering

by



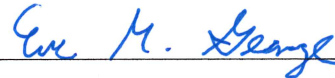
Colin Cooper



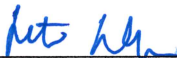
Kyle Foster



Amanda Dings



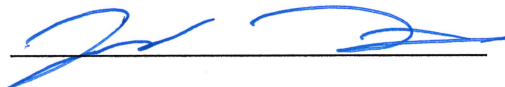
Eve George



Peter Dohn



Nicholas Lapierre



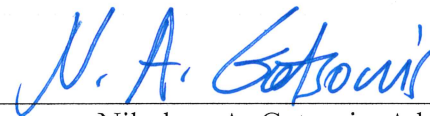
Jacob Fennick



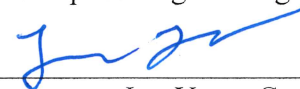
Ty Moquin

March 11, 2019

Approved by:



Nikolaos A. Gatsonis, Advisor
Professor, Aerospace Engineering Program



Jun Yang, Co-Advisor
Teaching Assistant Professor, Aerospace Engineering Program

Abstract

The high-powered model rocket (HPMR) is designed for an apogee of 457 m, with clustered engines, staged propulsion, actively controlled stabilizing fins, a deployable autorotating rotor recovery system, three cameras, an inertial measurement unit and three strain gauges. This project involves component design and fabrication, HPMR integration, structural, aerodynamic, and thermal analysis as well as functionally testing. SolidWorks is used for component design and integration. ANSYS simulations provide the structural loads on HPMR components and safety factors. FLUENT simulations and analytical modeling determine the drag forces during ascent. COMSOL simulations provide component temperatures using heat loads expected from the solid motors. Flight test analysis is presented.

Certain materials are included under the fair use exemption of the U.S. Copyright Law and have been prepared according to the fair use guidelines and are restricted from further use.

Acknowledgements

We would like to thank the following individuals and groups for their help and support throughout the entirety of this project.

Project Advisor

Professor Nikolaos Gatsonis

Assistant Project Advisor

Professor Jun Yang

Flight Stability and Controls Team

Professor Michael Demetriou and students Alexander Alvarez, Grace Gerhardt, Evan Kelly, Jack O'Neil and Jackson Whitehouse

Propulsion, Staging and Recovery Team

Professor John Blandino and students Nicolas Lucena Farias, Jean Furter, Steffany Halfrey, Mason Handy, Vanessa Legere, Connor Murphy, Nicholas Songer and Justin Tavares

Barbara Furhman

Nicholas Dal Porto

CATO Executive Staff

Table of Authorship

Section	Author(s)
<i>Introduction</i>	All
<i>1.2,1.3,1.4</i>	All, JB3-1901, MAD-1901
<i>2. Mechanical Design</i>	PD, KF
<i>3. Structural Analysis</i>	AD, NL, TM
<i>4. Aerodynamic Analysis</i>	CC, EG
<i>5. Thermal Analysis</i>	JF
<i>6. Integration and Testing</i>	PD, EG, KF, JF, AD, NL
<i>7. Conclusions and Recommendations</i>	PD, JF, TM, NL

Table of Contents

1	INTRODUCTION	11
1.1	BACKGROUND AND LITERATURE REVIEW	12
1.1.1	<i>Fundamentals of Model Rocket Design</i>	13
1.1.2	<i>Review of Previous Model Rockets</i>	15
1.1.3	<i>Structural Analysis</i>	17
1.1.4	<i>Aerodynamic Analysis</i>	19
1.1.5	<i>Thermal Analysis</i>	20
1.2	HPMR PROGRAM GOALS	21
1.3	HPMR PROGRAM DESIGN REQUIREMENTS, CONSTRAINS, STANDARDS AND OTHER CONSIDERATIONS	22
1.4	HPMR PROGRAM MANAGEMENT AND BUDGET	24
1.5	MSAT MQP OBJECTIVES AND METHODS	27
1.6	MSAT MQP ORGANIZATION	28
1.7	MSAT MQP TASKS AND TIMETABLE.....	29
2	MECHANICAL DESIGN, CONSTRUCTION AND INTEGRATION	30
2.1	AIRFRAME	30
2.2	PAYLOAD BAY	32
2.3	ELECTRONICS BAY	33
2.4	MOTOR BAY	38
2.4.1	<i>Fins</i>	44
2.4.2	<i>Boosters</i>	44
2.5	NOSECONE	47
2.5.1	<i>Cameras</i>	48
3	STRUCTURAL ANALYSIS	52
3.1	DETERMINATION OF FLIGHT-CRITICAL COMPONENTS.....	52

3.2	RECOVERY MOUNTING BULKHEAD ANALYSIS.....	53
3.3	STAGE SEPARATION ANALYSIS	58
3.4	FIN BRACKET MOUNTING SYSTEM ANALYSIS	62
3.5	DESIGN AND IMPLEMENTATION OF STRAIN GAUGE SYSTEM	65
3.5.1	Code.....	70
3.5.2	Physical Integration.....	70
4	AERODYNAMIC ANALYSIS.....	72
4.1	DRAG COEFFICIENT EVALUATION	72
4.1.1	Analytical Calculations	72
4.1.2	OpenRocket Analysis	74
4.1.3	Fluent Analysis.....	75
4.1.4	Fluent Results	81
4.1.5	SimScale Analysis.....	82
4.1.6	Comparison Between Various Approaches.....	82
4.2	ASSESSMENT OF WIND DISTURBANCE.....	83
4.3	CENTER OF PRESSURE CALCULATIONS	85
5	THERMAL ANALYSIS.....	88
5.1	COMSOL ANALYSIS	88
6	MECHANICAL INTEGRATION AND TESTING PROCEDURES.....	92
6.1	MECHANICAL INTEGRATION	92
6.2	STRUCTURAL TESTING.....	94
6.3	AERODYNAMICS TESTING	95
6.4	THERMAL TESTING	97
7	SUMMARY, CONCLUSIONS, RECOMMENDATIONS, AND BROADER IMPACTS	100
7.1	SUMMARY.....	100

7.2	CONCLUSIONS	101
7.2.1	<i>Mechanical Design and Integration</i>	101
7.2.2	<i>Structural Analysis</i>	102
7.2.3	<i>Aerodynamic Analysis</i>	102
7.2.4	<i>Thermal Analysis</i>	102
7.3	RECOMMENDATIONS FOR FUTURE WORK	103
7.4	HPRM PROJECT AND ITS BROADER IMPACTS	104
7.4.1	<i>Economic Impacts</i>	104
7.4.2	<i>Environmental Impacts</i>	105
7.4.3	<i>Social Impacts</i>	106
8	REFERENCES	108
	APPENDIX A.....	111
	APPENDIX B	112
	APPENDIX C	115
	APPENDIX D.....	116
	APPENDIX E	121
	APPENDIX F	122
	APPENDIX G.....	144
	APPENDIX H.....	145
	APPENDIX I	146

Table of Figures

Figure 1. SolidWorks rendering(left) and image (right) of component layout of the HPMR12	
Figure 2. Blue Tube airframes available from Always Ready Rocketry (c) 2018.	13
Figure 3. Possible nosecone shapes. Stine (c) 2004	14
Figure 4. Drawing of a typical motor mount assembly. Stine (c) 2004.....	15
Figure 5. The assembled model of the HPMR airframe.....	30
Figure 6. Model of the assembled electronics bay.	33
Figure 7. Black Powder separation system charge well.	35
Figure 8. Model of the CO2 separation mechanism.....	36
Figure 9. Model of the completed CO2 ejection system integrated into the body of the rocket.	37
Figure 10. Model of the assembled motor bay, including the passive variant of the active control fins designed by the FDC team. One fin has been removed for viewing purposes.....	39
Figure 11. Model of the removable motor mount assembly with three motor tubes (left) and a single motor tube (right).	41
Figure 12. Image of the motor retention system over empty motor mount tubes.	42
Figure 13. Model of the fin and bracket assembly separated from the motor bay tube. The 8 bracket pieces can be seen with fixtures through some of the provided holes.	43
Figure 14. Image of the completed motor bay, with the motor retention system attached. ..	44
Figure 15. SolidWorks model of the side booster.	45
Figure 16. Model of the custom magnet mount for the outside of the booster airframe.	46
Figure 17. Image of 3D-printed booster hooks and booster tube.	46
Figure 18. Model of the assembled nosecone subassembly.	47
Figure 19. Image of the nosecone windows.	48

Figure 20. Model of the passive 2-axis camera gimbal.	49
Figure 21. Images of the side camera mounted to the airframe. The red fairing can be independently removed from the rocket to access the camera.	50
Figure 22. Forces on nosecone bulkhead over time.	55
Figure 23. Force on main body bulkhead over time.	56
Figure 24. Safety Factors of nosecone bulkhead.	57
Figure 25. Safety factors of main body bulkhead.	57
Figure 26. Safety factor of nosecone bulkhead.	59
Figure 27. Equivalent stress of nosecone bulkhead.	60
Figure 28. Physical properties of cured epoxy. © 2004 West System (West System, 2014)	60
Figure 29. Equivalent stress and safety factor of body tube.	61
Figure 30. Fin bracket system modeled in SolidWorks.	63
Figure 31. Safety factors of area of concern 1.	64
Figure 32. Safety factors of area of concern 1 update.	64
Figure 33. Safety factors of area of concern 2.	65
Figure 34. Safety factors of area of concern 2 update.	65
Figure 35. Strain gauge information. 2019.	66
Figure 36. Concept of strain gauge placement in motor bay of the HPMR.	67
Figure 37. Actual placement of strain gauge on bulkhead of HPMR.	67
Figure 38. Actual placement of longitudinal strain gauge on the HPMR.	68
Figure 39. Single supply bridge amplifier. © 1997 Burr-Brown Corporation.	69
Figure 40. Pseudoground bridge measurement, 5V single supply. ©	69
Figure 41. Amplifier circuit on prototyping board. (c) 2019.	70

Figure 42. Partially complete amplifier circuit on perfboard. © 2019.	70
Figure 43. Testing of strain gauge integration with processor.	71
Figure 44. First ANSYS model of slender HPMR.	76
Figure 45. Close-up view of slender HPMR in ANSYS.	77
Figure 46. Second ANSYS model; two mesh boundaries.	78
Figure 47. Mesh of second ANSYS model.	79
Figure 48. Third ANSYS model; three mesh boundaries.	80
Figure 49. ANSYS model shown in fluent results window.	81
Figure 50. Plot showing the height of the HPMR vs. the predicted wind velocity.	84
Figure 51. Altitude vs. velocity of the HPMR.	84
Figure 52. Predicted wind speed vs. altitude of the HPMR.	85
Figure 53. Aerodynamic forces affecting flight stability in model rockets.	86
Figure 54. Motor bay thermal conductivity simulation result.	90
Figure 55. OpenRocket graph showing the altitude, velocity and vertical acceleration of the HPMR during flight.	96
Figure 56. Stationary (left) and Following (right) visualizations of the HPMR's trajectory. (c) 2019 (MAD-1901)	97
Figure 57. Diagram of the construction of the solid rocket motors (Anon., 2016).	98
Figure 58. Aft motor section post-launch.	99

List of Tables

Table 1. Inputs for the Calculations of Force on Each Bulkhead	54
Table 2. Material data of vulcanized fiber. © Oliner (Anon., n.d.)	62
Table 3. Equations for estimating drag coefficients on a slender rocket body. (Cannon, 2004)	73
Table 4. Analytical calculations of coefficient of drag.....	74
Table 5. Criteria of Structural Components.....	95

1 Introduction

Model rocketry is a widely enjoyed pastime dating back to 1957 (Stine & Stine, 2004). Model rockets are miniature aerospace models which include an airframe, solid-propellant motor(s) (typically purchased from a hobby store), and some type of recovery device. Model rockets can range in size from six inches to more than ten feet tall. The Federal Aviation Administration (FAA) has defined a series of classes pertaining to high powered model rocketry. Each class of rocket has a maximum mass and each class requires certain clearances to be able to fly (Anon., 2008). In addition to general size classification, the motor used to power the rocket has an additional classification. The National Association of Rocketry has defined three regulated levels of rocket motors. A level one rocket is a rocket whose motors provide a total impulse of between 320 and 640 Newton seconds. (Stine & Stine, 2004)

This Major Qualifying Project (MQP) team was part of the High-Powered Model Rocket (HPMR) Program consisting of two additional MQP teams, (JB3-1901, MAD-1901). The goal of the Program is to design, integrate, and test fly a HPMR capable of reaching an altitude of 457.2 m (1500 ft). The rocket designed and built for the HPMR is a Class-2 rocket with design options that included two Level-1 motor configurations.

The objectives of this MQP are: perform mechanical design; perform structural, aerodynamic, and thermal analysis; acquire and fabricate components; integrate all components of the HPMR shown in its final configuration in Figure 1.



Figure 1. SolidWorks rendering (left) and image (right) of component layout of the HPMR

1.1 Background and Literature Review

Building model rockets is a complex design challenge involving substantial mechanical design and integration. The following review focuses on the mechanical design, structural, aerodynamic, and thermal analysis of model rockets that are relevant to this MQP.

1.1.1 Fundamentals of Model Rocket Design

The rocket body or airframe is the main structural component of the HPMR. It is the platform on which the motor mount, stabilization hardware (e.g. fins), recovery system, payload, and nosecone are built. The rocket body is made from one or more body tubes joined using couplers and bulkheads (Stine & Stine, 2004). For models weighing under three ounces, the rocket body is typically made from thin-walled paper tubes. These may be purchased from hobby shops and cut to length by the hobbyist using a modelling knife. For larger models, more robust materials such as model aircraft plywood or fiberglass can be used. The airframe for this project will be constructed using Blue Tube, a vulcanized cardboard material purchased from Always Ready Rocketry © 2018. An example of Blue Tube is shown in Figure 2.



Figure 2. Blue Tube airframes available from Always Ready Rocketry (c) 2018.

The nosecone shown in Figure 3. Possible nosecone shapes. Stine (c) 2004 is the front end of the airframe, and its shape varies greatly. The purpose of the nosecone is to reduce aerodynamic drag on the forward end of the rocket. In order to mate with the body tube, the bottom portion of the nosecone is typically smaller in diameter than the rocket body. This also allows the nosecone

to eject reliably. The tip of the nosecone may be shaped in a variety of ways, as shown in Figure 3. Nosecones can be purchased from model rocket manufacturers and are made from balsa wood or polystyrene. The nosecone for this project will be purchased from Always Ready Rocketry © 2018.

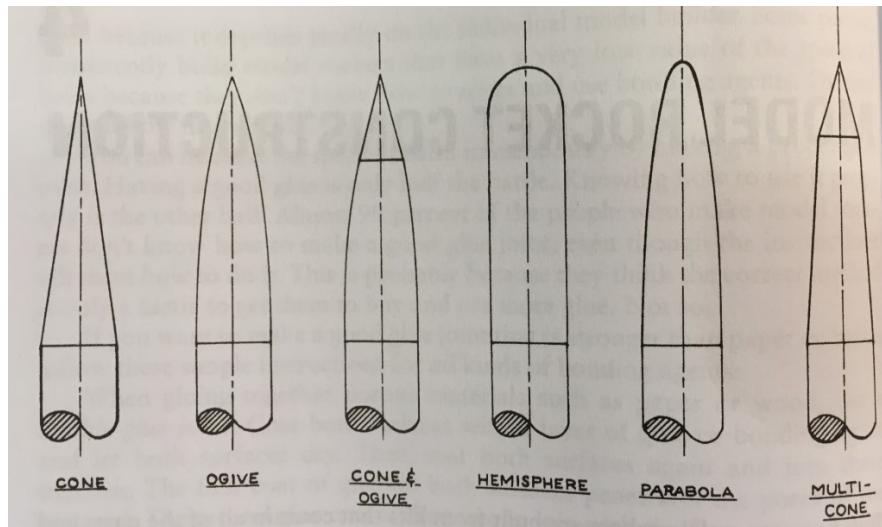


Figure 3. Possible nosecone shapes. Stine (c) 2004

To ensure stable flight, most model rockets have stabilizing surfaces (i.e. fins) attached to the aft end of the airframe. Properly designed fins counteract changes in the rocket's orientation during flight and ensure stable flight. Adding fins to a rocket moves its center of pressure (CP) behind its center of gravity (CG). This causes the rocket to fly straight when launched and overcome perturbations from aerodynamic forces such as wind. As a rule of thumb for model rocketry, the CP should be no less than one body diameter behind the CG to ensure stable flight. Fins for small models are typically constructed using cardboard, balsa wood or plastic. For larger models, fins are often constructed using model aircraft plywood or fiberglass.

At the aft end of the airframe lies the rocket's motor mount system. The motor mount is responsible for both holding the motor in place and ensuring that it remains aligned with the airframe's central axis during flight. The motor mount consists of the following parts (see Figure

4): the motor mount tube, which holds the motor in place; the thrust ring, which prevents the motor from moving forward into the airframe during launch; the centering rings, which maintain the alignment of the motor; and the motor retaining clip, which prevents the motor from falling from the aft of the airframe.

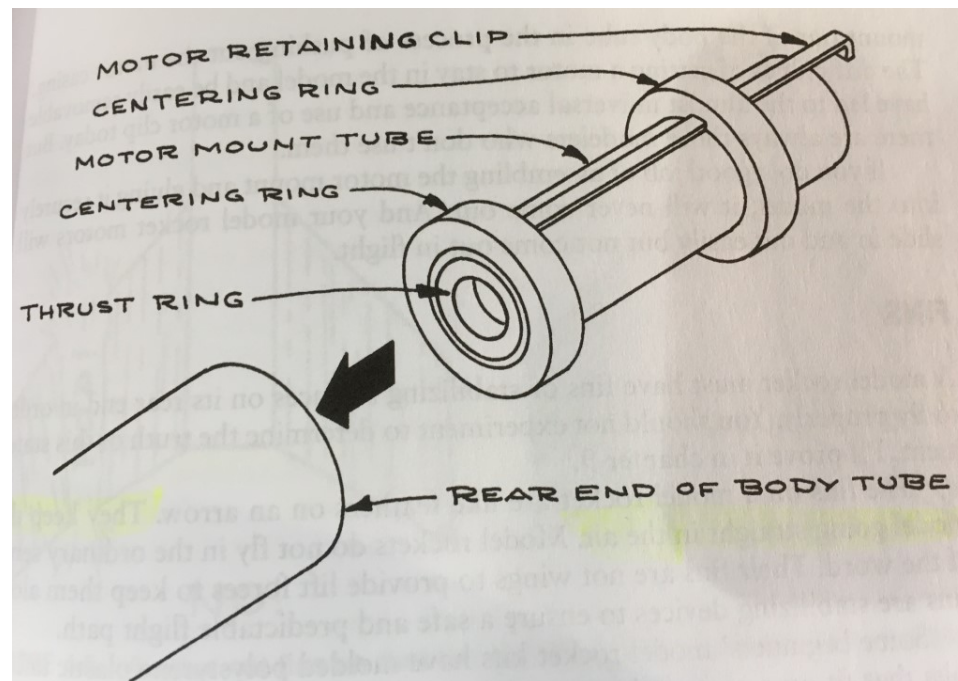


Figure 4. Drawing of a typical motor mount assembly. Stine (c) 2004.

Some model rockets have been designed to carry payloads. These include passive payloads (e.g. lead weights) that serve no function other than to provide stability, electronic payloads such as scientific equipment, and optical payloads (e.g. cameras). For this project, a window will be installed in the nosecone, where a gimbaled camera will be included to observe the horizon. Several smaller cameras will be included on the sides of the airframe pointed towards aft of the rocket to observe launch and stage separation.

1.1.2 Review of Previous Model Rockets

The following review presents the mechanical design aspects of comparable high-power model rocketry initiatives from other colleges and amateur rocketry competitions.

Most model rockets used a combination of fiberglass and epoxy to construct the body tube. (Behlman N, 2007) (Buhler J, 2008) (Barrowman, 1967). The WPI AIAA Research Rocket for the Investigation and Observation of Recovery and Staging (WARRIORS) I team used an Easyglas™ Sock (JB3-RCK1), while the WARRIORS II team used G-10 Fiberglass that had been reinforced with two layers of carbon fiber to increase stiffness (JB3-RCK2). For the rocket frame, the WARRIORS II team used three carbon fiber stringers for longitudinal strength and plywood bulkheads for torsional rigidity. The AJAKS team, which competed in the Intercollegiate Rocket Engineering Competition (IREC) in 2012, reinforced their rocket body using an internal skeleton of carbon fiber rods (Bowman et al, 2012). Additionally, a team from the US Naval Academy used purely carbon fiber to construct their airframe (Anon., 2017-2018). The rockets referenced above differed greatly in the fabrication of the nosecone. The WARRIORS III team purchased their nosecone from an online vendor (JB3-RCK3). The team from the US Naval Academy used a combination of fiberglass and Kevlar. Finally, Team Narwhal from Loyola Marymount University 3D printed their nosecone (Calcara, et al., 2016)

The construction of stabilization fins also varied greatly between teams. MQP team members have previously worked with WPI teams that competed in Battle of the Rockets (BOR). The BOR teams used a 4-fin design, constructed from ¼" plywood, slotted into the rocket body to improve strength. Oregon State's team competing in NASA's University Student Launch Initiative (USLI) used a combination of carbon fiber and Nomex® Honeycomb to make their fins light and strong (Anon., 2018). Team Narwhal used G-10 fiberglass fins slotted into the rocket body (Calcara, et al., 2016). Most teams constructed their centering rings for the motor mounts using plywood. In addition, the WPI BOR teams used 54mm Blue Tube for their motor mount tube, and the Naval Academy team used PVC (Anon., 2017-2018)

1.1.3 Structural Analysis

Structural analysis of a HPMR is critical in determining if it will survive the mission. The analysis will determine if it is safe enough and strong enough to hold up to the many different loads during launch, stage separation, and recovery as well as what materials to use for each of the different components. A pre-launch structural analysis allows for more iterations in design before launch to ensure that the HPMR is structurally sound.

The University of Louisville rocket had the most developed structural analysis of all the reviewed teams (Exeler M, 2017). They used ANSYS software to find the safety factor of components under approximated loads during flight. For the bulkheads, they investigated the force applied on the bulkhead when each of the payload and parachute bays open. For shear pins used in the airframe, they investigated the pressure differential from the outside air and the inside of the rocket to ensure the pressure inside would not be too great for the shear pins (Schilter, 2019).

Other universities were not detailed in what types of structural analysis was performed on their rockets, but they did mention the use of finite element modeling (FEM) to determine load paths, and how to reinforce weaker sections of the rocket to make them meet their structural criteria (Anon., n.d.). More so, other universities use FEM to determine what materials to use for their airframe components.

Loyola Marymount University's Narwhal team conducted a failure modes and effects analysis (FMEA) to identify the most critical potential failure modes of the rocket (Calcara, et al., 2016). To conduct this method, risk priority numbers from 1 to 10 were assigned to potential failure actions, their effects, and their causes. The failure mode with the highest number was the most likely failure to occur and was addressed first. Using this method, the Narwhal team was able to perform some basic fixes such as checking that components were securely fastened and conducting

ground testing. Additionally, the Narwhal team performed a nosecone drop test to determine if the nosecone could withstand multiple impact landings. Using OpenRocket, they determined the expected landing velocity, and then calculated the proper height of the drop test to recreate this with a safety factor of 10%. This was a qualitative test, but the nose cone was still structurally sound after the drop tests (Calcara, et al., 2016).

The WARRIORS I MQP team conducted some basic structural tests, but no structural analysis with software (Belliss M, 2006). The team tested the body tube strength of two different types of rocket body tubes in order to determine the best body tube to use. This was done by adding weights on one end of the body tube to test the normal forces the rocket would experience in flight with a safety factor of 2.5. They tested a fiberglass reinforced body tube as well as a standard body tube. The reinforced tube retained its basic shape after repeated testing, while the standard body tube suffered significantly in its radial axis (Belliss M, 2006). The WARRIORS II MPQ rocket utilized a glider wing decedent method and required much more structural analysis than the WARRIORS I and III MQPs. The WARRIORS II MQP used a central servo and crossbar to deploy the glider which underwent significant structural stresses due to the high amount of drag on the mechanism. SolidWorks FEM was used by the team to determine the yield strength and bending of the crossbar. With this they were able to analytically prove that the crossbar was sufficiently strong enough to hold the rocket. Additionally, the body of the WARRIORS II MQP rocket used four carbon fiber stingers with a fiber glass outer casing (Behlman N, 2007). In order to test this structure, the critical bulking load was calculated and used to determine the diameter of the carbon fiber struts. The crossbar was assumed to be a fixed-fixed beam. The WARRIORS III MQP did not perform a structural analysis (Buhler J, 2008).

1.1.4 Aerodynamic Analysis

Aerodynamics is applicable across many industries, including motor vehicles, marine transportation, and of course, the aerospace industry. For the purpose of designing a HPMR, aerodynamic analysis is an especially important step that needs to be taken in order to ensure the stability and overall success of the vehicle during flight. If a HPMR is even slightly unstable, it can spiral out of control under the smallest disturbances (Anon., n.d.). Thorough aerodynamic analysis in model rocketry is often completed through a combination of Computational Fluid Dynamics (CFD) and Wind Tunnel Testing (WTT).

After reviewing a variety of high-powered rocketry projects, some similar themes were found amongst the aerodynamic analysis methods. As a preliminary step, many teams used OpenRocket or RockSim to determine variables such as altitude, airspeed, Mach number, etc. RockSim allows users to design a HPMR within the program, and then simulate the launch to see how the HPMR will perform, while also calculating aerodynamic coefficients and forces. RockSim allows the user to alter specifications of events during flight such as sequencing of parachutes and staging, or environmental conditions like wind, altitude, and angle of attack (Bowman, et al., 2012). Both the WARRIORS I MQP and WARRIORS II MQP utilized RockSim. WARRIORS I MQP used it specifically to determine launch velocities (Belliss M, 2006), while WARRIORS II MQP made use of the program to size the fins of their HPMR and verify its stability (Behlman N, 2007). WARRIORS III MQP developed a model to characterize fin flutter and provide different estimates on flutter characteristics through different flight conditions and fin designs (Buhler J, 2008).

WARRIORS III MQP used both the CFD and a WTT testing approach. The team employed a variety of methods, starting with the use of FinSim to determine which fin designs were optimal

for WTT. Data was obtained through LabVIEW and compared to the FinSim calculations. From there, MATLAB was used with the known data to calculate velocity and natural frequency for each fin geometry. In addition, both FLUENT and GAMBIT were used to provide a wide range of physical models. The team used GAMBIT to mesh the HPMR geometry, which was then directly imported into FLUENT for analysis. This analysis was valuable because it provided the team with visuals such as contour plots, velocity flow fields, and path-lines (Buhler J, 2008).

Research of past high-powered model rocketry projects indicated the value of aerodynamic analysis techniques to different design aspects of the vehicle. CFD proved to be a powerful and inexpensive way to predict reactions of certain mechanical designs in an aerodynamic environment. Comparing testing results across multiple CFD platforms ensures more credible results and allows for comparisons that ensure design modifications can be properly justified. In addition, to provide an even more accurate analysis, CFD results can be compared to WTT. All these lessons learned from previous model rocketry projects will help guide the MSAT MQP team to proper analysis techniques.

1.1.5 Thermal Analysis

Review of the literature revealed that thermal analysis of high-powered model rockets is often overlooked in favor of more thorough research into mechanical design and aerodynamic analysis. Nonetheless, thermal analysis is necessary to ensure there is no impact of thermal loads from the motor to subsystems as well as to resolve possible failure modes of the rocket during flight.

Team Narwhal designed their rocket to accommodate estimations of thermal loading from the motor. The team had originally designed a 3D-printed ABS plastic boat tail to improve aerodynamic performance. In its original configuration, the boat tail was fastened to the end of the rocket without concern for the exhaust of the rocket motor. After noting the relatively low melting

point of the ABS material used, the motor was moved to sit just beyond the end of the boat tail so that the exhaust did not contact the plastic surface. Furthermore, discussions with the motor manufacturer confirmed that the outer surface of the motor reaches a maximum of 100°C during its burn period. Given a motor burn time on the order of one second and the 105°C melting point of ABS, the team determined that no further action was required to protect the rocket from thermal loads. Upon launching their rocket, the team discovered a secondary problem due to the thermal expansion of 3D printed parts. As with the boat tail, the nosecone of the rocket was printed using ABS. It was designed to have a sliding fit with the body tube, to ensure proper separation upon parachute deployment. However, the nosecone did not successfully separate during the rocket's second launch. The team speculated that this was due to the thermal expansion of the nosecone caused by solar heating during launch and recovery. The team calculated an expansion of more than four thousandths of an inch (Calcara, et al., 2016) . This expansion made the nosecone slide much less effectively in the body tube, resulting in the parachute deployment failure.

1.2 HPMR Program Goals

The goals of the HPMR Program were shared among the three MQP teams involved: NAG-1901 , JB3-1901, and MAD-1901. They are:

- Design, integrate, and fly a reusable, Class-2 high-powered model rocket capable of reaching an altitude of 457.2 m (1500 ft) using Level-1 motors.
- Provide the 21 members of the three MQP teams with a major design experience of a moderately complex aerospace system.

1.3 HPMR Program Design Requirements, Constrains, Standards and Other Considerations

The design requirements for the HPMR Program were shared among the three MQP teams involved (NAG-1901, JB3-1901, MAD-1901) and consisted of the following:

- Use on-board cameras to record video during flight.
- Use an autorotation recovery system to slow the descent and prevent damage upon impact.
- Use a CO₂ stage-separation system to eject the nose cone and deploy the recovery system.
- Use an electromagnetic stage separation system to separate boosters from the main rocket body.
- Use actively-controlled, actuated fins to control the trajectory of the rocket to ensure vertical flight.
- Use single or clustered, Level-1 main motors, and boosters if necessary, to provide the necessary thrust-to-weight for a safe launch, while remaining below the total impulse limit.

The design constraints for the HPMR Program were shared among the three MQP teams and consisted of the following:

- The overall weight of the rocket must be minimized to ensure a high enough thrust-to-weight ratio to launch safely and meet project height requirements.
- The rocket must leave the launch rail at a high enough speed to ensure there is no chance of injury to those present at the launch site.
- Each motor must be able to individually provide a 5:1 thrust to weight ratio off the launch rail to provide an adequate safety factor.
- The dimensions and location of all internal subsystems must be compatible with constraints imposed by the height and width of the rocket body.

The design standards imposed by the National Association of Rocketry (NAR) (Stine & Stine, 2004) for high-powered model rockets applied to the three MQP teams and included the following:

- The rocket is built with lightweight materials (paper, wood, rubber, plastic, fiberglass, or when necessary ductile metal).
- Only certified, commercially made rocket motors are used to launch the rocket.
- Motors and rocket body materials used were purchased from reputable hobbyist sources.
- For flight tests, the motors are ignited electronically with commercial ignitors, purchased from reputable hobbyist sources.
- The rocket is launched with an electrical launch system, and with electrical motor igniters that are installed in the motor only after the rocket is at the launch pad or in a designated prepping area. The launch system includes a safety interlock in series with the launch switch that is not installed until the rocket is ready for launch and will use a launch switch that returns to the “off” position when released. The function of onboard energetics and firing circuits will be inhibited except when the rocket is in the launching position. The switch is installed and tested before launch.
- The rocket uses a recovery system to land the rocket safely and undamaged in such a manner that it can be flown again. Any wadding used in the recovery system is flame-retardant. For the test launch, this consisted of an appropriately sized parachute. An autorotation recovery system was designed for later launches.

The following design considerations for the HPMR Program were shared among the three MQP teams and included the following:

- Safety: A primary consideration during construction, integration, and launch, for both the MQP teams and the public.

- Simulation of possible landing places to insure the safety of not only the project teams, but also the launch site.
- Thrust-to-weight ratio: Designed to be relatively high, to ensure safe levels and guarantee the rocket maintained a vertical orientation after leaving launch rail.
- Proper disposal of partially burned motors to ensure safety and minimize environmental impact.
- Social impact: The broader impacts of model rocketry as a hobby was researched by the individual teams with findings described in the individual reports.
- Environmental factors: Means of limiting potential environmental impact of model rocketry (e.g. material disposal, damage during launch and flight mishaps) was researched by the individual teams with findings described in the individual reports.
- Community outreach: considered to potentially engage those wishing to learn more about STEM related topics explored with this project.

1.4 HPMR Program Management and Budget

The HPMR Program consisted of three separate MQP teams, each responsible for different aspects of the Program.

The Mechanical, Structural, Aerodynamic, and Thermal (MSAT) MQP team (NAG-1901), with 8 members, performed the overall HPMR design and was responsible for the physical assembly and mechanical integration of all subsystems designed by the PSR and FDC teams. The MSAT team was responsible for enforcing volume limitations that affected subsystem designs by the PSR and FDC teams. The MSAT MQP team fabricated also several components and performed functionality testing of cameras. The MSAT MQP team also performed structural, aerodynamic,

and thermal analysis on the various subsystems of the HPMR to ensure safety margins and no adverse impacts from structural and thermal loads on components.

The Propulsion, Staging, and Recovery (PSR) MQP team (JB3-1901), with 8 members, was responsible for the design of the propulsion and recovery subsystems of the HPMR. The PSR MQP team performed analysis on motor sizing to choose the appropriate motors for the rocket and determined a parachute size that would return the rocket to the ground at a safe velocity. An autorotation recovery subsystem was also designed, which was meant to replace the parachute. The PSR MQP team also designed the systems that would separate the nosecone section from the rocket body and the system that attaches/separates the boosters from the main body via electromagnets.

The Flight Dynamics and Control (FDC) MQP team (MAD-1901), with 5 members, was responsible for the design of the avionics for control and dynamic stability of the HPMR. For the first launch the FDC MQP team had to ensure parachute ejection at apogee as well as dynamic stability of fin design. While communicating with MSAT they were given maximum electronics bay dimensions to ensure sufficient volume for parachute and motors.

The three MQP teams met weekly with each of the faculty advisors involved as a conglomerate organization titled the Systems Engineering Group (SEG). Each week, the MQP teams presented an update of the past week's activities, discussed open action items between the teams, and sought input from the faculty advisors.

Funding for the construction of the rocket was provided by the WPI Aerospace Engineering Department. Per school policy, each student was allotted \$250 for use in the project. With 21 students, the budget for the construction of the rocket totaled \$5,250. The total funds were split between the three MQP teams comprising the HPMR Program. The MSAT and PSR teams each

had 8 members, corresponding to a budget of \$2000 each. The FDC team received the remaining funds for its 5 members, with \$1250. Overall, the SEG spent \$1947.94 in development of the rocket. The full cost breakdown can be seen in Appendix A.

The Code of Ethics for Engineers (National Society of Professional Engineers) states that

“Engineers, in the fulfillment of their professional duties, shall:

1. Hold paramount the safety, health, and welfare of the public.
2. Perform services only in areas of their competence.
3. Issue public statements only in an objective and truthful manner.
4. Act for each employer or client as faithful agents or trustees.
5. Avoid deceptive acts.
6. Conduct themselves honorably, responsibly, ethically, and lawfully to enhance the honor, reputation, and usefulness of the profession.”

The first canon is especially relevant to this project, since model rocketry can be a dangerous hobby if certain regulations are not strictly followed. The HPMR Program took this canon very seriously, by adhering to all FAA and NAR guidelines and regulations throughout the design process, as well as by following all guidelines set forth by the executive staff at the launch site.

The second canon was addressed partially by placing students in each MQP team that they would be most interested and qualified for, thus creating a project wherein students are performing work in their area of expertise.

The third and fourth canons are less relevant to the HPMR Program, since there were no public statements to be issued; nor were there separate employers to speak of.

The fifth and sixth canons are covered by WPI’s Academic Honesty Policy, which all three MQP teams (and all MQPs) must follow.

1.5 MSAT MQP Objectives and Methods

The objectives of the MSAT MQP and methods used to achieve them are:

- Design the following HPMR components using SolidWorks: Airframe & Bulkheads; Electronics Bay; CO₂ Separation system integration; Fin Attachment Brackets; Camera (nosecone); Cameras (side). SolidWorks components provide accurate sizing data for the other sub-teams.
- Construct the following HPMR components using tools provided in the MQP Laboratory and Foisie Makerspace: Airframe & Bulkheads; Electronics bay mounting mechanism; Camera Mounts; Fin attachment brackets. Construction consists of drilling and epoxy which allow the team to separate the HPMR into components.
- Perform physical integration of the following components: Airframe & Bulkheads; Electronics Bay; Autorotation System; CO₂ Separation System; Camera System; Fins. Communication with other sub-teams is maintained in order to guarantee integration quality.
- Perform aerodynamic analysis using analytical models of the airframe to obtain the drag over the HPMR for different parts of the ascent. Perform also computational fluid dynamics modeling of the full-scale HPMR to obtain the drag for speeds in the range of 100 to 150 m/s using ANSYS FLUENT.
- Perform the following structural analyses using ANSYS Workbench: bulkhead pressure analysis; weight vs. thrust analysis; camera mount force analysis. Structural analysis ensures mechanical components have a reasonable factor of safety for high velocity loads.

- Perform the following thermal analyses using COMSOL Multiphysics Software: thermal loading of the tail region (motor section, boosters, fins).
- Perform camera functionality and view testing by ensuring mount is designed properly. A successful design will view both the horizon and boosters in flight.
- Perform scale model wind tunnel tests (if possible) in order to confirm accuracy of Lift vs. Drag curves.
- Perform a test launch (if possible) to obtain data that will allow the team to determine whether it meets mission constraints.

1.6 MSAT MQP Organization

The MSAT MQP team was subdivided into the following subgroups: mechanical design and integration; structural analysis; aerodynamic analysis; and thermal analysis. The mechanical sub-team was responsible for designing and constructing the HPMR's airframe, and any mounting components required to integrate other sub-systems. The mechanical sub-team was also responsible for integrating the sub-systems designed and built by the PSR and FDC teams. The structural sub-team was tasked with conducting computer simulations of the various components of the airframe and bulkheads. The goal of these simulations was to ensure all components would withstand launch and landing loads without having to risk loss of the HPMR through destructive testing. The structural sub-team also developed a system of strain gauges to confirm the accuracy of their simulations. The aerodynamic sub-team, in a similar manner to the structural sub-team, developed and ran computational fluid dynamics (CFD) simulations. These simulations were used to produce drag coefficients for the HPMR and its control surfaces. The aerodynamics sub-team also provided drag coefficients to the FDC team for use in their control law development. The

thermal analysis sub-team produced a COMSOL model of the motor cluster to ensure that the thermal loading of any of the parts would not endanger the structural integrity of the HPMR.

Each of the sub-teams used a series of tools to manage the execution of the product. These tools included a team expectations agreement, an action item list, and a Gantt chart. A team expectation agreement is a document that all the team members write together at the start of a project. It serves to lay out team protocols and expectations. Additionally, it defines the course of action undertaken if a team member is found to be neglecting their responsibilities. An action item list is an Excel document that lists each action item, the person or group responsible for its completion, the dates when the item was assigned, when it's due, and the status of the item. This was used as a fair method for delegating tasks and keeping track of due dates. The Gantt chart was a document that listed all the tasks required to complete the different objectives of the project. The Gantt chart assigned a predicted start and end date for each of those tasks. The function of this was to establish a critical path of tasks. This allowed for the MSAT team to plan out long-term objectives and prioritize critical tasks.

1.7 MSAT MQP Tasks and Timetable

A Gantt chart was used throughout the project to organize tasks. This Gantt chart was shared by all three MQP teams and updated regularly. The Gantt chart covered tasks for the active control fins, autorotation recovery mechanism, CO₂ stage separation, boosters, nosecone and side cameras, electronics bay, airframe and bulkheads, propulsion system, launch day procedure, and the final report. The Gantt chart can be found in Appendix B. In addition to the Gantt chart, the SEG used an action item list to track tasks assigned from one of the MQP teams to another. This action item list is displayed in Appendix C. A MSAT-specific action item list was also used to delegate tasks to individuals on the MSAT MQP team. This full list of action items appears in Appendix D.

2 Mechanical Design, Construction and Integration

This chapter lays out the considerations made during the design of the HPMR, as well as the process for the construction of each section. The HPMR is broken down into six main assemblies: airframe, payload bay, electronics bay, motor section, boosters, and nosecone, as seen in Figure 5. The payload, electronics, and motor section, as well as the nosecone and boosters, are all individual assemblies, each containing various systems. The airframe is the compilation of each subsection into a completed HPMR.

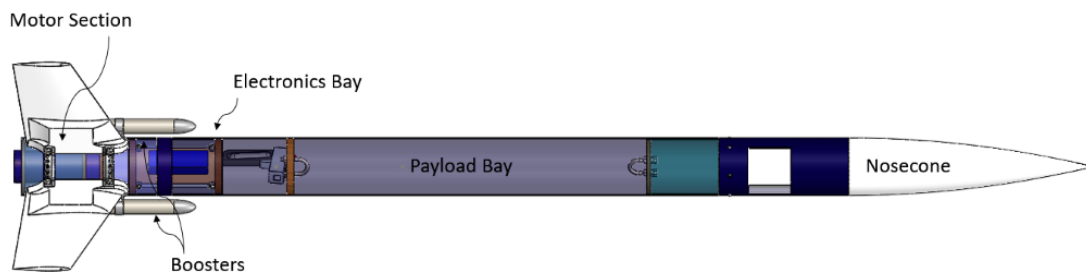


Figure 5. The assembled model of the HPMR airframe.

Throughout the design, modularity and ease of assembly were major considerations. The three MQP teams developed systems concurrently, and each needed to be accessed in preparation for launch. Each subsection can be separated from the HPMR by unfastening the connecting bolts. Further disassembly is possible in the motor section, electronics bay, and nosecone to facilitate the replacement of damaged motor tubes, removal of electronic components, and access to the internal camera.

2.1 Airframe

The airframe is the assembly of each subsection into the completed rocket. As such, it is comprised of a large tube which provides shape and structure to the rocket. Determining the proper material for the airframe required considering weight, strength, cost, and ease of manufacturing.

The MSAT team considered four of the most common materials used in model rocketry: Kraft phenolic paper, fiberglass, carbon fiber, and Blue Tube.

As with all the materials considered, Kraft phenolic paper is a composite, composed of a cardboard-like material impregnated with resin. Phenolic body tubes are the cheapest material of those considered. Furthermore, it is available for purchase from multiple manufacturers and can be found in sizes common for model rocketry. However, though reasonably strong, Kraft phenolic paper suffers from brittleness, and can easily crack if dropped or impacted. It was this weakness that prompted the MSAT MQP team to pick a different material.

Fiberglass and carbon fiber are the strongest materials the MSAT MQP team considered. Each consist of fibers of material--glass or carbon respectively--bound together with an epoxy resin. The resulting material is much stronger and resistant to cracking than phenolic tubes. Many model rocket builders use fiberglass for high-altitude or high-speed rockets and use carbon fiber for strong, lightweight fins. However, both materials are much more difficult to manufacture than the pre-made tubes. Working with either materials requires epoxy, vacuum chambers, and curing ovens, as well as protective equipment to prevent irritation or injury from sharp airborne fibers. Combined with the much higher cost and increase in estimated weight, the MSAT MQP team determined that neither fiberglass nor carbon fiber would be used in the rocket.

The material chosen for the airframe was Blue Tube, a proprietary vulcanized fiber material made by a company called Always Ready Rocketry. Much like Kraft phenolic, Blue Tube comes ready to use, as a tube sized for most rocketry applications. Although it is more expensive and slightly heavier than phenolic, the material is much stronger and more flexible. Blue Tube is also approximately 36% lighter than fiberglass (Anon., 2019). Blue Tube's greatest weakness is its susceptibility to water damage. Light rain or very high humidity can cause severe warping of the

tube. However, the surface can be sealed with paint or other waterproof sealer, eliminating this problem. Furthermore, Blue Tube is very easy to work with. It comes ready to use and can be cut with many woodworking tools. The MSAT MQP team determined that Blue Tube had the greatest balance of strength, cost, and manufacturability, even if it was not the lightest material considered.

The MSAT MQP team purchased 2 pieces of 4-inch (101.6 mm) diameter Blue Tube, each 48 inches (1219 mm) long, to make up the airframe. Two pieces of coupler tube were also purchased, each with a diameter of 3.876 inches (98.45 mm) in order to slide snugly into the main body tube and connect two tubes together. The 4-inch diameter was chosen as a reasonable size for the allotted total impulse of the HPMR. A larger rocket would have been unreasonably heavy, whereas a smaller diameter would have restricted the space for the various subsystems.

2.2 Payload Bay

The payload bay makes up the center section of the HPMR. It is included as a compartment large enough to hold any payload the HPMR may be carrying. In most cases, this includes a parachute and anything to be deployed based on mission requirements. In place of a parachute, the PSR MQP team elected to design a deployable autorotating blade system. Consequently, the payload bay had to be large enough to contain sufficiently long blades for recovery and any extra deployment mechanisms developed by the PSR MQP team.

The payload bay is the least complicated section of the HPMR, as it consists of a single empty tube. Though the length of the autorotation mechanism was limited to 24 inches (610 mm), the tube for the payload bay was cut to 38 inches (965 mm) in length. This was to include 5 inches (127mm) for mounting the payload bay to the nosecone, 3.5 inches (88.9 mm) for mounting to the electronics bay, and the remaining 5.5 inches (139.7 mm) for the payload deployment system.

The construction of the payload bay was simple: the correct length of Blue Tube was cut from the original manufacture length using a hacksaw; the surface of the cut was then sanded to remove any burs left from the cutting process and allow for a piece of coupler tube to slide easily through the tube once more.

2.3 Electronics Bay

The electronics bay (e-bay) is the central hub of all power and control systems in the HPMR (see Figure 6). The e-bay holds the battery, altimeter, IMU, and microcontroller to organize events and data during flight. It is designed to contain these systems securely in the HPMR while allowing manual access for the purpose of arming and disarming any deployment charges while on the launchpad.

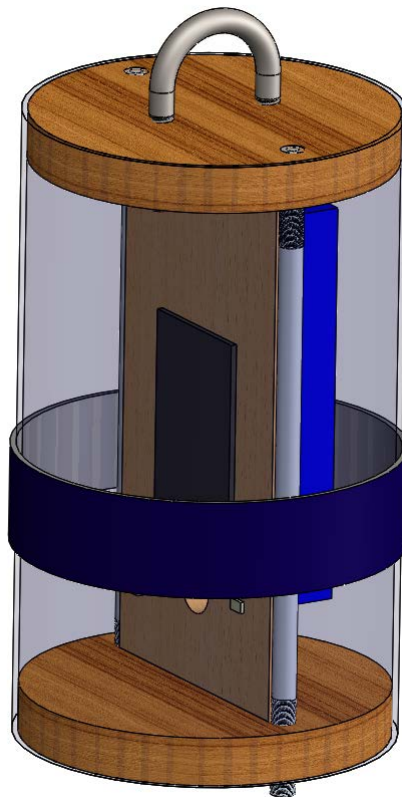


Figure 6. Model of the assembled electronics bay.

The design for the e-bay followed the design of most standard high-powered rockets. The main body of the electronics bay was constructed from a length of the coupler tube. This was done to allow the electronics bay to serve the additional function of connecting the motor section to the payload bay. The center of the e-bay was fitted with a thin 1-inch (25.4 mm) band of body tube material around the outside to prevent the enclosure from sliding through the HPMR. The purpose of this was to transfer the force from separation and recovery system deployment to the rest of the HPMR and prevent the electronics bay from sliding into either the motor section or the payload bay. This ring also provides access to the e-bay from the outside of the HPMR, as the ring sits in line with the rest of airframe. The ends of the e-bay tube are capped with plywood bulkheads. Unlike the ¼" (6.35 mm) bulkhead material used elsewhere on the HPMR, these bulkheads were made from ½" (12.7 mm) plywood to increase their strength. On the side of the e-bay facing the payload bay, the bulkhead is epoxied in place to support parachute mounting, as well as withstand the forces of deployment. The other bulkhead is held in place with nuts and threaded rods. This allows it to be removable for access to the internal electronics.

While it is possible to purchase off-the-shelf electronics bays of a similar design, the MSAT MQP team decided to build the electronics bay from scratch to allow for greater customization and to meet the mission requirements. In addition to the electronic components included in a standard electronics bay, the mission required electrical systems to control the active fins, the booster separation, and strain gauge system. Furthermore, the electronics bay also had to serve as the mounting point of the stage separation system, as well as the anchoring point for the recovery system.

The e-bay was designed to accommodate two different separation and recovery systems. The first separation system used the combustion of black powder to pressurize the payload bay and

cause the nosecone assembly to separate. The recovery system would be pushed out with the nosecone and deploy for a safe recovery. This was to be used as a simpler alternative to the CO₂ system in preliminary testing and launches. The design of this system was straightforward. A small plastic well for holding the black powder, pictured in Figure 7, and a connection point for the ignition wires were bolted to the outside of the fore end bulkhead of the electronics bay.



Figure 7. Black Powder separation system charge well.

The second stage separation system utilizes pressurized carbon dioxide in place of black powder. Designed and built by the PSR MQP team, the CO₂ separation system utilizes a gas canister and magazine from a gas-powered airsoft gun as the source of pressure. The canister stores CO₂ at 932 psi (6.43 MPa), enough to pressurize the entire payload bay to approximately 14.5 psi (0.10 MPa) and deploy the recovery system. To trigger the ejection, a custom lead-screw linear actuator was designed to press a button located on the side of the magazine, releasing the gas in the canister in under 500ms (JB3-1901). This actuator was fixed to the CO₂ magazine with a 3D printed bracket. The full sub-assembly is pictured in Figure 8.

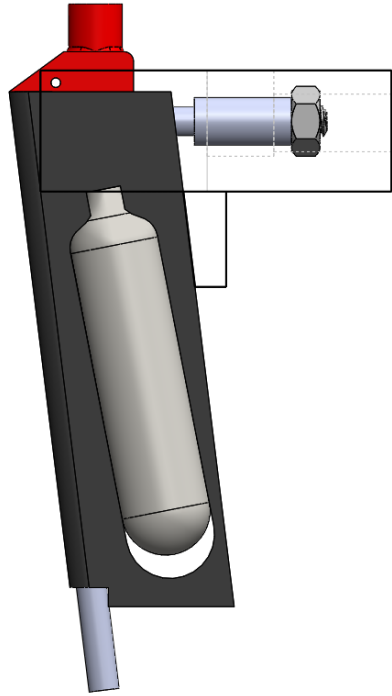


Figure 8. Model of the CO₂ separation mechanism.

Both recovery systems, a parachute and a set of autorotating blades, were designed to connect to a U-bolt which was fastened to a bulkhead. In the case of black powder ejection, the U-bolt was mounted directly to the top of the E-bay. This reduces the need to add additional bulkheads, therefore minimizing complexity. To accommodate the increased size of the CO₂ system, the MSAT team added a bulkhead above the E-bay to hold the U-bolt mounting for the recovery system. A hole in the bulkhead allows the gas from the canister to pass through uninhibited, while a second hole allows the IMU to reach the CG of the HPMR. Simulations of the stresses on both bulkheads are discussed in Chapter 3.

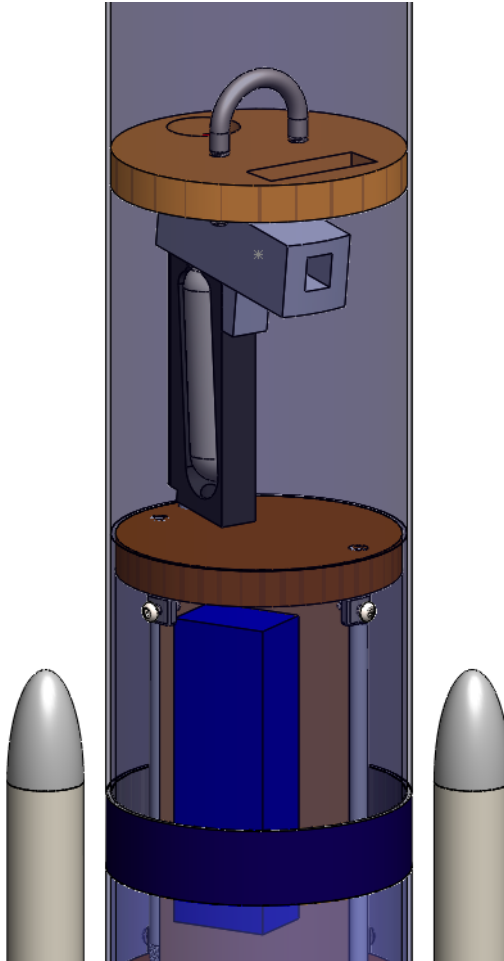


Figure 9. Model of the completed CO₂ ejection system integrated into the body of the rocket.

The MSAT MQP team was responsible for the integration of the CO₂ system into the rocket. By coincidence, the magazine selected to hold the gas canister was made with a channel approximately ¼" (6.35 mm) in diameter. The MSAT MQP team used epoxy to secure a ¼" (6.35 mm) threaded rod into this channel. This rod screws into the e-bay, just as the black powder cap does for the black powder separation. The bulkhead used to hold the recovery system is epoxied in place above the CO₂ system, with the hole located directly above the nozzle (see Figure 9).

To construct the electronics bay, a 6.5-inch (165 mm) length section of coupler tube was cut using a hacksaw. This length was chosen through communication with the FDC MQP team, who determined they would need a 5-inch (127 mm) vertical space for the e-bay. Then the retaining

band of body tube was epoxied in place. Finally, eight nuts—four on each end of the e-bay—were secured radially with epoxy to the interior of the electronics bay. These nuts served to retain the bolts that secured the electronics bay to the payload bay and the motor section. The rest of the electronics bay, the bulkheads, and internal electronics mounts were designed and constructed by the FDC MQP team to allow them greater flexibility in the layout. Once these parts were completed, they were delivered to the MSAT MQP team for physical integration into the airframe. Finally, the U-bolt for connecting the recovery system to the HPMR was fixed to the upper bulkhead.

2.4 Motor Section

Located at the aft of the HPMR as shown in Figure 10, the motor section was designed to securely hold the motor(s) for launch and retain them after burnout. Further, the motor section contains the mechanical and electrical systems for booster burn and separation. The outer surface of the motor section provides locations to mount the HPMR's stabilizing fins. Contained within the motor bay of the motor section was the motor mount, the detachable tube where the motor(s) are inserted. The original design of the motor mount included three 38 mm motors clustered radially. After a failed launch attempt, these motors were replaced with a single 54 mm motor. The fins are mounted around the outside of the motor section tube using custom 3D printed brackets. The forward area of the motor section is designed to simultaneously hold the magnetic separation system, as well as provide a mounting interface for the e-bay.

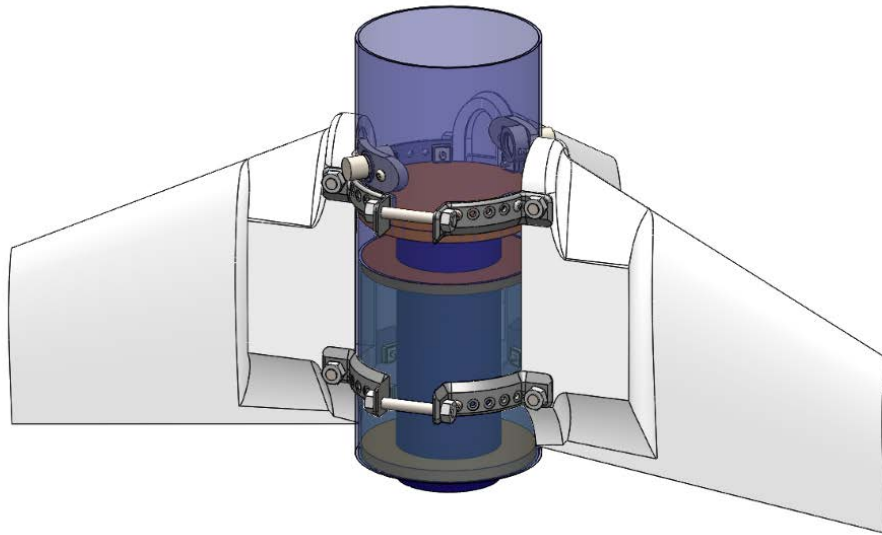


Figure 10. Model of the assembled motor section, including the passive variant of the active control fins designed by the FDC team. One fin has been removed for viewing purposes.

The principle driver of the design of the motor section was the number, length, and diameter of the original motor tubes, which were required in order to hold the motors specified by the PSR MQP team. The PSR team decided to utilize three H73J motors. These motors required mounting tubes 38 mm in diameter by 6 inches (152.4 mm) tall. In standard model rocketry practice, there are two methods to arrange three motor tubes, either in-line or radially. Each method can either have a surrounding tube or be exposed. The team decided to enclose the motors rather than leave them exposed. This was done for two reasons: First, enclosing the motors follows the designs employed on previous WPI teams (Belliss M, 2006). As a result, some of the team members were familiar with the design and construction of this type of rocket. Second, the motor section needed to attach to the e-bay and payload bay. Each of these are a single, enclosed tube. By enclosing the motors in a tube of the same diameter, connecting the motors to the rest of the HPMR was easily accomplished with a coupler tube. Deciding to enclose the motors in the body tube automatically required the motors to be clustered radially. Because each motor has a diameter of 38 mm, it was impossible for the three motors to be arranged linearly inside a 4-inch (101.6 mm) tube. After a

review of a failed test launch, the PSR team made the decision to change the main motor to an I218 54 mm-diameter motor. This new motor required a redesign of the motor mount. The new motor mount had the same layout of centering rings as the original design. However, the new centering ring only had a single axial hole to mount the larger motor. Figure 11 shows both configurations of the motor mount.

One major requirement of the motor section was the ability to remove the spent motor casings from the HPMR. In order to accomplish this, two centering rings for the motors were fixed to a 3.75-inch (95.25 mm) long piece of coupler tube, with the motor tubes placed in these rings. This coupler was fixed with nuts similarly to the nuts in the e-bay. This allowed the whole assembly, pictured below, to slide into the motor bay and mount securely, while still being removable. The final centering ring and main bulkhead, used to separate the heat of the motors from the electronics, were epoxied into the main motor section 5.45 inches (138.43 mm) from the lower end. At this distance, the fully inserted motor mount fits into the centering ring and extends approximately 1/3” (8.47 mm) from the end of the HPMR. This distance was added to assist in the removal of the motor mount, which would be difficult to grasp when mounted flush with the bottom of the HPMR.

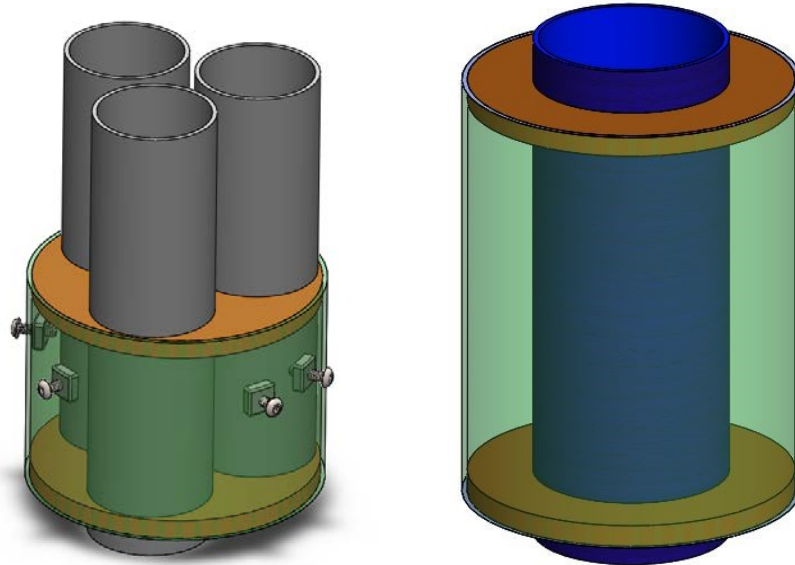


Figure 11. Model of the removable motor mount assembly with three motor tubes (left) and a single motor tube (right).

In addition to holding the motor tubes, the internal motor mount also holds the motor retention system. The motor retention satisfies a launch site safety requirement. It is designed to hold the motors in place after burnout to prevent the ejection of uncontrolled debris from the rocket. The MSAT MQP team decided to use a commercial-off-the-shelf (COTS) part, mainly because the commercial system was inexpensive and highly reliable. The system consists of three bolts secured by T-nuts into the aft end of the motor mount. Each bolt held two retaining hooks, one for each adjacent motor, shown in Figure 12.



Figure 12. Image of the motor retention system over empty motor mount tubes.

The motor mount was secured to the larger motor section by four bolts. These bolts performed two functions, since they were also responsible for holding the lower fin mounting brackets in place. There was some difficulty in finding locations for the four bolts without intersecting the motor tubes. This was due to the fact that there were three radially symmetric motor tubes whereas there were four radially symmetric fins. Furthermore, the bolts are not able to intersect with either the motor tubes or the fins. To solve this, the MSAT team attached the fins with a set of eight custom 3D printed brackets (see Figure 13). The brackets were designed with five holes each, to allow for a range of possible bolt positions around the motor bay. This allowed the MSAT team to print multiple copies of the same bracket without the need to tailor each bracket to the location of each bolt. Each bracket could be secured by at least one bolt and have enough space around the end of the bolt for a retaining nut. Each fin was then secured to the appropriate brackets by two bolts threaded through the fins---one at the leading edge and the other at the trailing edge. The fin attachment system is shown in Figure 13

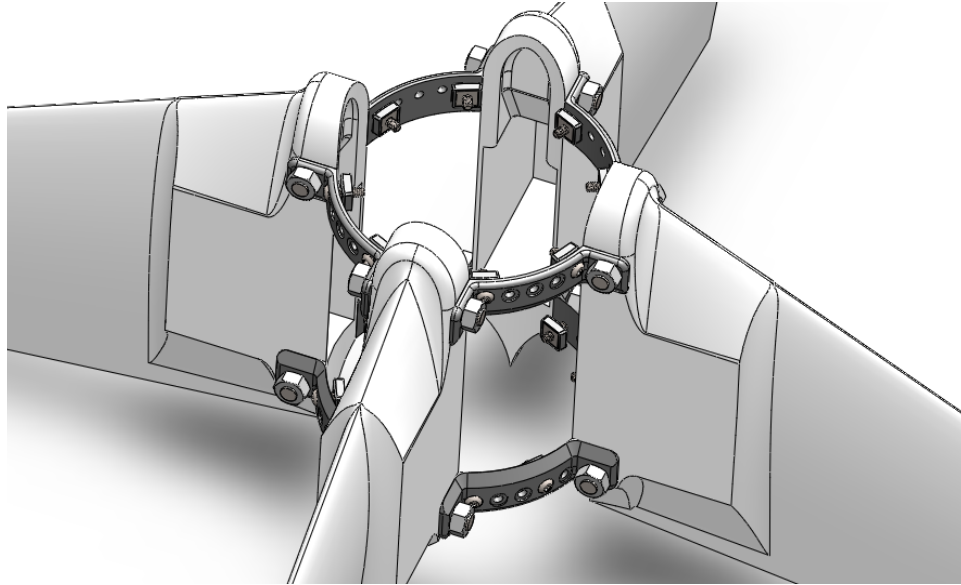


Figure 13. Model of the fin and bracket assembly separated from the motor bay tube. The 8 bracket pieces can be seen with fixtures through some of the provided holes.

To construct the motor section, the materials were first modeled in SolidWorks and then cut to the appropriate size and length. The motor tubes, motor mount coupler tube, and motor section body tube were cut to length using a hacksaw and sanded, just as with the electronics bay. Next, the centering rings and solid bulkhead were laser cut from ¼-inch (6.35 mm) plywood. Two centering rings were cut with a smaller diameter in order to fit into the coupler tube. These centering rings were aligned and epoxied in place at each end of the coupler tube. The motor mount was then fitted into the motor bay, after the fin mounting brackets had been dry-fit around the section. Holes were then drilled through the holes in the mounting brackets, so that the holes were aligned through each layer of tube. Next, the MSAT team installed retaining nuts within the motor mount, in line with the holes drilled previously. With the nuts installed, the motor tubes were epoxied into the centering rings, taking care to keep them parallel and vertically aligned. The third alignment centering ring and the solid bulkhead were epoxied in place in the main body tube to hold the motor mount in line with the bottom of the HPMR.

2.4.1 Fins

The fin assembly was attached concurrently with the motor mount (see Figure 14). The same series of bolts which were used to secure the motor mount also functioned to attach the fin mounting brackets. With the holes drilled and the motor mount assembly inserted in the HPMPR, the brackets were bolted in place. Subsequently, the fins were bolted to those brackets. Once the fin location was confirmed, the brackets were attached to the body tube with epoxy.

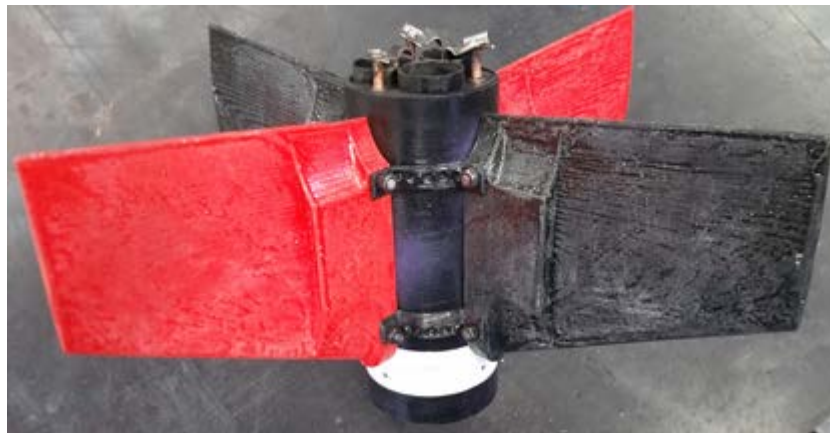


Figure 14. Image of the completed motor bay, with the motor retention system attached.

2.4.2 Boosters

To maximize the total impulse available to the HPMPR, the PSR MQP team elected to create a booster stage to propel the HPMPR off the launch pad and then separate from the HPMPR after motor burnout. While the separation system is included in the motor bay, the PSR team delegated the design and construction of the booster airframe and external mounting to the MSAT team.

The boosters had a very similar layout to the main HPMPR. As discussed in section 2.5, the forward end of the booster was capped with a tangent ogive nosecone. This nosecone was attached to the body of the booster with a length of shock cord, which was also attached to a recovery system. Like a normal model rocket, each booster also contains a motor, a nosecone, and a recovery system. Each booster utilizes an elliptical 3D printed nosecone, with a streamer to allow the low-

mass booster to fall at a reasonable speed. In addition, the boosters are equipped with mounts to hold magnets for the electromagnetic separation system. The model of the completed booster is viewable in Figure 15.

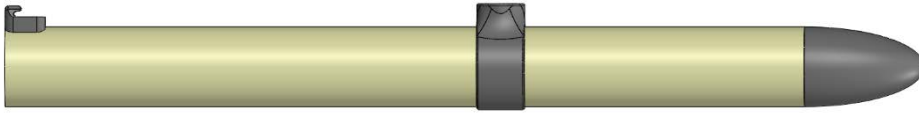


Figure 15. SolidWorks model of the side booster.

Mounting the booster to the side of the HPMR was the main concern of the booster airframe design. The booster airframe had to contain a permanent magnet to interface with the electromagnet mounted within the motor bay. The electromagnet, designed by the PSR team, is the mechanism that separates the booster from the HPMR. Thus, the boosters must be designed to interfere with the electromagnet as little as possible.

Secondary to the magnet mounting, the boosters were designed to use motor ejection to deploy a streamer for recovery. The MSAT team elected to use the motor ejection charge to remove as much complexity as possible from the booster system. Unlike a black powder, CO₂ ejection, or mechanical separation system, the motor ejection charge comes premade in the motors. Furthermore, it does not require any external trigger to activate; a time delay sets off the charge a set time after motor burnout. In order to allow the motor ejection charge to act effectively, the entire booster airframe must remain mostly clear, so as not to block the expanding gasses. The only items placed inside the booster are the streamer, to slow its descent, and the nosecone, which is ejected to release the streamer.

In order to satisfy both constraints, the team designed a mount to hold the permanent magnet to the outside of the HPMR. The mount slides over the outer diameter of the tube, while the magnet

slides into a hole oriented perpendicularly. The model of this mount is pictured in Figure 16. Both the booster tube and magnet are held in place with epoxy.

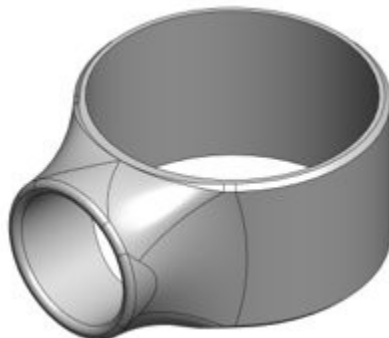


Figure 16. Model of the custom magnet mount for the outside of the booster airframe.

At the base of each booster, the team designed hooks to support the booster as its motor fires (see Figure 17). Without the addition of these hooks, the electromagnetic separation system would be required to sustain the full force of launch and separate successfully with the added friction from the force of the motors. The booster hook was a 3D printed plastic hook which interfaced with a similar hook mounted on the motor bay. The hooks are designed so that, after the booster has finished firing and the magnetic separation has activated, the hooks will no longer keep the boosters fixed to the rocket body.



Figure 17. Image of 3D-printed booster hooks and booster tube.

The booster tubes were made of 10-inch (254 mm) cardboard tube that was already in stock in the lab. The top 3.5-inches (88.9 mm) of the tube contained the streamer and nosecone shoulder.

Directly below that level, the permanent magnet mount was epoxied in place to hold the permanent magnet component of the electromagnetic separation system designed by the PSR team. The lower 6.5-inches (165.1 mm) provided distance between the mounting hook and the magnet separation. This distance reduces the angular deflection of the magnet as it exits the electromagnetic separator, limiting the possibility that the magnet becomes jammed in the mount, and increasing the likelihood of a successful separation.

2.5 Nosecone

The nosecone assembly (see Figure 18) exists to reduce the drag of the otherwise cylindrical rocket by adding a pointed nose with a smooth transition to the body tube. Furthermore, the nosecone is ejected at apogee to allow the recovery system to deploy and slow the rocket's descent. On this HPMR, the nosecone serves the added purpose of housing an internal GoPro camera to record the flight.



Figure 18. Model of the assembled nosecone subassembly.

The fore end of the nosecone section consists of a COTS plastic nosecone, which was purchased to avoid the complexity of constructing a nosecone while maintaining reliability. The shoulder of the nosecone was fixed to a length of body tube with windows cut in the side. This section was designed for use as a camera bay. Below the length of body tube, a piece of coupler tube acts as the new shoulder of the now-extended nosecone for connection to the payload bay. As with previous sections, each connection between tubes was facilitated by nuts epoxied on the inside of the body. Bolts can be threaded in from the outside, fastening the HPMR in place. At the bottom

of the coupler tube, a bulkhead with an attached U-bolt was epoxied in place in order to attach the smaller nosecone parachute. Instead of using metal bolts to fix the nosecone to the payload bay, shear pins were used. The shear pins hold the HPMR together during launch but allow the nosecone to separate when pressurized by the deployment charge.

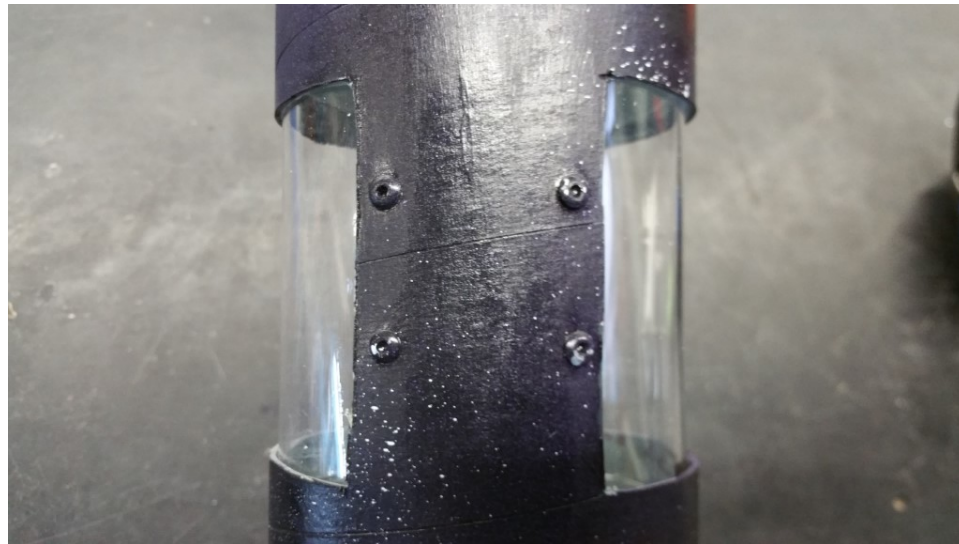


Figure 19. Image of the nosecone windows.

In order to allow the GoPro camera to see out of the nosecone assembly, two windows were cut out from the tube and covered with clear acrylic sheets. To ensure the camera could adequately see out of the HPMR, the windows were made to be large, measuring 3-inches (76.2 mm) tall and subtending an angle of 120° each (see Figure 19). To cover the holes left by the windows, the team used clear acrylic sheets. The MSAT team used a heat gun to bend and warp the sheets to fit the contour of the body tube. Pop rivets were used to secure the acrylic to the Blue Tube.

2.5.1 Cameras

The HPMR has three cameras, one mounted in the nosecone section looking towards the horizon, and one on each side looking aft at the boosters and fins. The nosecone camera is designed to provide stabilized footage facing the horizon during launch. The purpose of the aft facing

cameras is to observe both the boosters throughout their firing and separation, as well as the actuated fins, to observe and document in case any fault developed in either system.

The team had originally planned to use a COTS actively stabilized gimbal to reduce movement and vibration in the nosecone-mounted camera. However, this was changed to a passive design after no COTS part could be found that would meet the sizing requirements for the assembly. The nosecone camera stabilizing system was constrained by the maximum rocket body diameter of four inches. Furthermore, active gimbals rely on the acceleration of gravity to align the camera. With much of the upward trajectory of the HPMR occurring in freefall, the gimbal would not experience gravity relative to the HPMR. Thus, the gimbal would be unable to stabilize effectively. As a result, the team elected to design a passive gimbal to counter any rapid rolling and pitching motions of the HPMR (see Figure 20).

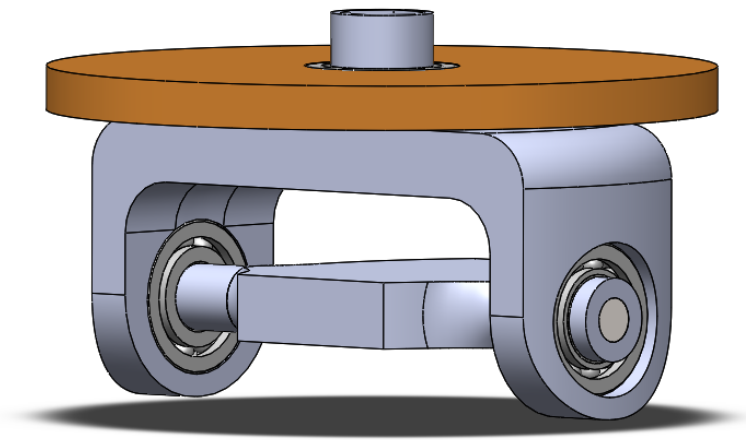


Figure 20. Model of the passive 2-axis camera gimbal.

The goal of the passive design was to stabilize the camera view by isolating the movement of the camera from the movement of the rocket body. The isolation was accomplished with bearings. The gimbal was designed to fit within the four-inch (101.6 mm) diameter body tube and was confirmed through integration in the nosecone CAD model. The entire system was mounted to a

bulkhead in the base of the original plastic nosecone. This mount is the location of a bearing which functions to provide isolation from rolling motion. This connection is threaded to allow for the replacement of the gimbal system in the case of damage. A “U” shaped bracket was designed to hold two bearings, to provide support for the pivot on both ends, as opposed to a single point of support which would add unnecessary torque. The camera is then mounted securely in the open section of the “U” by a COTS mounting system, with care taken to ensure that the camera hangs at its center of mass. To construct the mount, the three-dimensional CAD parts were 3D printed and then assembled with the bearings.



Figure 21. Images of the side camera mounted to the airframe. The red fairing can be independently removed from the rocket to access the camera.

The greatest constraint on the side camera mount design was that, between the two cameras, all boosters and fins needed to be in view. Therefore, two cameras were employed, separated by 180 degrees (see Figure 21). Additionally, the cameras needed a streamlined housing to reduce their impact on the aerodynamic stability of the HPMR. This housing was designed to have an outer profile of a tangent ogive curve like that of the nose cone. The cameras were mounted in place using high strength Velcro. The proper location was determined by streaming the camera feed to a computer to make sure that each camera would have two boosters in view. The fairings were fabricated using a 3D printer and secured, over the cameras, to the HPMR separately with more high strength Velcro.

3 Structural Analysis

The flight-critical components of the HPMR are the main body tube, the nosecone parachute bulkhead, the main body parachute bulkhead, and the mounting brackets for the fins. This section presents the methods and results of the structural analysis on each component. This section also presents the design and integration of a series of strain gauges for measuring strain in flight and confirming the values predicted by the simulations.

3.1 Determination of Flight-Critical Components

The structural analysis of the HPMR began with the determination of all flight-critical components. These components must be fully functional for the entire flight to be successful. If any flight critical components fail, the HPMR risks severe damage to itself, and directly endangers those in its immediate vicinity. For each critical component, the team considered various possible failure modes. The stresses and safety factors were computed using hand calculations and confirmed using ANSYS. The results were used to determine whether the components were safe to use during flight, and to inform design revisions if needed.

The planned flight sequence of the HPMR was examined to find any potential sources of flight failure. The MSAT MQP team determined four main components most critical to launch success: the main body tube; the e-bay bulkhead; the nosecone bulkhead; and the fin mounting brackets.

The main body tube is required to support all the forces acting on the HPMR during a period of high acceleration at launch. The body tube must also contain the pressure created for the deployment of the recovery subsystem. If the body tube were to be damaged or burst in any way, the HPMR would be unable to launch safely, and the recovery system may fail to deploy. Thus, the body tube was determined a flight-critical component.

Bulkheads on both the fore end of the e-bay and the aft end of the nosecone subassembly are used to connect recovery systems to their respective section of the rocket. These bulkheads were deemed flight critical, as failure to survive recovery deployment and use would result in the freefall of the rocket. This scenario would not only lead to severe damage to the HPMPR upon impact with the ground, but potentially endanger to observers on the ground who may be hit by the falling components.

The MSAT MQP team determined the fin mounting brackets to be the final flight critical structure. As discussed in Chapter 2, these brackets are used to fix the fins developed by the FDC team to the outside of the motor bay. These brackets form the sole mounting method of the fins to the motor bay. If these brackets fail during flight, the aerodynamic stability of the HPMPR will be severely affected, possibly causing the rocket to lose control entirely, similarly endangering itself and those around it.

3.2 Recovery Mounting Bulkhead Analysis

The recovery mounting bulkhead provides a U-bolt to attach the recovery system to the HPMPR. The main body of the HPMPR and nosecone bulkheads each utilized individual recovery system, as they separated upon deployment. For the main body recovery system, the MSAT MQP team developed two bulkhead configurations to account for the differences in black powder and CO₂ separation systems. The first incorporated the bulkhead into the forward end of the e-bay as the forward closure for that section. The second design added a bulkhead 4.5 inches above the e-bay to accommodate the larger CO₂ system. It was important to consider the forces on this bulkhead to ensure that the recovery system would remain fixed to the HPMPR during deployment and descent.

The MSAT MQP team used the ANSYS structural analysis tool to perform the analysis on the bulkheads due to the deployment of the recovery system. These components can be seen below in Figure 24 and Figure 25. The team imported SolidWorks assemblies of each bulkhead with an attached U-bolt into ANSYS, and calculated the estimated force of the recovery system on the U-bolt for use in the simulations. The force of a parachute acting on the bulkhead is given by equation 1:

$$\mathbf{F}_d = \frac{1}{2} \rho C_d S V^2 \quad (1)$$

Where C_d is the drag coefficient, ρ is the density of air, S is the surface area of parachute, and V is the descent velocity of the HPMR

Since the force of the parachute on the bulkhead varies with velocity, the equations of motion due to the parachute are listed as follows in equations 2 and 3:

$$a = \frac{F}{m} \quad (2)$$

$$V = V_i - at \quad (3)$$

Where, m is mass, t is time, V_i is the initial velocity of the HPMR, and a is its acceleration. The MSAT MQP team developed a MATLAB code, found in Appendix E, and iteratively determined the force of the parachute over flight time. The same method was similarly used to find the forces on the nose cone bulkhead. The inputs for the main body and nosecone calculations are available below in Table 1.

Table 1. Inputs for the Calculations of Force on Each Bulkhead

Main Body	Parachute Surface Area	1.225 m ²
-----------	------------------------	----------------------

	Component Mass	4 kg
	Initial Velocity	49.05 m/s
Nosecone	Parachute Surface Area	0.23 m ²
	Component Mass	0.6 kg
	Initial Velocity	49.05 m/s

The plots shown in Figure 22 and Figure 23 show the forces on each of the bulkheads over time:

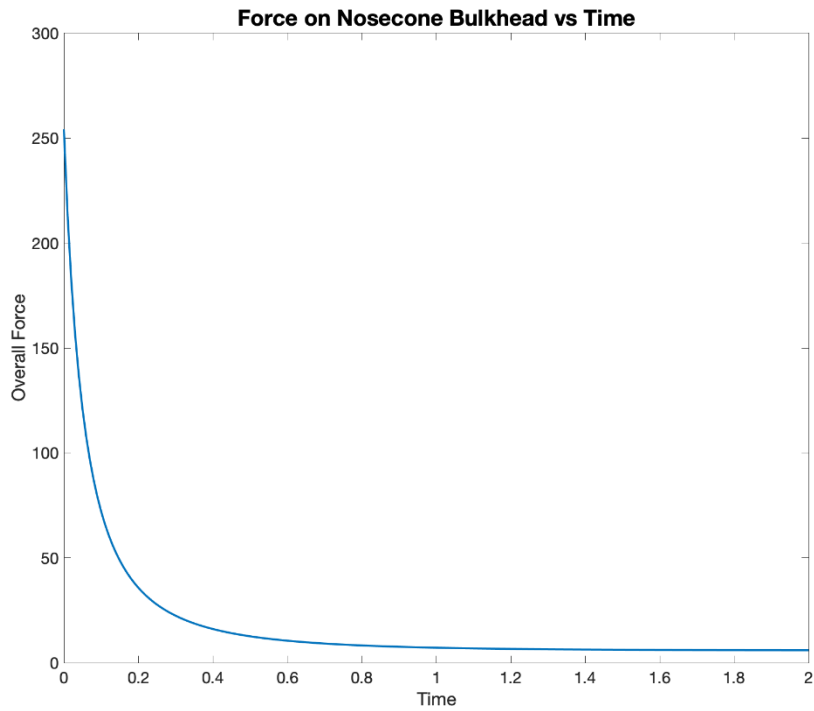


Figure 22. Forces on nosecone bulkhead over time.

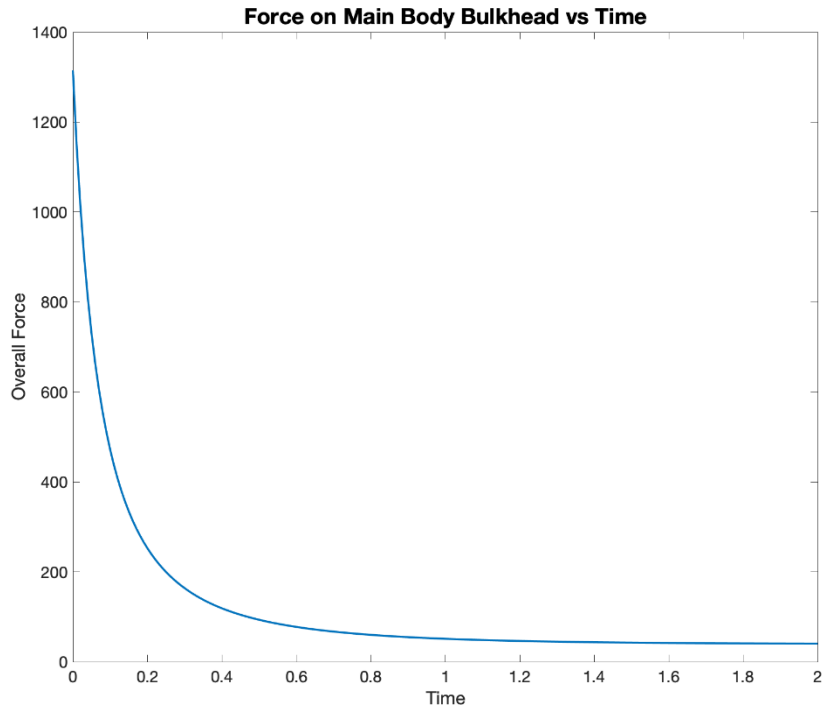


Figure 23. Force on main body bulkhead over time.

The results from the MATLAB plot were used as initial conditions for the ANSYS structural simulation. The MSAT team input an initial 1400 N force, linearly decreasing to 100 N, into the simulation to find the safety factors of the main body bulkhead. Similarly, for the nosecone bulkhead, the safety factors were determined using an initial 300 N force that decreases linearly to 10 N. Figure 24 and Figure 25 show the safety factors to be greater than one, which indicates that the bulkheads are likely to survive the forces of deployment.

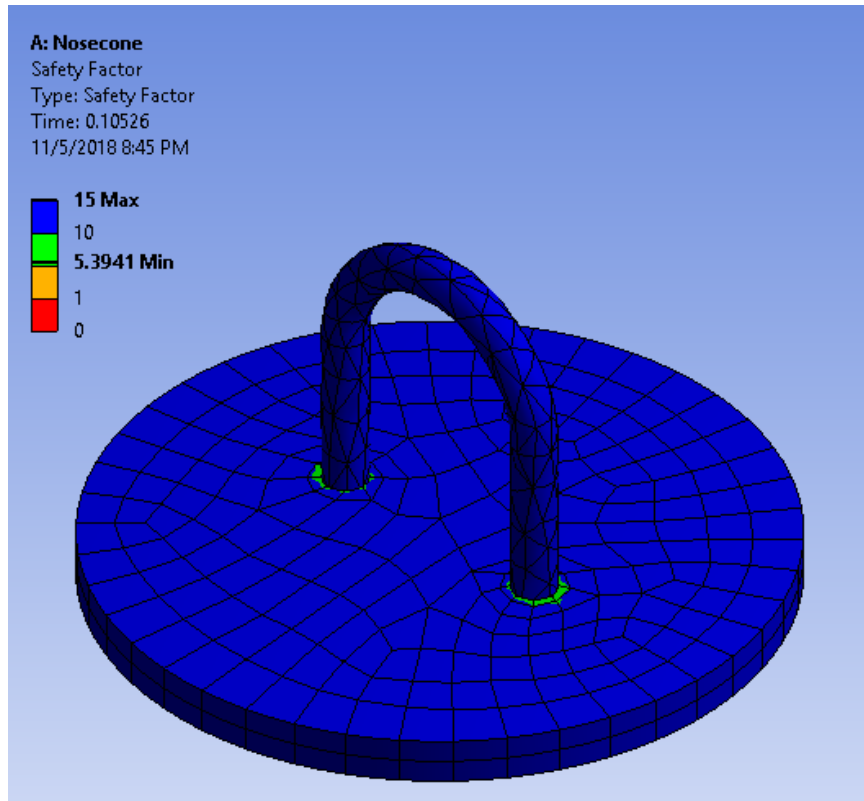


Figure 24. Safety Factors of nosecone bulkhead.

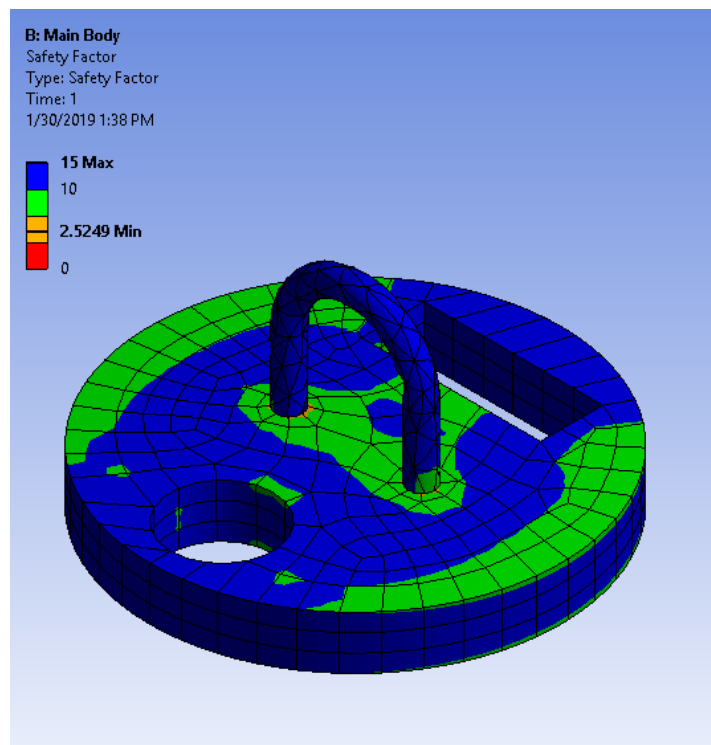


Figure 25. Safety factors of main body bulkhead.

The ANSYS analysis determined that the safety factor is greater than one for both bulkheads. This indicates that both bulkheads are highly likely to survive parachute deployment. Furthermore, the assumptions used to calculate the forces on the bulkheads were made to greatly overestimate the real-world experiences during launch. The initial velocity chosen corresponds to a freefall of nearly five seconds. In practice, the recovery system is designed to deploy at apogee, where the velocity of the rocket reaches a minimum. The estimated mass of the bodies was also increased for the simulations, further increases the simulated forces on the bulkhead. The simulations provided the MSAT MQP team with confidence that neither bulkhead would fail during launch.

3.3 Stage Separation Analysis

When the HPMR reaches the highest point of its trajectory, the onboard computer triggers the stage separation system. This system consists of a pressurized canister of CO₂ that released gas inside the rocket. The system rapidly increases the internal pressure of the rocket body in order to shear the pins holding the nosecone in place. This ejects the nosecone from the front of the rocket, pulling the recovery system with it. Analysis of the structure of the payload bay was necessary to ensure that the pressure increase wouldn't harm the airframe.

Most of the analysis was performed in ANSYS, with the remaining portion done analytically. By calculating the safety factors and margins of safety, the MQP team determined whether each of the individual components could withstand the pressure inside the body tube during separation.

To analyze the bulkhead, the team used ANSYS Static Structural. A pressure of 20 psi was applied to the bottom of the bulkhead. To represent the epoxy mounting the bulkhead to the body tube, the sides of the bulkhead were manually fixed in place. The team also used ANSYS Static Structural for the body tube analysis. As with the bulkheads, a pressure of 20 psi was applied to the inside of the body tube. The ends of the body tube were fixed in place to represent a sealed

body. The MSAT MQP team obtained the material properties of Blue Tube from the manufacturer. This material data was then put into ANSYS for use in the simulation.

The MSAT MQP team analyzed the epoxy holding the bulkheads analytically. The stress on the epoxy and the margins of safety are given by equation 4:

$$MOS = \frac{\sigma_{allowable}}{\sigma_{applied}} - 1 \quad (4)$$

where $\sigma_{allowable}$ is the allowable stress and $\sigma_{applied}$ is the actual stress applied to the epoxy.

To analyze results of the bulkhead analysis, the team examined the equivalent stress and safety factors over the mesh of the body tube and bulkheads to determine if the components could withstand the forces of stage separation. A safety factor greater than 1 was needed for the component to be used safely. Figure 26 shows the results of the bulkhead analysis with a pressure of 20 psi applied to the underside of the bulkhead. The most concerning areas were the sides of the bulkheads, where the epoxy adheres to the body tube.

Figure 26 shows the results of the bulkhead analysis with a pressure of 20 psi applied to the underside of the bulkhead. The only areas of concern were the sides of the bulkhead where the epoxy adheres the bulkhead to the body tube.

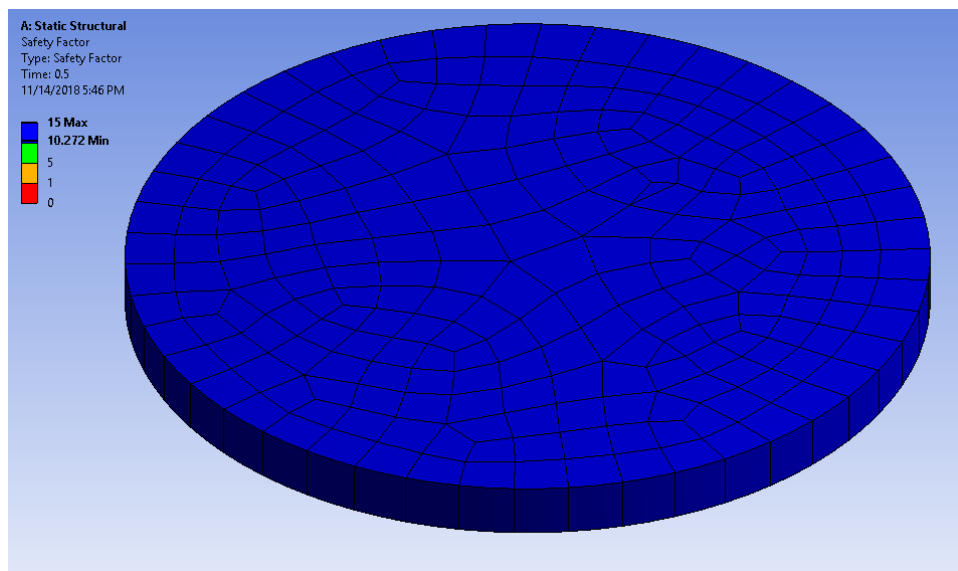


Figure 26. Safety factor of nosecone bulkhead.

The bulkhead was determined to have a safety factor of 10. Figure 27 shows a color gradient of the stress on the bulkhead due to the separation. The maximum stress, shown in red, was used to find the margins of safety.

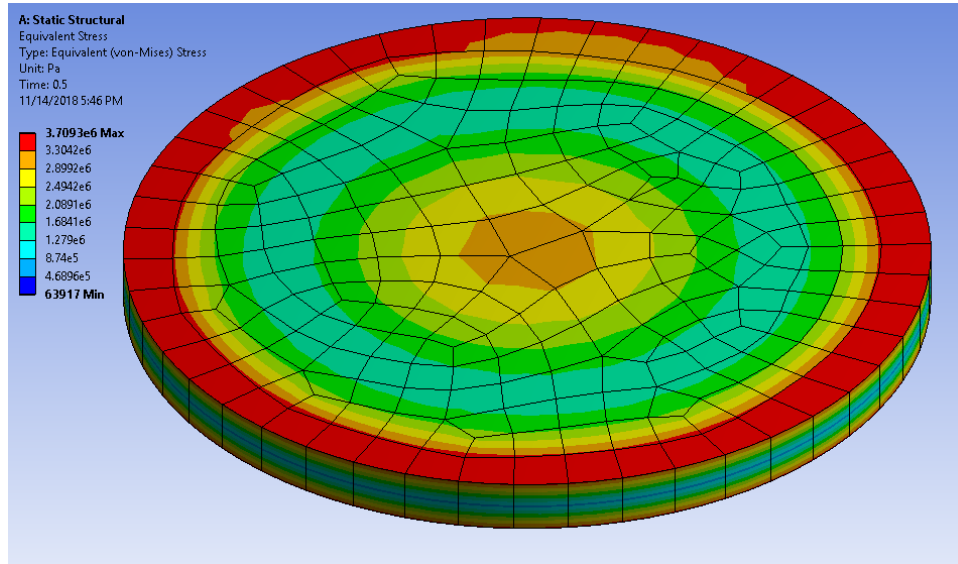


Figure 27. Equivalent stress of nosecone bulkhead.

From the simulation, the team predicted that the stress of the bulkhead on the epoxy to be about 3.7 MPa. The team checked the results from ANSYS through analytical calculations. The calculated maximum stress on the epoxy was 3.7 (see Figure 28).

Physical Properties of Cured Epoxy

Specific gravity	1.18
Hardness (Shore D) ASTM D-2240	83
Compression yield ASTM D-695	11,400 psi
Tensile strength ASTM D638	7,900 psi
Tensile elongation ASTM D-638	3.4%
Tensile modulus ASTM D-638	4.08E+05
Flexural strength ASTM D-790	14,100 psi
Flexural modulus ASTM D-790	4.61E+05
Heat deflection temperature ASTM D-648	118°F
Onset of Tg by DSC	129°F
Ultimate Tg	142°F

Figure 28. Physical properties of cured epoxy. © 2004 West System (West System, 2014)

The team determined the margin of safety of the epoxy from the material data sheet and maximum calculated stress. The shear strength of adhesives, according to the Inch Fastener

Standards, is about 60% of the tensile strength (International Fastener Institute, 2018). Thus, the strength of the epoxy becomes 4740 psi, or 32.7 MPa. The resultant margin of safety is 7.8. This is acceptable, as the margin of safety is much greater than 1. The results of the body tube analysis with a pressure of 20 psi applied are available in Figure 29.

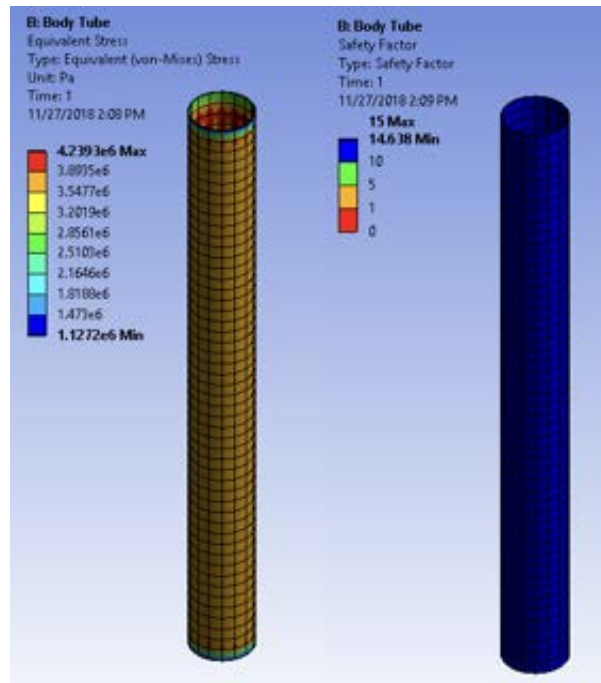


Figure 29. Equivalent stress and safety factor of body tube.

The material data for Blue Tube provided by the manufacturer is listed in Table 2.

Table 2. Material data of vulcanized fiber. © Oliner (Anon., n.d.)

Property	Thickness (in)	Unit	ASTM Test Method	Typical Value
Density	1/16	gm/cc	D-619	1.20
Specific Volume	1/16	cu in/lb		23.0
Tensile Strength				
MD	1/16	psi	D-638	18,000
CD	1/16	psi	D-638	9,000
Modulus of Elasticity in Flexural x 10 ⁵				
MD	1/16		D-790	10
CD	1/16		D-790	7
Modulus of Elasticity in Tension x 10 ⁵				
MD	1/16		D-638	12
CD	1/16		D-638	8
Flexural Strength				
MD	1/16	psi	D-790	26,000
CD	1/16	psi	D-790	16,000
Compressive Strength	1/16	psi	D-695	35,000
Impact Strength				
MD	1/16	ft lbs/in	D-256	2.0
CD	1/16	ft lbs/in	D-256	1.8
Rockwell Hardness, R Scale	1/16	divisions	D-785	80
Bond Strength	1/16	psi	D-952	900
Dielectric Strength	1/64	volts/mil	D-149	230
	1/16	volts/mil	D-149	200

ANSYS analysis and hand calculations show that the safety factors of most components are far above one. In practice, it is best to make sure that each structural component will be able to handle the stresses from varying sources--for example, stage separation and aerodynamic forces. The epoxy analysis compares the applied stresses to the allowable stresses to calculate a safety factor for each epoxied component. In this case, this MSAT MQP team concluded that the airframe will not fail due to the recovery system deployment during launch.

3.4 Fin Bracket Mounting System Analysis

The fin mounting system (shown in Figure 13) includes of a series of brackets which affix the fins to the motor section. Each fin is attached to four brackets which are fixed to the rocket body with bolts that driven through the airframe. It is important that the fin brackets be able to withstand the forces of transport and launch, as a loss of a fin would result in an imminent launch failure.

The analysis of the fin bracket mounting system was conducted using ANSYS Static Structural. The bracket system was ported into ANSYS and subjected to a 100 N force applied to the side of the fin. 100 N was chosen because it is well above the expected aerodynamic forces. This overestimation increased the MSAT team's confidence that the brackets would not fail in flight. Figure 30 shows the model that was imported into ANSYS:

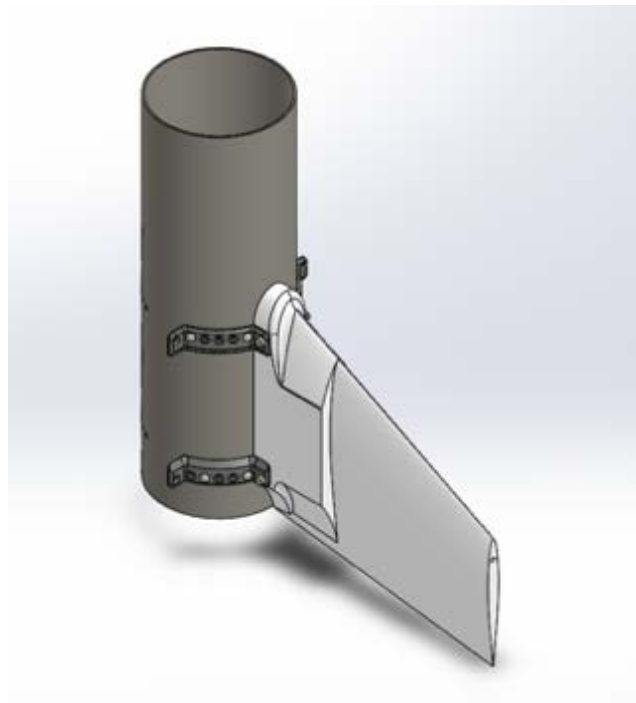


Figure 30. Fin bracket system modeled in SolidWorks.

The post processing of ANSYS simulations consisted of evaluating the equivalent stress and safety factors over the mesh of the bracket. As with the bulkheads and body tube analysis, a safety factor of one or greater was required to qualify the brackets for the expected forces.

Figure 31 shows the results of the bracket with a 100 N force applied to the side of the fin with a focus on the area of concern. The area of concern is the orange highlighted section on the left bracket, which is where a bolt attaches to the fin. A suggestion was made to the mechanical sub-team to thicken the material at the area of concern. Figure 32 shows the repeated analysis with

the improved bracket models. The increased safety factor clearly indicates the increased strength of the part.

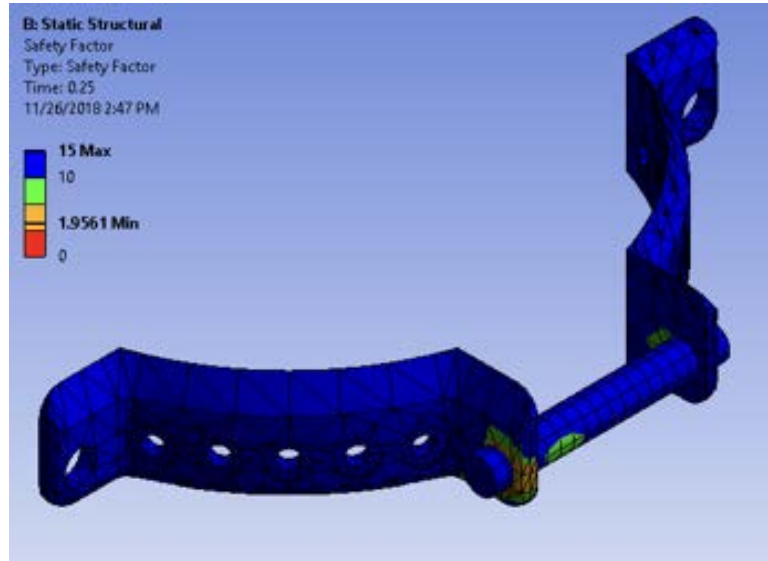


Figure 31. Safety factors of area of concern 1.

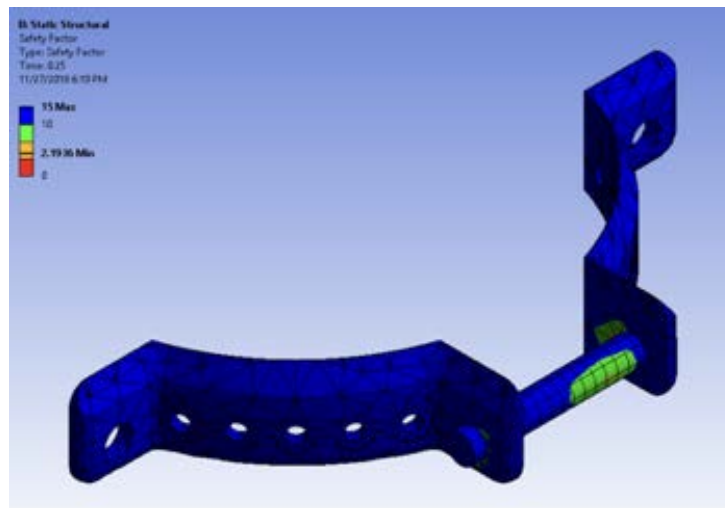


Figure 32. Safety factors of area of concern 1 update.

A second area of concern was found on the side of the bracket which attaches to the body tube. As discussed in Chapter 2, some of the brackets contained only a single bolt to connect it to the side of the motor bay. In this case, the stress on the bracket is greatly increased around the single mounting point. Simulations of this bracket returned a safety factor of only 1.3, much lower than with other brackets (see Figure 33).

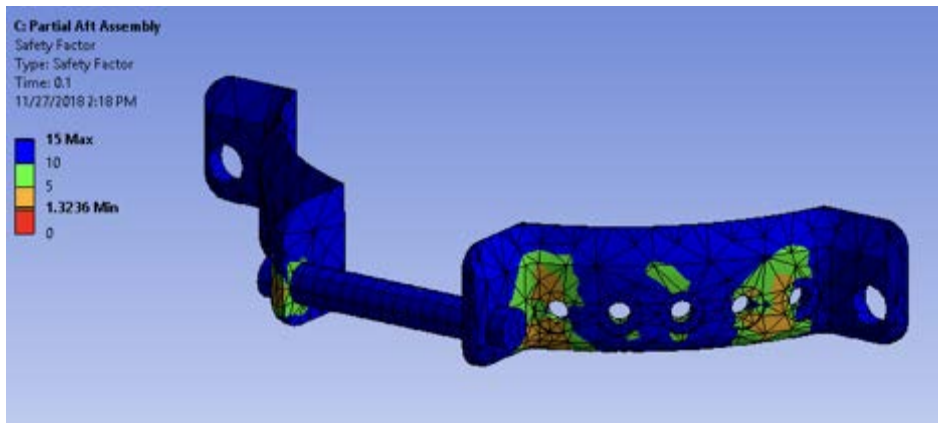


Figure 33. Safety factors of area of concern 2.

After discussion with the mechanical sub-team, the problem was addressed by filling the unused holes with epoxy, as well as using epoxy to attach the bracket to the body tube. This configuration provides a better distribution of stress along the bracket. Figure 34 shows the stresses with the bracket being epoxied to the body tube.

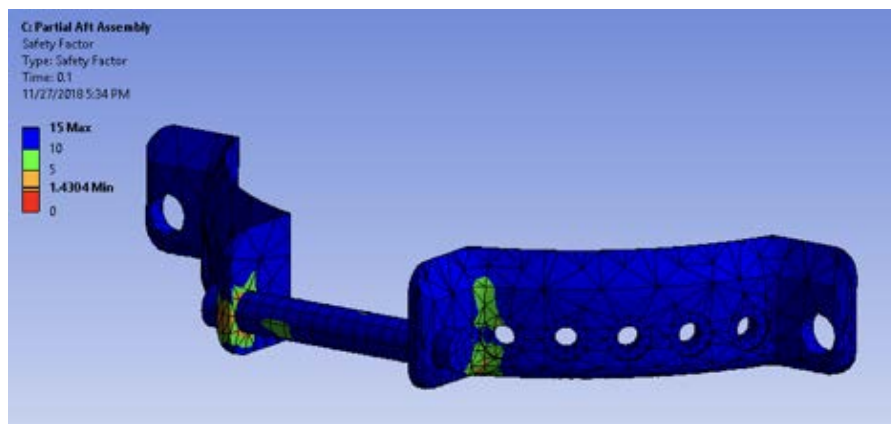


Figure 34. Safety factors of area of concern 2 update.

Upon review of the ANSYS simulation, the MSAT team determined that the fin brackets were structurally sound and could sustain large aerodynamics loads during the extent of the flight.

3.5 Design and Implementation of Strain Gauge System

To corroborate the loads predicted by the analysis of the bulkheads and body tube, the MSAT team employed the use of a strain gauge system. Based on the predicted strain values, strain gauges

were acquired from Micro-Measurements with a gauge factor of approximately 2.1. The details of the strain gauges are shown in Figure 35.



Figure 35. Strain gauge information. 2019.

The MQP team designed a system that employed the use of three strain gauges: one to be placed in the center of the bulkhead separating the electronics bay from the payload bay; two to be placed on the payload bay body tube--one facing longitudinally, and one facing laterally. (See Figure 36, Figure 37, and Figure 38 for strain gauge placement.)

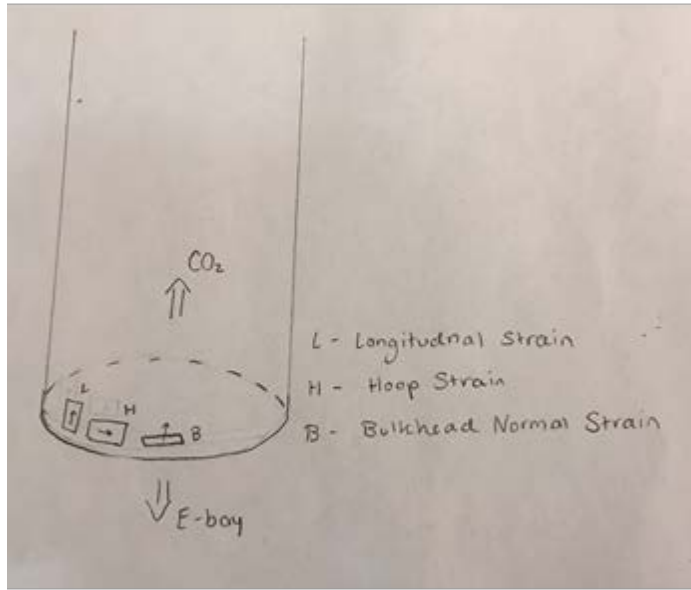


Figure 36. Concept of strain gauge placement in motor bay of the HPMR.

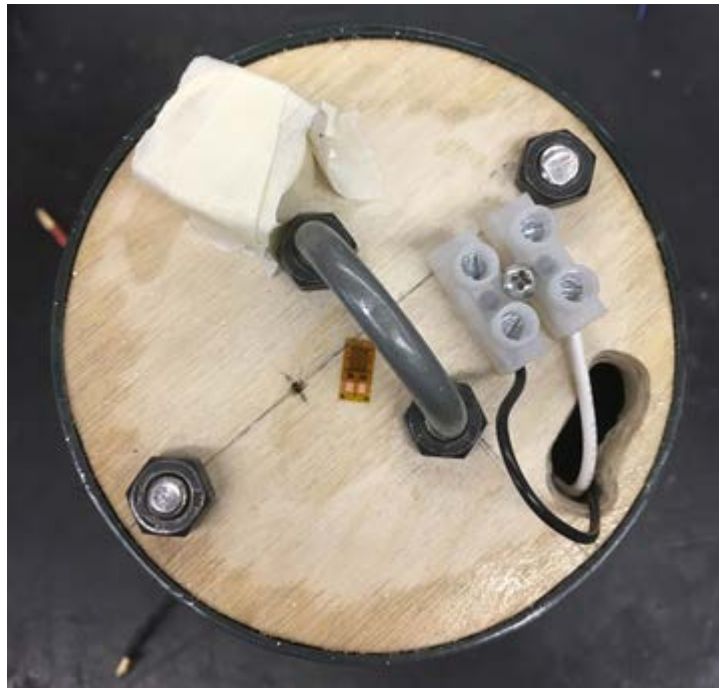


Figure 37. Actual placement of strain gauge on bulkhead of HPMR.



Figure 38. Actual placement of longitudinal strain gauge on the HPMR.

The circuitry for this strain gauge was based around the INA125, an instrumentation amplifier from Texas Instruments. This integrated circuit receives input from both sides of a Wheatstone bridge, and amplifies it to a value between zero and five volts, the output voltage of the Arduino. An onboard voltage reference was necessary for the amplifier to operate with a single polarity power supply, versus a dual polarity supply common in most strain gauge applications. The MQP team also used an extra strain gauge mounted on a scrap of wood to test the amplifier circuit. This allowed the strain gauge to be manipulated by hand without causing damage to the strain gauges

in the rocket. This testing block is shown in Figure 41. Figures Figure 39 and Figure 40 show the circuit diagrams for the INA125.

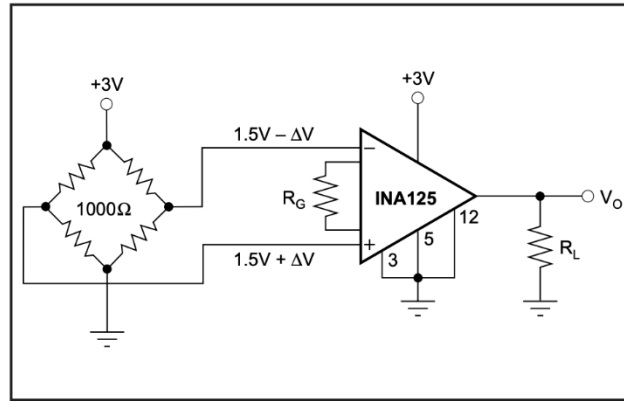


Figure 39. Single supply bridge amplifier. © 1997 Burr-Brown Corporation.

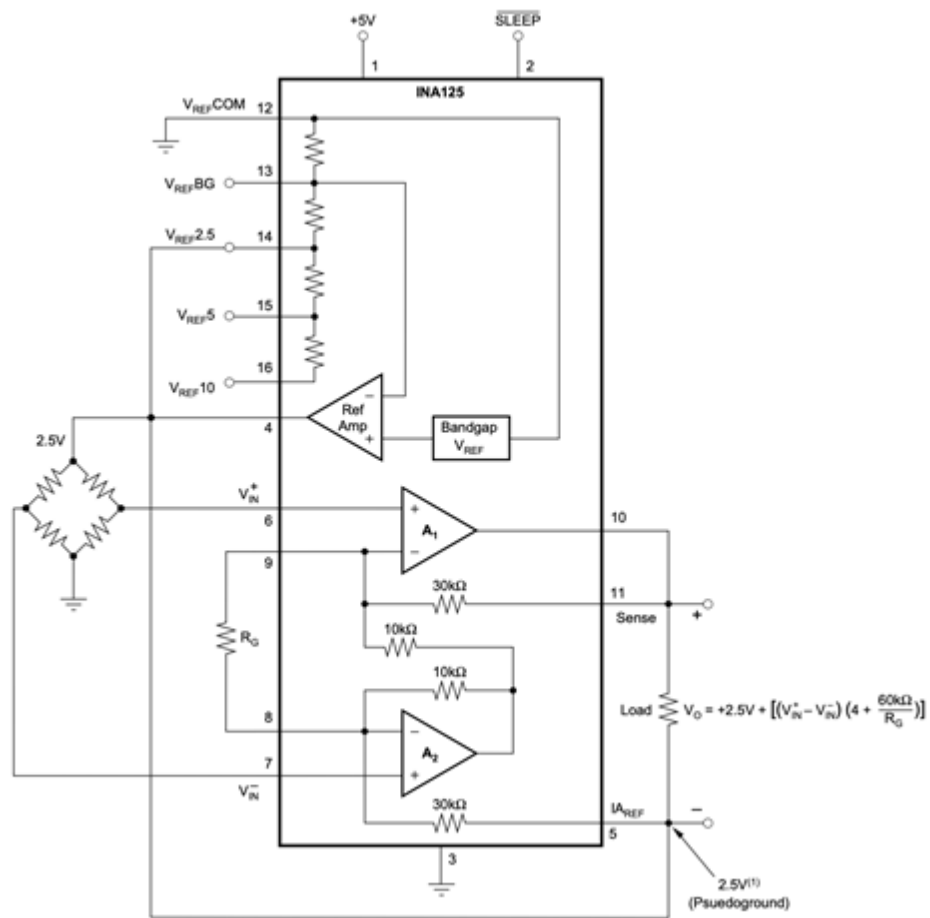


Figure 40. Pseudoground bridge measurement, 5V single supply. ©

1997 Burr-Brown Corporation.

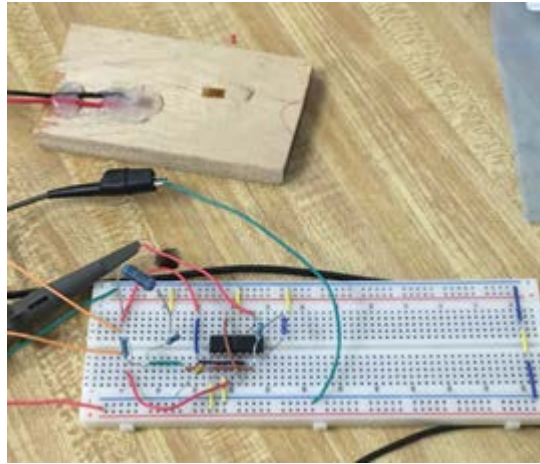


Figure 41. Amplifier circuit on prototyping board. (c) 2019.

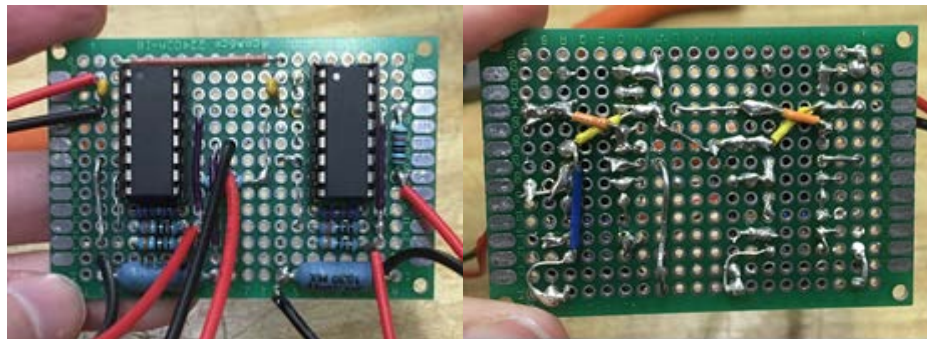


Figure 42. Partially complete amplifier circuit on perfboard. © 2019.

3.5.1 Code

The computer code to operate the strain gage system was delegated to the FDC team. This allowed the team to more effectively integrate the strain gauge measurements with the code they were developing for the HPMR control systems.

3.5.2 Physical Integration

MSAT team worked with the FDC team to integrate the strain gauge circuitry into the electronics bay. The strain gauges were wired to the processor via the ribbon cable connecting the IMU to the Arduino (see Figure 43).

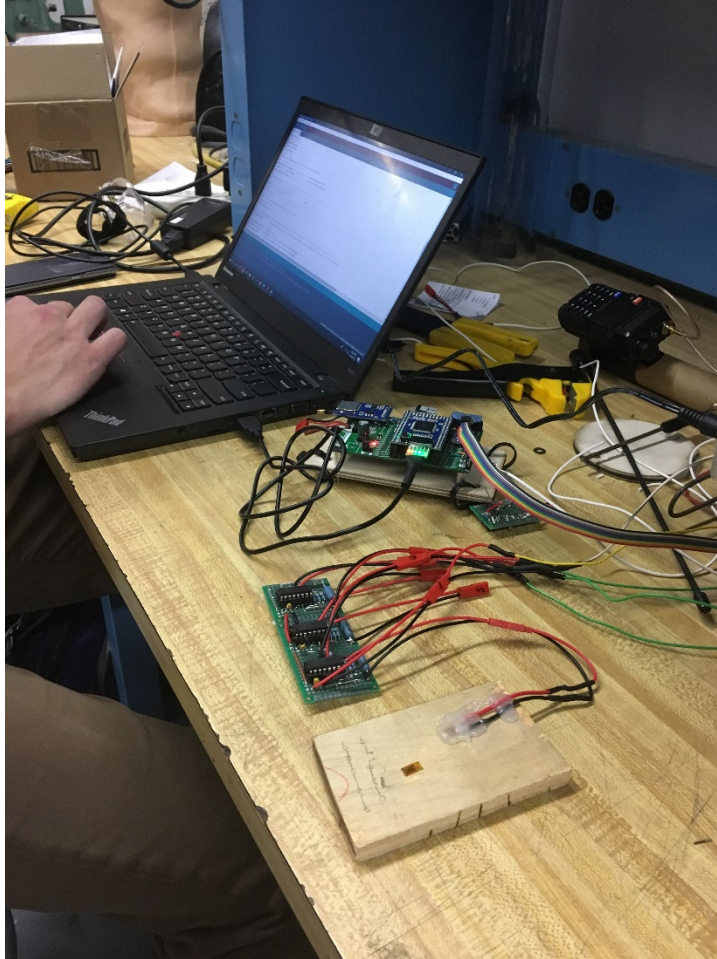


Figure 43. Testing of strain gauge integration with processor.

4 Aerodynamic Analysis

This section presents the aerodynamic analysis that was performed by the MSAT Aerodynamic sub-team. These team members performed computational fluid dynamics (CFD) analysis using ANSYS Fluent and SimScale, and simulated the HPMR trajectory using the open source OpenRocket software. This chapter also presents the possible wind disturbances surrounding the HPMR on the day of flight.

4.1 Drag Coefficient Evaluation

The primary goal of the aerodynamic analysis was to predict the coefficient of drag that the HPMR would experience during flight. This was achieved first performing analytical calculations and supplemented two separate CFD analyses. Comparisons were made between the three methods. Aerodynamics results were also provided to the FDC MQP team for further analysis.

4.1.1 Analytical Calculations

One of the most important tasks regarding aerodynamic stability was the determination of the drag coefficient of the rocket in flight, using both analytical calculations and CFD software. The calculated coefficient of drag could then be delivered to the FDC Team, for use in their MATLAB simulation of the expected HPMR trajectory. First, the team estimated the drag coefficient analytically as a function of airspeed. This calculation is based on equations shown in Table 3.

Table 3. Equations for estimating drag coefficients on a slender rocket body. (Cannon, 2004)

Component	Value	Symbols
$C_{D_{Total}}$	$C_{D_N} + C_{D_{BT}} + C_{D_B}$ $+ C_{D_F} + C_{D_L} + C_{D_I}$	A_{BT} = cross-sectional area of body tube, m^2 A_{LL} = cross-sectional area of launch Lug, m^2 C_{Ave} = average fin chord, m C_R = root fin chord, m C_{D_B} = base drag coefficient, dimensionless $C_{D_{BT}}$ = body tube drag coefficient, dimensionless C_{D_F} = fin drag coefficient, dimensionless C_{D_I} = interference drag coefficient, dimensionless C_{D_L} = launch lug drag coefficient, dimensionless C_{D_N} = nose drag coefficient, dimensionless C_F = skin-friction coefficient, dimensionless S_{BN} = wetted surface area of body and nose, m^2 S_F = wetted surface area of fins, m^2 S_{LL} = wetted surface area of launch lug, m^2 d = body diameter, m L = length of body and nose, m n = number of fins, dimensionless t = fin thickness, m v = velocity, m/s Δy = boundary layer thickness, m μ = viscosity, m^2/s ρ = air density, kg/m^3
$C_{D_N} + C_{D_{BT}}$	$1.02 C_F \left(1 + \frac{1.5}{(L/d)^{3/2}} \right) \frac{S_{BT}}{A_{BT}}$	
C_{D_B}	$\frac{0.029}{\sqrt{C_{D_N} + C_{D_{BT}}}}$	
C_{D_F}	$2 C_F \left(1 + 2 \frac{t}{c_{Ave}} \right) \frac{S_F}{A_{BT}}$	
C_{D_L}	$\frac{1.2 A_{LL} + 0.0045 S_{LL}}{S_{BT}}$	
C_{D_I}	$C_F \left(1 + 2 \frac{t}{c_{Ave}} \right) \frac{c_R}{S_{BT}} dn$	
C_F	$\frac{2\mu}{\rho v \Delta y}$	

It's important to note that in Table 1, C_{D_I} represents the launch lug drag coefficient. This value accounts for the drag caused by the launch lugs and any other externally mounted features. For the team's purposes, C_{D_I} included both the area of the launch lug and the area of the external camera housing. This is an important nuance to note, because the CFD analyses include only the slender HPMR body, as the smaller external components would be very computationally time consuming to mesh. Using analytical methods, the MSAT MQP team determined drag coefficient of the HPMR to be 150 m/s is 0.433. The spreadsheet automating this process is shown in Table 4.

Table 4. Analytical calculations of coefficient of drag

A_BT (m^2)	0.008	C_F	0.000322	C_DI	6.26807E-05	C_D_total	0.433221
A_LL (m^2)	0	$(2 \cdot \mu) / (\rho \cdot v \cdot \Delta y)$		C_DL	0		
C_Ave (m)	0.1397			C_DF	0.208796182		
C_R (m)	0.1778			C_DN + C_DBT	0.020170809		
S_BN (m^2)**	1.997			C_DB	0.204190881		
S_BT (m^2)	0.482						
S_F (m^2)**	1.9975						
S_LL (m^2)	0						
d (m)	0.1016						
L (m)	1.885696						
n	4						
t (m)	0.0208						
v (m/s)	150						
delta_y (m)	0.0005						
mu (m^2/s)	1.48E-05						
rho (kg/m^3)	1.225						

4.1.2 OpenRocket Analysis

After the analytical calculation was completed, the team examined the HPMR using OpenRocket, an open source software that allows the user to quickly simulate the performance of an approximated HPMR. Inputs that can be specified include individual component geometry and mass, as well as the motor configuration. The input geometry is shown in Figure 43.

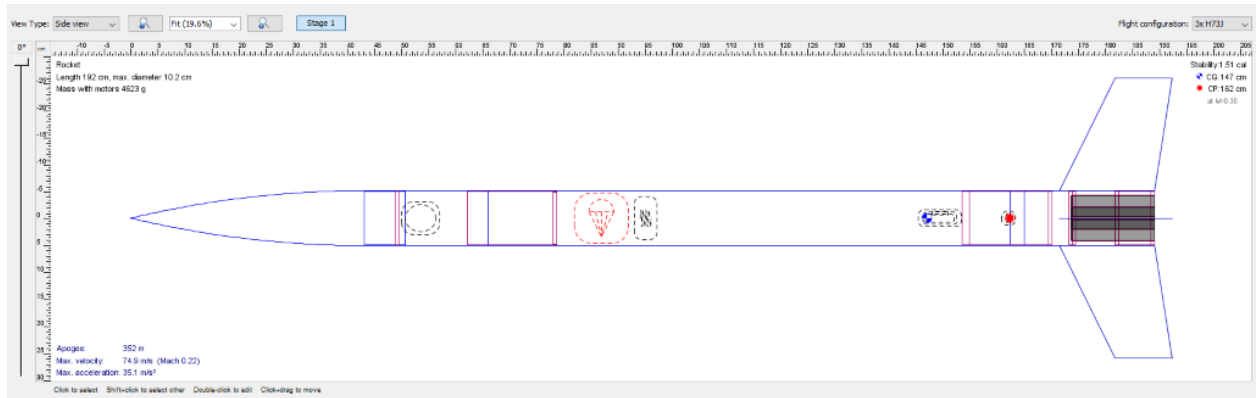


Figure 43. OpenRocket Simulation of Full HPMR Body

The team used OpenRocket to confirm the results of the analytical calculations, as well as to create preliminary estimates of predicted apogee, the velocity over the full flight, and the lateral distance traveled during launch and recovery.

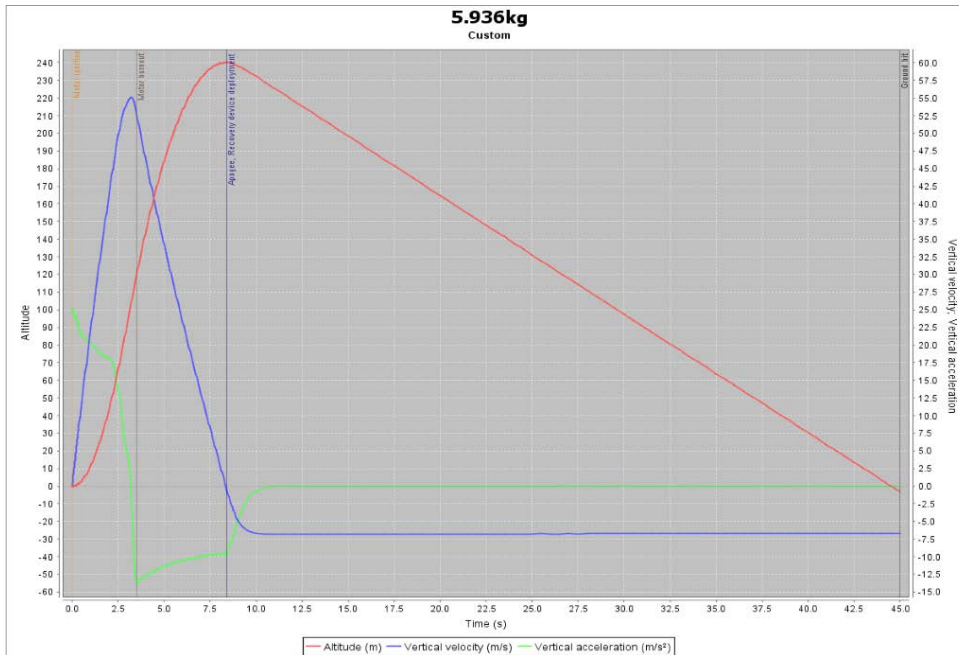


Figure 44. OpenRocket Simulation Results Plotted

To be cleared for flight on the day of launch, the range safety officer at the launch site requires an OpenRocket simulation similar, the results in Figure 44, to confirm that the HPMR has adequate aerodynamic stability and sufficient acceleration for a safe takeoff.

4.1.3 Fluent Analysis

In conjunction with the analytical calculations and OpenRocket simulations, the team performed CFD analysis of the defeatured slender HPMR body using ANSYS Fluent.

The Fluent analysis was an iterative process that involved creating a model in ANSYS to be simulated in Fluent. The simulated model excluded the fins and external camera housing units. The external features were excluded because they would not have made a significant difference to the results for the coefficient of drag. Furthermore, these features would have greatly added to the computational time and power needed to complete the simulations. The sub-team spent much of its time optimizing the mesh design to reduce computation time.

Fluent allows users to create multiple mesh boundaries, each with varying cell size. This allows for a highly detailed mesh to remain near the boundary layer of the HPMR, while a region of much larger cells further from the area of interest reduces the overall cell count in the simulation. In all iterations, the team created a fine mesh in a small boundary closely surrounding the HPMR body, while a larger mesh extended outward to cover a larger area representing the fluid flow.

The first design of the simulation included a large fluid flow boundary, and a small mesh boundary surrounding the HPMR body. This model included the entire HPMR body and excluded all external features. An image of this model is shown in Figure 44 with a face of the larger boundary hidden so that the inner boundary and HPMR is visible.

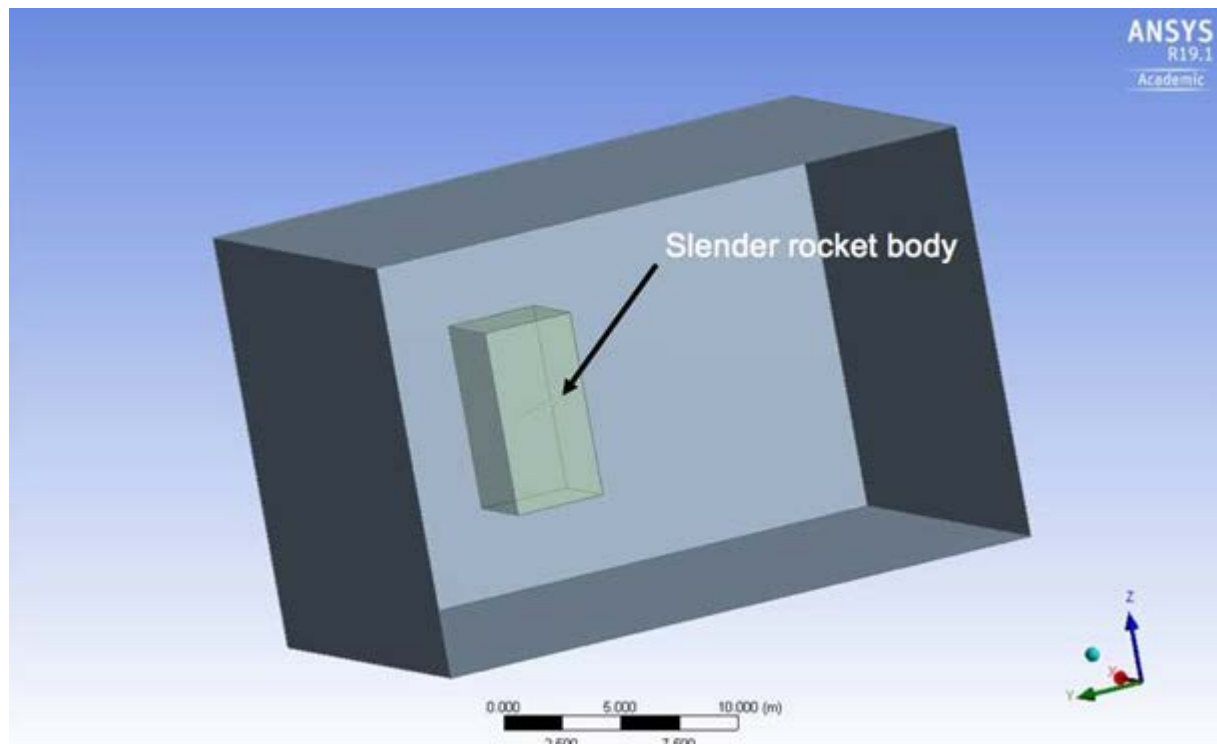


Figure 44. First ANSYS model of slender HPMR.

A closer image of the slender HPMR body is shown in Figure 45 to give a better understanding of the size of the fluid flow boundary compared to the actual object of analysis.

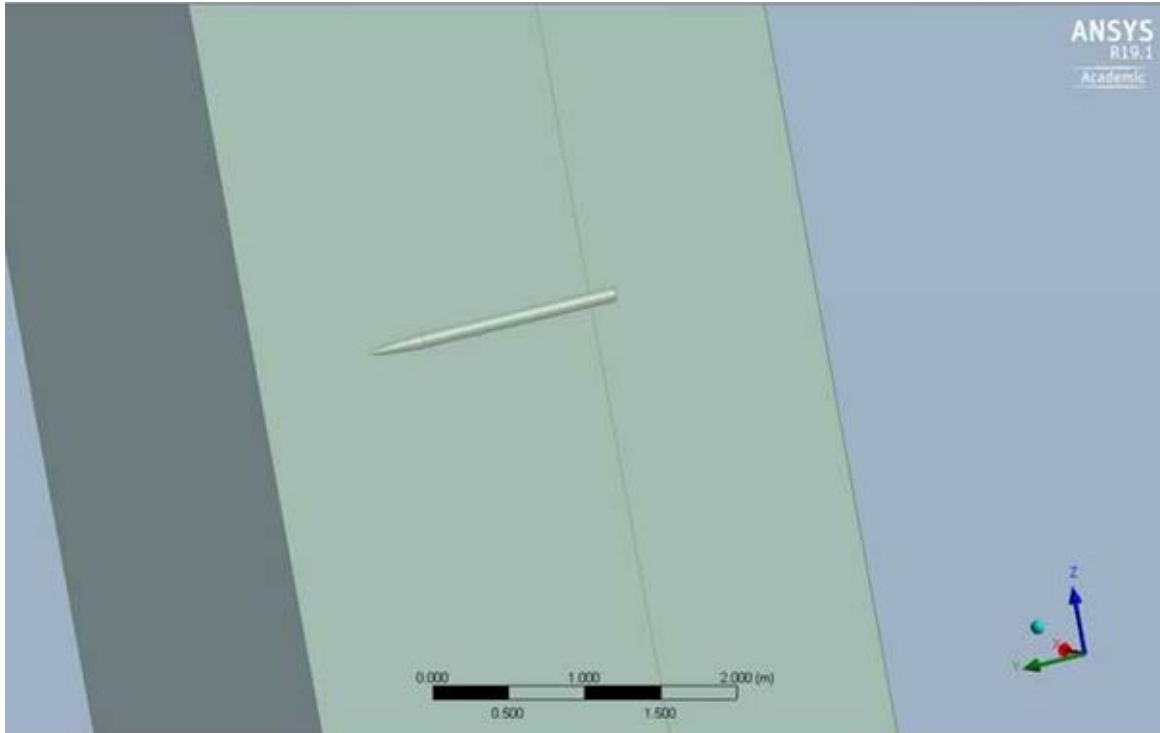


Figure 45. Close-up view of slender HPMR in ANSYS.

Because the model was so large in fluid flow size, it was very troublesome to mesh, and the sub-team did not make it to the meshing stage with this geometry. It was decided that a smaller fluid flow boundary would be more reasonable to complete for the purposes of this project.

Figure 46 depicts the second iteration of the simulation model.

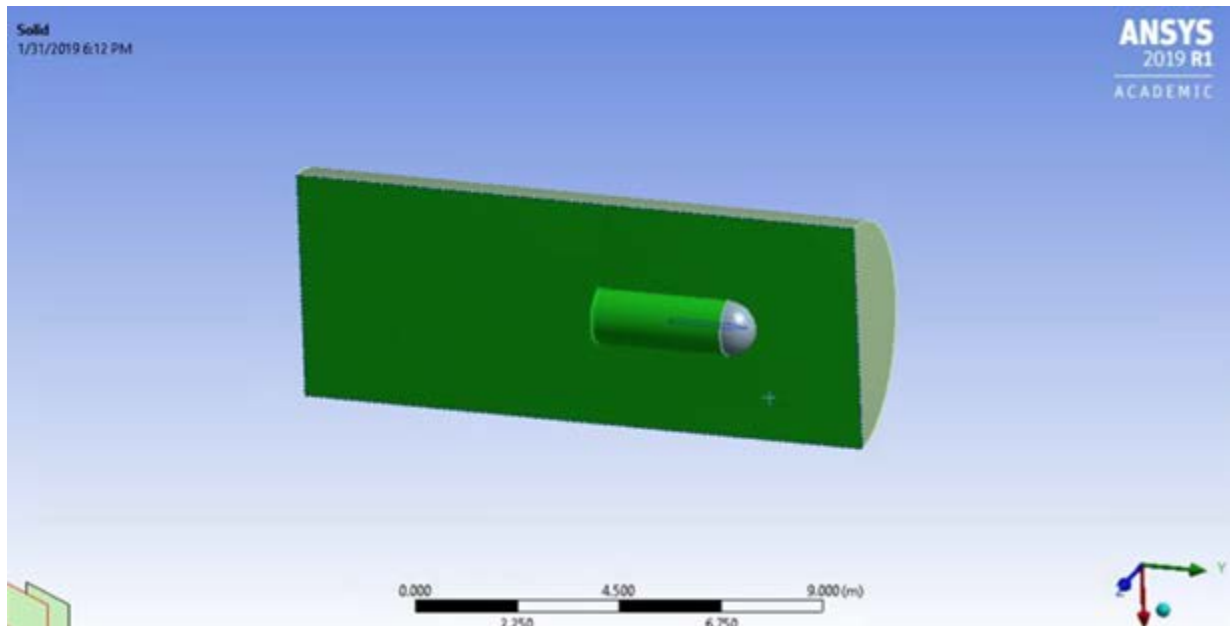


Figure 46. Second ANSYS model; two mesh boundaries.

The MSAT MQP team made multiple changes between the first and second boundaries. The fluid flow boundary is much smaller than the previous version, and only half of the HPMR is used due to its vertical symmetry. This made for a simpler model; and the mesh was completed in this iteration as shown in Figure 47.

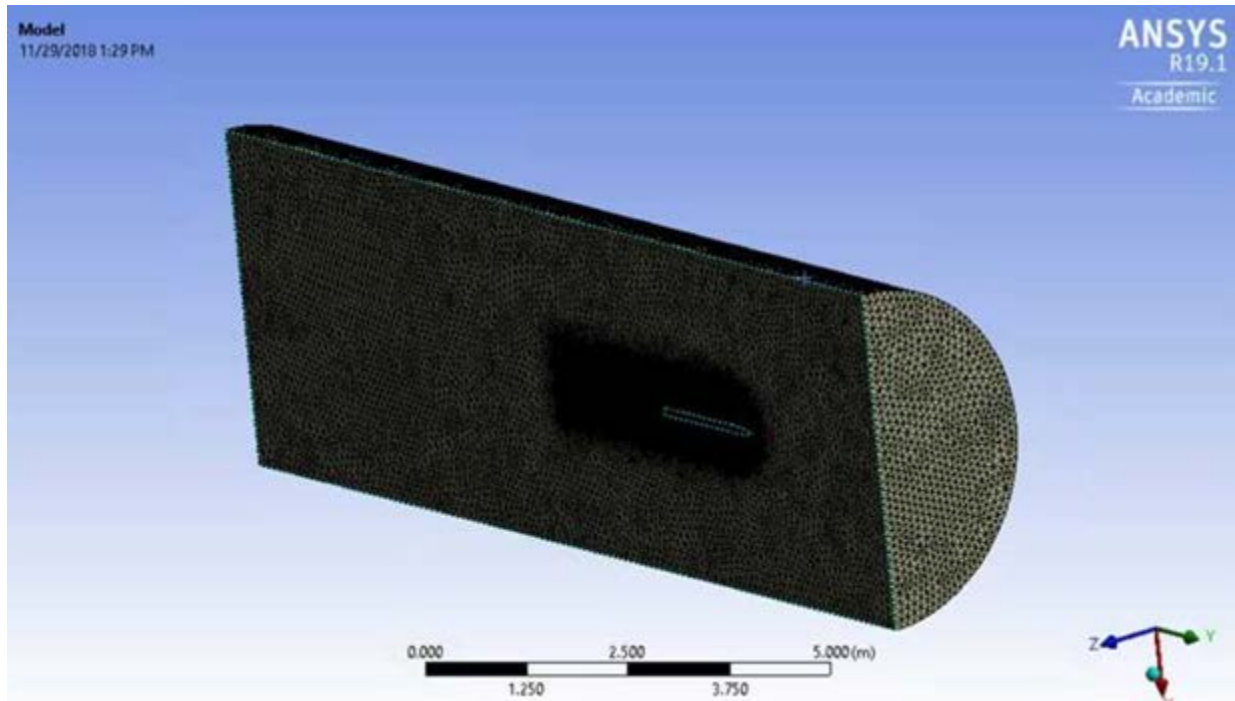


Figure 47. Mesh of second ANSYS model.

Although this configuration allowed for a reasonable mesh, the sub-team decided that a more precise configuration could be created without adding too much complexity to the model. This would still allow it to be realistically completed within the project timeframe. A third, mid-size mesh boundary was added to the model (see Figure 48).

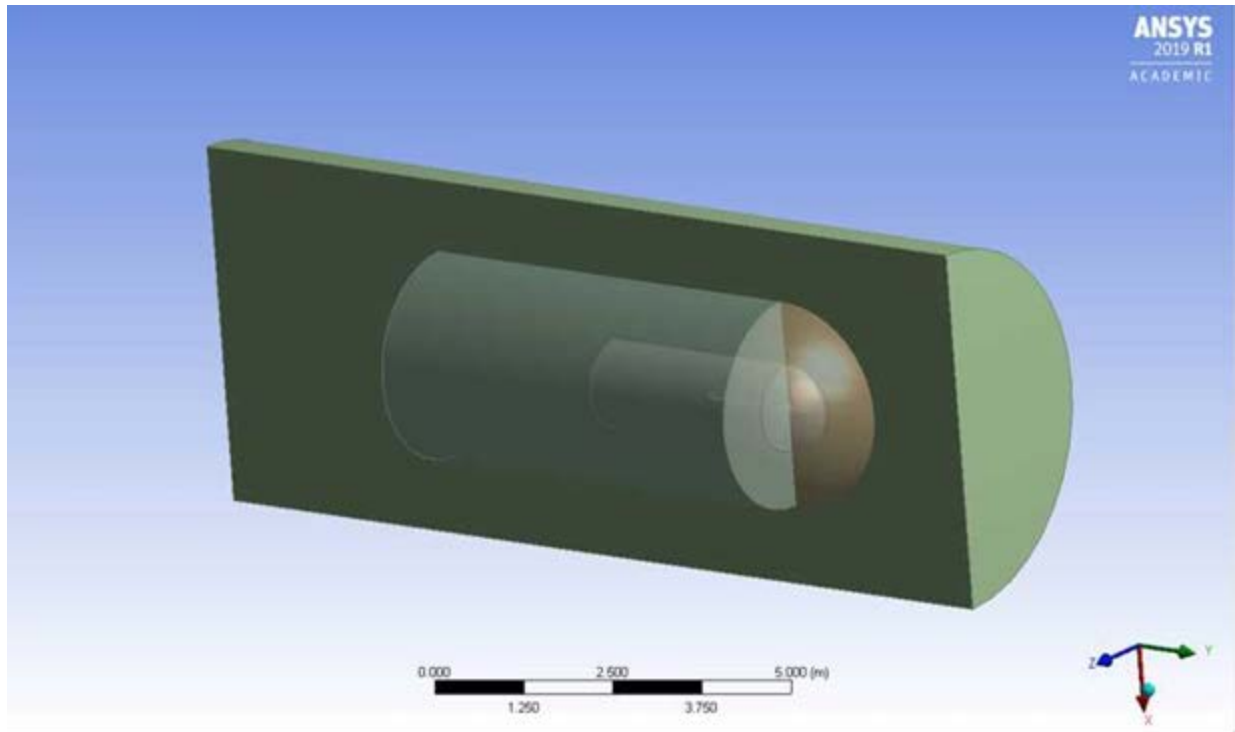


Figure 48. Third ANSYS model; three mesh boundaries.

This iteration of the simulation model was used to obtain values for the coefficient of drag of the HPMR during flight. Adding the third, mid-sized boundary while keeping only half of the HPMR allowed for a smooth mesh and reasonable computational time. In the final version of the ANSYS model, the largest boundary contained an element size of 0.3 meters; the medium body contained an element size of 0.1 meters; and the small body contained an element size of 0.002 meters. The final meshed model represented in Fluent is shown in Figure 49.

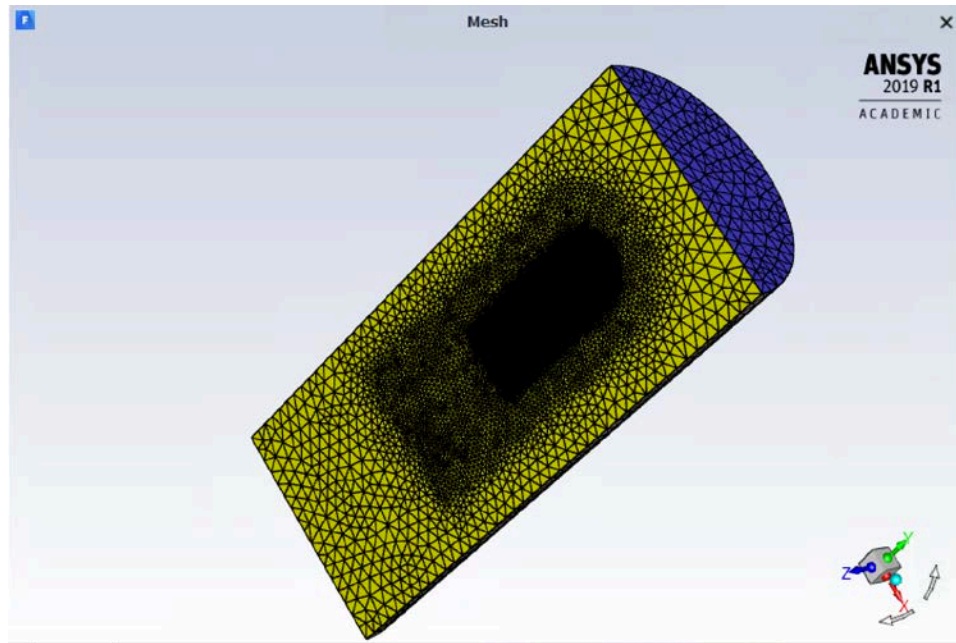


Figure 49. ANSYS model shown in fluent results window.

4.1.4 Fluent Results

The results of the Fluent analysis are shown in Appendix F, for velocities ranging from 100-150 m/s at intervals of 10 m/s. This encompasses the graphs of coefficient of drag and scaled residuals, as well as contours of pressure and velocity. Iterations were computed until the coefficient of drag graphs stabilized.

The images in Appendix F show that C_d and speed are inversely related; the general trend of the C_d is to decrease as speed increases. In addition, the contours show that static pressure on the HPMR is the highest at the tip of the nosecone and the very end of the HPMR. The contours of dynamic pressure show that the dynamic pressure of the HPMR is the highest at the area surrounding the nosecone and at the end of the HPMR body. And finally, the velocity contours show that the velocity of the HPMR experiences is highest also at the area surrounding the nosecone and at the side end of the HPMR body.

4.1.5 SimScale Analysis

SimScale has similar functionality to ANSYS but employs a less complex user interface. Difficulties in mesh sizing and boundary inflation were resolved using SimScale. Once generated, the mesh was simulated at multiple velocities to get obtain the drag coefficient.

Initial drag coefficients calculated with Fluent were an order of magnitude larger than the analytical solution. ANSYS' user interface made it difficult to define the direction of the normal force in the drag direction. Unable to resolve this difficulty, the sub-team used a post processing software called ParaView. Switching software allowed for easier manipulation of force vectors. The combination of software allowed for a calculation that was much closer to the analytical solution.

4.1.6 Comparison Between Various Approaches

Although analytical calculations and OpenRocket were the easiest means of determining the HPMR's aerodynamic properties, the results they yield are not as accurate as those that can be obtained through powerful CFD software such as Fluent or SimScale. While Fluent can perform complex tests, it is neither user friendly nor straightforward. Small mistakes can quickly become time-consuming errors. This contrasts SimScale and ParaView, which provided the greatest balance of performance and an accessible user interface.

Fluent has a more complex user interface with more control over individual variables such as mesh sizing, shaping, etc. Although it is computationally powerful, ANSYS is overly complicated for calculating the drag coefficient for the purpose of this MQP. Software with a simplified user interface allowed for a swifter introduction into computational fluid dynamics (CFD) software. Additionally, with the aid of cloud computing, multiple calculations were run simultaneously in SimScale.

ParaView is the preferred method to process CFD solutions. Solutions processed in ANSYS generally took longer to generate, making it difficult to adjust graphical solutions. Similar problems were found in SimScale's solution processor. Post processing software allows for stronger manipulation of

surface forces generated by a velocity field. Although ANSYS provides similar solutions, it does not allow the same control over individual surface polygons.

4.2 Assessment of Wind Disturbance

Aside from analyzing the baseline aerodynamic performance of the HPMR, the team was tasked with determining the wind profile in a topography typical to that of the area that the HPMR would be launched from. The wind profile provided an approximation of average windspeed across the range of altitudes the HPMR would encounter during flight. If the wind speed is not to be assumed to be significantly lower than the vertical velocity of the HPMR, assumptions of symmetric flow around the HPMR would no longer be accurate. An asymmetric wind profile could also threaten the stability of the HPMR. The wind profile is determined from the topography of the surrounding land, as well as the height of the target object and temperature of the profile. The team calculated the wind profile using equation 5 (John & Spyros, 2006).

$$u(z) = u(h_r) * (z * h_r) * P \quad (5)$$

Here, $u(z)$ is the velocity of the wind in meters per second, z is the height of the object, h_r is the reference height in meters, and P is the roughness length defined as the height above ground level where the wind speed theoretically should be zero. In general, the more pronounced the roughness of the earth's surface, the slower the wind in that area, and the smaller the roughness length (Schilter, 2019). A roughness length of 0.143 was assumed for neutral stability conditions, similar to the conditions in the area where the HPMR was launched.

Using this equation, the team used MATLAB to plot the estimated wind profile that the HPMR was expected to encounter during flight. The plot can be seen in Figure 50, and the MATLAB code used to plot the results is available in Appendix G. Figure 51 plots the FDC's estimates of the altitude of the HPMR versus the vertical velocity during flight.

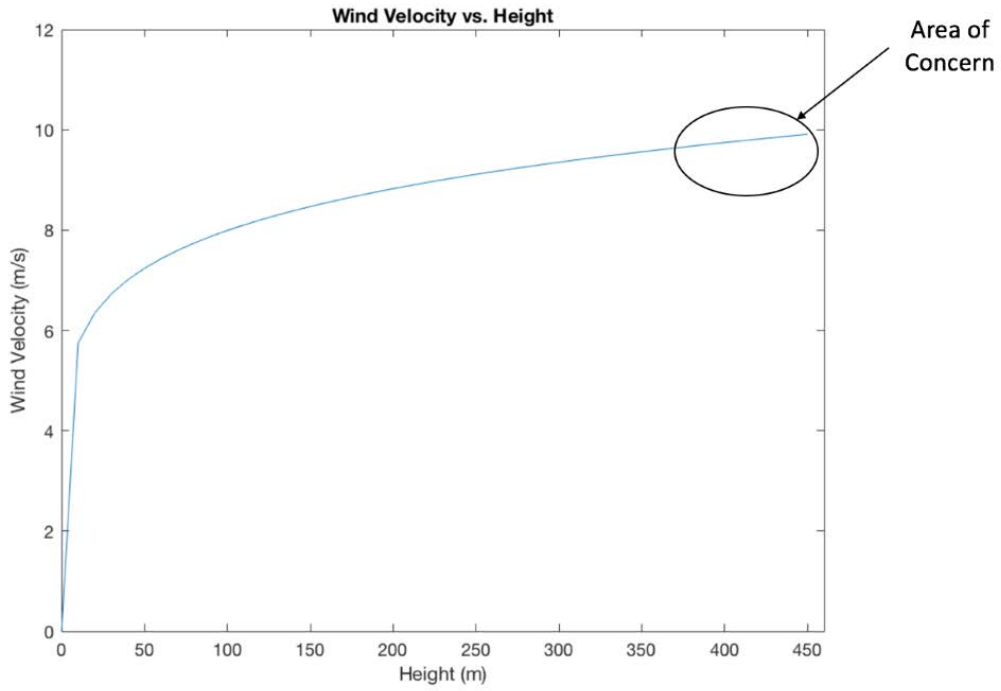


Figure 50. Plot showing the height of the HPMR vs. the predicted wind velocity.

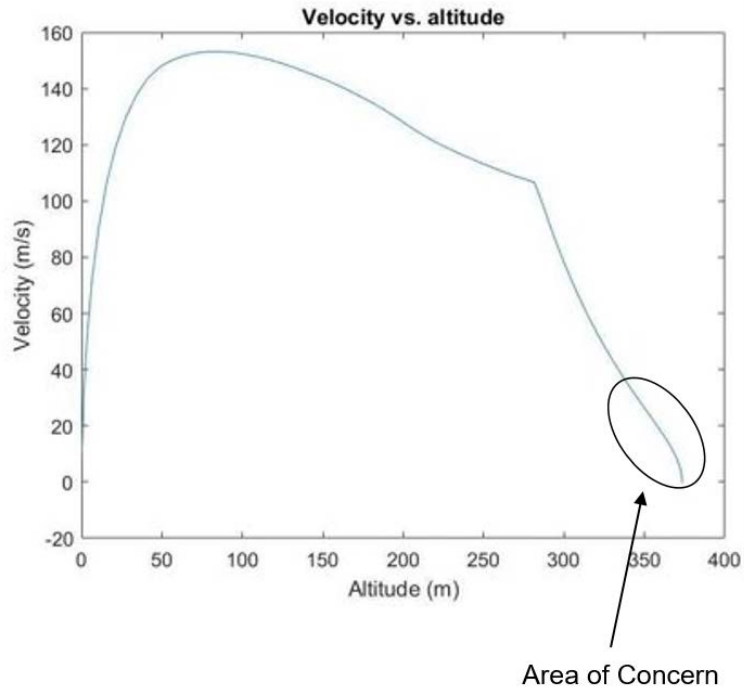


Figure 51. Altitude vs. velocity of the HPMR.

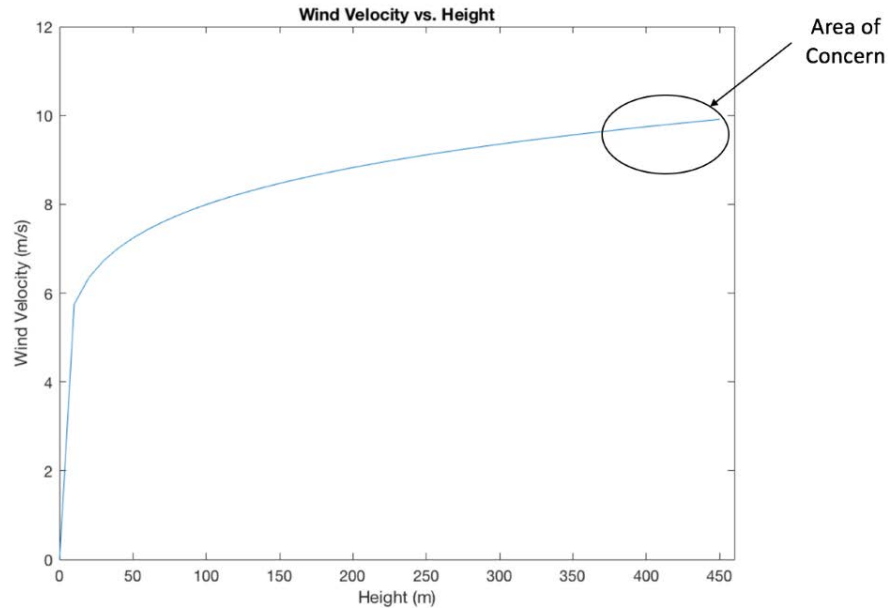


Figure 52. Predicted wind speed vs. altitude of the HPMR.

Each plot shows a potential area of concern near apogee when the surrounding wind speed approaches the speed of the HPMR. The HPMR slows while it approaches apogee, while the wind speed increases with altitude. While the stability of the HPMR at this altitude is in question for this brief period, deviations from simulated values do not affect the overall behavior of the HPMR. Stage separation occurs at apogee, transitioning the HPMR from a stable aerodynamic regime to a descent controlled by a separate recovery system.

4.3 Center of Pressure Calculations

Determining the center of pressure (CP) of the HPMR was essential to ensure stability. The center of pressure is the point through which the sum of all aerodynamic forces acts upon. For the HPMR to be stable, the CP needs to be aft of the center of gravity (C_g). Because the center of mass and center of pressure are separated, aerodynamic forces acting on the center of pressure generate a torque during flight. When the CP is aft of the C_g , this torque corrects the pointing direction to

face along the velocity vector. Figure 53 depicts the aerodynamic forces affecting a rocket body during flight.

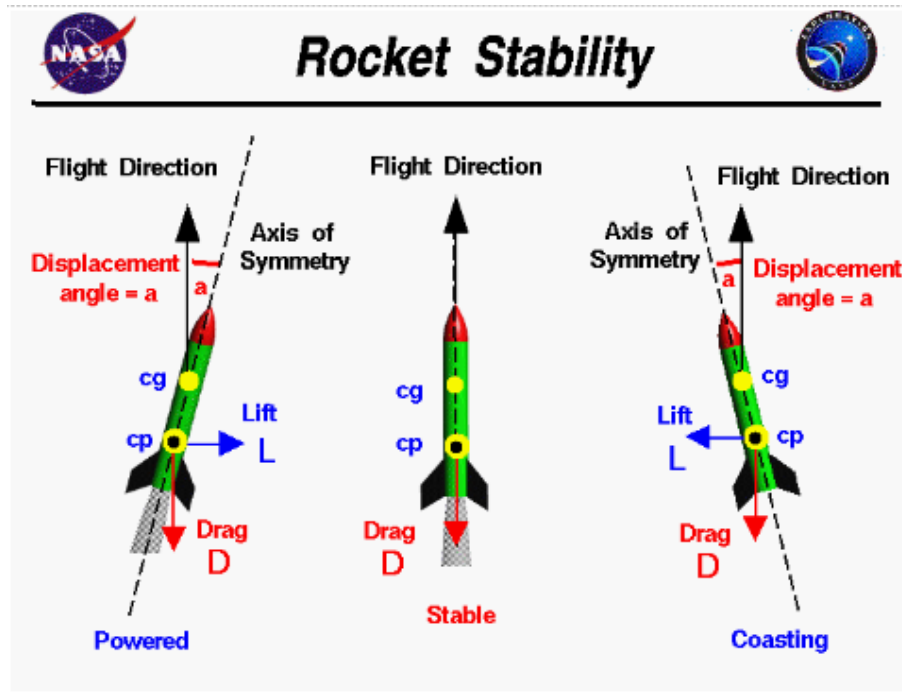


Figure 53. Aerodynamic forces affecting flight stability in model rockets.

To calculate the center of pressure of the HPMR, the team utilized the Barrowman Method, developed by James Barrowman in 1967. This process analytically determines an approximate center of pressure of a rocket. Specifically, the Barrowman Method assumes zero surface drag on the rocket body and considers any stabilizing fins as flat plates. The team determined the center of pressure to lie 1.63 m from the tip of the nosecone. With the center of mass located 1.44 m from the nosecone, the team calculated the HPMR stability to be 1.87 calibers, or 1.87 times the diameter of the main body tube.

To confirm the results of the Barrowman calculations, the team used CP measurements provided automatically in OpenRocket. However, OpenRocket placed the center of pressure much higher than the team had calculated, leading to a stability of 1.53 calibers. This discrepancy could

be due to the different assumptions made with each method. For example, while the Barrowman Method assumes the fins to be flat plates, OpenRocket factors in material thickness.

5 Thermal Analysis

This chapter presents the thermal analysis of the HPMR. The primary focus of the thermal analysis is to evaluate the thermal conduction of the burning fuel in the motor casings to the HPMR body. This analysis was performed using COMSOL, a finite element analysis software package. The results of this analysis served to confirm that the HPMR would be safe from any thermal damage that could be caused by the motors, and to give insight on how the motors interact thermally with the airframe and other body components.

5.1 COMSOL Analysis

The rocket's motor mount consisted of three motors placed radially about the center of the HPMR as shown in Figure 11. Each motor has an aluminum casing approximately 2 millimeters thick. The aluminum casing is friction fit into a Blue Tube segment the same length as the casing. These motor tubes are then aligned using plywood bulkheads which are epoxied Blue Tube motor section and inserted into the motor bay.

The cursory analysis performed by the PSR MQP Team provided a basis for the thermal analysis. It was their assumption that the temperature exposed to the interior of the aluminum motor casing increased linearly from the ambient temperature to the surface temperature of the burning fuel, ammonium perchlorate, as it was consumed over the length of the burn time. This assumption leads to equation 6 relating the temperature at the interior of the aluminum casing with time:

$$T_{casing}(t) = \frac{(T_{2f} - T_{2i}) * t}{t_b} + T_{2i} \quad (6)$$

In this equation T_{2f} is the surface temperature of burning ammonium perchlorate, 1800 K (Powling & Smith, 1965), T_{2i} is standard temperature, and t_b is the burn time, 2.6 seconds (Anon., 2019).

The density, thermal conductivity, and specific heat of the materials that make up the motor bay were needed for the simulation. These materials are aluminum for the motor casings, five-ply plywood for the bulkheads, and vulcanized fiber for the Blue Tube (The properties of aluminum were already included within the COMSOL materials library). A manufacturer data sheet for a commercial version of vulcanized fiber, called Vulcanex, was used as a close approximation for the Blue Tube (Anon., 2019). The physical properties of solid birch (Goss & Miller, n.d.) were used in place of plywood for ease of research.

To begin the simulation, a 3D time dependent study was initialized in COMSOL. A 3D model of the motor bay was imported from SolidWorks. The appropriate properties were then assigned to each material. The temperature function above was placed on the interior wall of each motor casing. This allowed for the temperature to increase linearly with time, reaching a maximum of 1800 K at the end of the burn time. A fine mesh was generated from the geometry of the motor bay. Careful attention was paid to ensure that the element size was smaller than the thickness of the motor casings. The simulation ran for the burn time of 2.6 seconds.

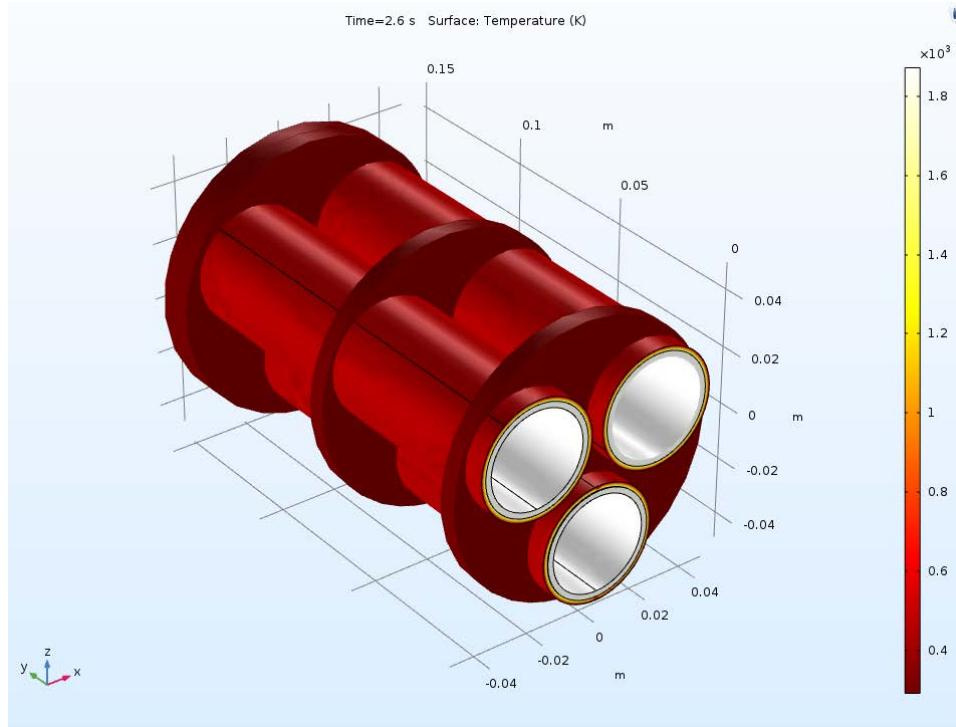


Figure 54. Motor bay thermal conductivity simulation result

Figure 54 depicts the temperature distribution of the motor bay at the end of the burn time of 2.6 seconds. The exterior of the Blue Tube motor tubes and bulkheads did not appear to reach unsafe temperatures. However, according to the simulation, the maximum temperature of 1800°K occurs at the contact point of the fuel and the aluminum casing. Though this temperature seems extremely high and is well above the melting point of the aluminum casing, this is not cause to worry about the integrity of the motor casings.

One possible explanation for the excessive temperature estimates is the simplified nature of the simulation. This simulation assumes that the interior boundary of the aluminum casing is exactly the temperature given by the formula above. In practice, the fuel in the motor would not directly contact the motor casing. While the burning propellant may reach these temperatures, insulating materials in the motor prevent the aluminum casing from reaching dangerously high temperatures. This simulation also excludes heat transfer through convection in air, and only observes

conduction through surface contact. In practice, aluminum motor tube suffers little to no damage on a given launch. Even a severe motor failure, as described in Chapter 7.3, does little to provide significant thermal damage. Despite this, as a “worst case scenario” test, it confirms that the bulkheads and airframe should not experience thermal damage from launch. Though the thermal analysis described was sufficient for the purposes of this MQP, a more accurate simulation would include the calculation of the heat flux provided by the motor and apply that to a more realistic model of the aft section that includes heat conduction through the air. This is an intensive problem, and a more thorough analysis of the HPMR aft section is provided in the PSR MQP team’s report (JB3-1901).

6 Mechanical Integration and Testing Procedures

The purpose of this section is to detail the mechanical integration process that was used to assemble the HPMR before launch, as well as to describe the goals and outcomes of the test launch.

6.1 Mechanical Integration

The following is a break-down of the integration process followed for the first test launch of the HPMR. Refer to Appendix H for the pre-launch check list. The first step in rocket integration occurred before traveling to the launch site. The fins were secured in their brackets before travel. This was done because the bolts holding the fins were very stiff and the team decided that installing the fins earlier to avoid having to do so in the cold environment of the launch would be easier. Upon arrival, the first step was to inspect the HPMR components for damage and ensure that they were flight worthy. This was carried out by each team and sub-team that manufactured each component. After inspection, the e-bay was passed off to the FDC team so that they could integrate the electronics bus, and the motor mount was handed off to the PSR team for motor installation. This step demonstrates the importance of the modularity of the HPMR systems. It allows multiple teams to perform integration steps simultaneously. After the three loaded motors casings were installed in the motor mount, the motor retention system was installed and secured. While the motors were being loaded, the FDC team installed the electronics within the e-bay. Once the electronics were in place, the e-bay was supposed to be sealed with an aft bulkhead. However, the packing of the electronics did not allow for the bulkhead to be mounted properly and the aft of the e-bay was left open. This was not deemed a flight risk because the lower section of the e-bay opened onto the top of the motor section, which was empty at the time of launch.

After the FDC MQP team finished packing the e-bay, they handed the component off to PSR for the installation of the black powder separation charge. The charge and electric match were

loaded into the charge well and secured with tape. At this point, both the e-bay and the motor mount were mated to the motor section. After the two sections were secure, a length of nylon shock cord was passed through the payload bay section. This shock cord was used to mate the recovery system to the forward e-bay bulkhead. The e-bay was then secured to the aft end of the payload bay. The main recovery system was then packed and loaded into the payload bay.

Next, the MSAT MQP team integrated the internally mounted camera. The camera was affixed to the internal mount, and the nosecone, and then lowered into the camera housing. The nosecone parachute was secured to the aft end of the now fully assembled nosecone section, and both were loaded into the forward end of the payload bay and secured by shear pins. The final component attached before launch were the two external side cameras. Both the cameras and their faring were secured to the proper Velcro tabs.

The testing objectives for the mechanical sub-team centered around the quality of the footage from the onboard cameras, the success of the stage separation, and the retention of both the motors and the motor mount sub-section. A full breakdown of the testing criteria can be found in Appendix I. A successful test of the cameras would include the capture of clear footage that lasts for the whole duration of the flight. Though the HPMR failed to leave the launch pad, this criterion was met for each of the three cameras. Every camera returned footage for the entire setup process and remained active even as the motors violently failed. For a detailed analysis of launch failure, see section 7.3.4.

For stage separation, a successful test of the shear pins requires the nosecone to be fully ejected from the main airframe without damaging either component. While the PSR MQP team designed the motor ejection system, the MSAT MQP team was responsible for sizing shear pins to hold the nosecone before separation. This criterion was not tested in-flight due to the launch failure.

However, a ground test was performed in which the upper sections of the HPMR were assembled in the launch configuration and the separation charge was fired. In this test the shear pins functioned nominally and the HPMR separated completely, allowing the parachutes to smoothly exit the tube. The final mechanical test objectives dealt with retaining both the removable motor section, and the motors themselves during flight. Even though there was no flight, the ignition and failure of the motors provided a much more rigorous test of the motor mounting and retention systems than expected during flight. The motor section was retained throughout the motor firing and was determined to have passed the test. The results for the motor retention system were less conclusive. Although all the motors were contained during firing, the aft closures of each motor were blown out as a result of the motor failure. The failure produced significantly more force on the aft closure than anticipated during a nominal launch, suggesting that the retention system would have been successful. Nonetheless, the motors still ejected each aft closure and significantly damaged the retention system. Thus, the actual in-flight performance of the motor retention system remains unknown.

6.2 Structural Testing

The structural sub-team integrated the strain gauge system into the HPMR. As discussed in section 3.6.1, this involved attaching the strain gauges to the inside of the HPMR with CA glue. The team then secured the gauges and wiring with a small amount of hot glue to ensure the gauges remained in place (see Figure 43). The team integrated the circuitry for the strain gauge system on launch day by attaching the circuit board to the main E-bay assembly using Velcro.

The testing criteria for the strain gauge system included whether data was collected, and whether events such as launch, and stage separation could be discerned from the data. However, due to sizing constraints in the e-bay, the team was unable to make the suitable connections

between the circuitry and the gages, thus rendering the strain gage system unusable for the test launch.

Each of the structural components were to be tested during the launch. Table 5 shows a criterion to determine if the components passed or failed during the test flight. The components were to be looked over prior to the launch to check for any damage from transport and then again looked over after the launch to check for any damage. If there was damage to the components during the launch, the component would be assigned with a fail. A pass would be given only if the components sustained no visible damage and remained capable of immediate re-launch if necessary.

Table 5. Criteria of Structural Components

Structural	Fin	Are the fins capable of performing without damage?	Pass:	The fins are undamaged and capable of flying again immediately.
			Fail:	The fins collect damage, fall off, or are unable to fly again.
	Fin Bracket	Are the fin brackets capable of performing without sustaining damage?	Pass:	All eight fin brackets do not break or come detached during flight.
			Fail:	Any of the fin brackets break or come detached during flight.
	Vibrations	Do the attached strain gauges measure and record data correctly?	Pass:	Data was collected, and launch actions (such as stage separation) can be seen within the strain data.
			Fail:	No data collected or the data that was collected is too noise to be useful.
	Body Tube	Does the body tube survive launch? Can the body tube launch again?	Pass:	There are no cracks, dents, divets, bulges, or other structural concerns in the body tube post-launch.
			Fail:	There is any sign of structural concerns or damage to the body tube post-launch.
	Parachute Mounting Bulkheads	Do the bulkheads survive parachute deployment?	Pass:	The bulkhead doesn't break (ready to fly again, no visible damage) or detaches from the rocket body.
			Fail:	The bulkhead breaks (has cracks, movement, or visible damage) or detaches from the rocket body.

6.3 Aerodynamics Testing

Aerodynamic testing was required to confirm these results. The MSAT MQP team intended to use the test flight to perform much of the planned aerodynamic testing. Because a test flight was not successfully completed, the following details the aerodynamic testing that was completed using software.

The MSAT MQP team used simulations in OpenRocket to estimate the margin of stability of the HPMR. As discussed in Chapter 4, OpenRocket can rapidly provide estimates of rocket performance and stability. Furthermore, OpenRocket simulations are often required by the launch

sites during model rocket launches. From the OpenRocket simulation (see Figure 55), the HPMR was determined to be stable, reaching an altitude of approximately 250 m.

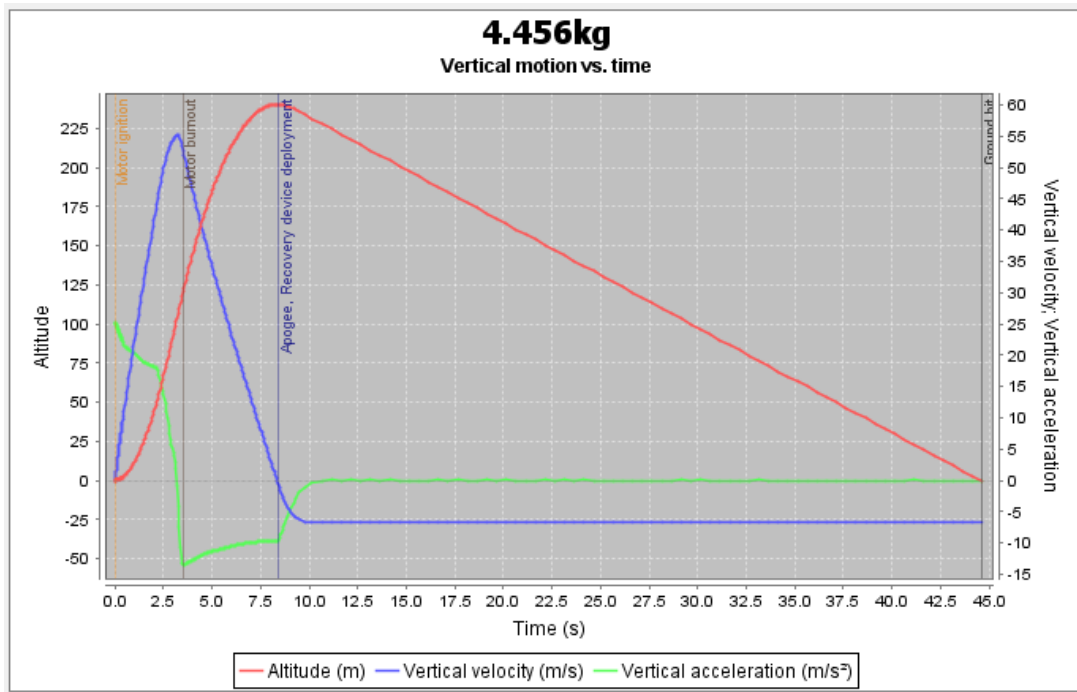


Figure 55. OpenRocket graph showing the altitude, velocity and vertical acceleration of the HPMR during flight.

In addition to the OpenRocket model completed by the MSAT MQP team, the FDC MQP Team completed a flight simulation using MATLAB. This simulation further confirms the stability of the HPMR during flight by predicting its trajectory. Details of this simulation can be found in section 2.4 of the Flight Stability and FDC Team’s final report (MAD-1901), and an image of the team’s simulation results are shown in Figure 56 below.

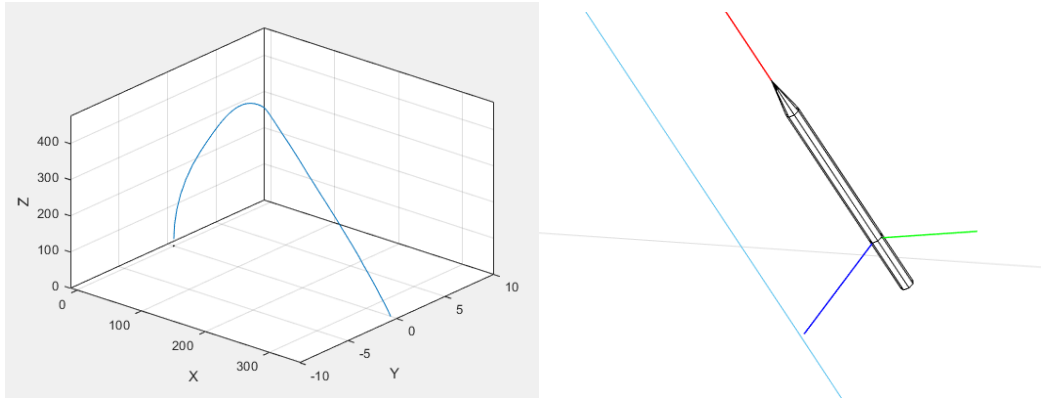


Figure 56. Stationary (left) and Following (right) visualizations of the HPMR's trajectory. (c) 2019 (MAD-1901)

6.4 Thermal Testing

There was no integration performed by the MSAT MQP thermal sub-team regarding the assembly of the HPMR. Integration of the propulsion subsystem was handled by the PSR MQP team. Monitoring the temperature of various subsystems within the HPMR during launch was not feasible, so the testing objectives for the thermal sub-team was primarily a visual analysis of the motor subsection after the HPMR had landed.

The passing criteria required no visible thermal damage on the motor tubes and the aluminum motor casings. The motor tubes passed, with a note that only one of the motors ended up burning due to difficulties experienced at launch. The aluminum motor casings did not pass, however, due to a failure of the O-rings in the motor assembly upon ignition. Each motor is constructed from pieces, or grains, of propellant stacked inside a disposable casing. At either end of the motor, visible in Figure 57, O-rings provided a seal to prevent expanding gasses from escaping and contacting the surface of the casings.

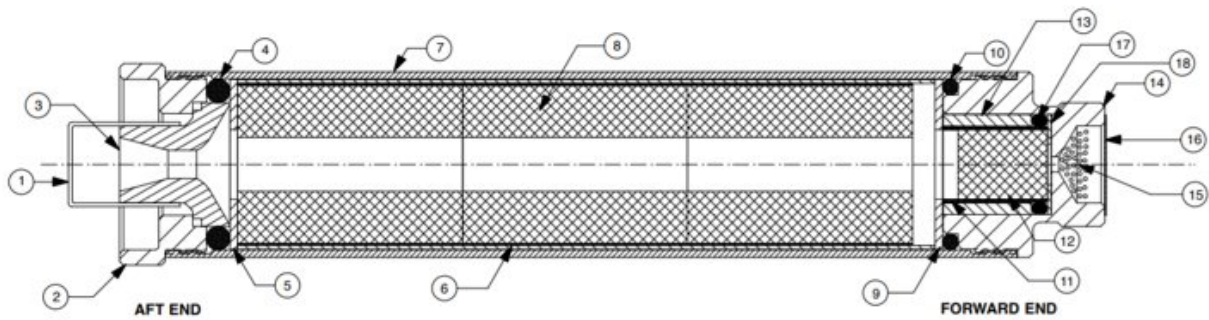


Figure 57. Diagram of the construction of the solid rocket motors (Anon., 2016).

It became apparent through analysis that the hot gas generated by the burning fuel had escaped past the O-ring and out the aft end of the motor casing, causing visible thermal damage to the casing exterior (see

Figure 58). Multiple causes for this failure were considered by the MSAT MQP team. First, it was possible that a lack of lubrication on the O-ring exposed the rubber material to hot gasses without protection from the oily lubricant. This would have caused near-immediate failure of the O-rings, allowing the expanding gasses to heat the aluminum casing and eject the aft closures. It is also possible that the low temperature at the time of launch, approximately 32°F, may have caused the O-rings to shrink and become less flexible. This change in material properties could have similarly allowed the gasses to escape and eject the casings. Further discussion of the possible failure modes is discussed in Chapter 7.2.4.



Figure 58. Aft motor section post-launch.

7 Summary, Conclusions, Recommendations, and Broader Impacts

This chapter presents a summary, conclusions, and recommendations generated through the completion of this MSAT MQP and the HPRM Program overall. The chapter reviews the steps taken throughout the project period and provides recommendations to teams performing future related work. The chapter concludes with a brief discussion covering some of the broader impacts of the HPMR Program.

7.1 Summary

The objectives of the MSAT MQP were to: design, analyze, build, integrate, and test the HPMR which achieves an altitude of 457.2 m (1500 ft); perform structural analysis of the HPMR airframe and bulkheads; perform aerodynamic analysis of the HPMR airframe; perform thermal analysis of the motor mount sub-assembly.

The SEG utilized the following methods to accomplish these objectives: the mechanical components of the HPMR were designed using SolidWorks; the various subsystems from the PSR and FDC teams were integrated first in SolidWorks and physically using bolts and epoxy. The structural analysis was conducted both with hand calculations and with the ANSYS Static Structural package. The aerodynamic analysis was conducted with analytical calculations, ANSYS Fluent and SimScale simulations with post processing in ParaView, and OpenRocket. The thermal analysis was conducted using the COMSOL Physics Modeling package.

Each sub-team of the MSAT MQP team reached results for each respective section of the project. The mechanical design sub-team was successful in designing, constructing and integrating each of the sub-assemblies into the HPMR. The structural sub-team completed each of the analyses of the sub-assemblies of the HPMR but was unsuccessful in integrating the strain gauge system into the HPMR. The aerodynamic sub-team completed modeling the HPMR CFD analysis in both

ANSYS Fluent and SimScale, obtaining coefficient of drag results. The launch failure prevented the sub-team from confirming the simulated results. The thermal sub-team was successful in modeling the temperature gradient of the motor section in COMSOL and analyzed possible causes of the launch failure.

7.2 Conclusions

We provide below conclusions for the mechanical, structural, aerodynamic, and thermal sub-teams.

7.2.1 Mechanical Design and Integration

The greatest takeaway from the mechanical design of the HPMR is the importance of modularity in the rocket design. With each subsection able to be completely separated from the HPMR, separate teams and sub-teams were able to work on construction of different sections simultaneously. Additionally, the separation of each section eased both transport to the launch site and final assembly. The placement of the three cameras also proved advantageous. All three angles provided valuable data in the analysis of the test flight failure. The cameras captured both video and audio that clearly showed the motors igniting and then failing in sequence.

Some shortcomings of the HPMR design and construction were also identified. The position of the rail buttons, originally offset to allow for potential integration of a booster motor, was closer to the fin mount than was desirable. The mounting bolts for the closest fin had to be partially unscrewed to allow for loading onto the launch rail. However, the fact that the fin retaining bolts were force threaded through the plastic fins was not a concern. Also, during construction, the amount of weight of each individual component not given the proper concern to allow for adequate performance. This resulted in a rocket much heavier intended. Even under ideal circumstances, the HPMR would have been unable to meet the originally stated altitude requirement.

7.2.2 Structural Analysis

As discussed in section 6.2, the strain gauge system was unable to be fully integrated during the test launch due to a lack of working space in the e-bay. Because of this, the team was unable to retrieve any test data from the strain gauge system for this launch attempt. Every simulation and analytical calculation returned safety factors greater than 1 for loads equal to or greater than the actual loads expected throughout the flight of the HPMR. Since the HPMR failed to launch, some testing criteria results remained inconclusive. However, the parachute mounting bulkheads and body tube successfully survived payload deployment during the launch day ground test.

7.2.3 Aerodynamic Analysis

Because aerodynamic testing and simulation has been relatively sparse and inconsistent in past MQPs related to model rockets, the aerodynamics team did not have significant background information to choose from when considering what sort of applications would be useful in the context of the MQP. The aerodynamics team decided to move forward with CFD simulations through FLUENT, without knowledge of ANSYS applications before the start of the project. While FLUENT is an incredibly powerful tool used for CFD simulations in large projects across the aerospace industry, it was difficult to learn and apply to a project in the timeframe of this MQP. In hindsight, it would have proven valuable for the aerodynamic sub-team to perform more thorough research into different CFD tools before relying on FLUENT as the only option for the analysis.

7.2.4 Thermal Analysis

The test launch was unsuccessful due to failure of the rubber O-rings in the motor caps. The purpose of these O-rings is to keep the hot pressurized gas generated by the burning fuel from escaping out of the top of the motor casings. There are three potential modes of failure: extrusion

caused by exposure to high temperature; shrinkage caused by exposure to low temperature and a lack of contact medium (lubricant); or a lack of pressure on the O-ring from the motor cap. Extrusion is unlikely, as the O-rings are designed to operate in contact with the pressurized gas, and it is unlikely for this mode of failure to occur with all three O-rings. The temperature at the launch site had a low of 24° F, and a lubricant had not been applied to the O-rings prior to launch. A contact medium--such as a lubricant--acts as a plasticizer, counteracting shrinkage and hardness that can occur with exposure to cold temperatures. It also reduces surface friction and makes it easier for the O-ring to seat itself. Therefore, the most likely scenario is that the O-rings failed due to a combination of lack of lubrication and exposure to cold temperature for a prolonged period. (Parker Hannifin, 2018).

7.3 Recommendations for Future Work

The MSAT MQP team has the following recommendations for future teams pursuing projects similar to the present work.

- Greater consideration of the overall HPMR weight will benefit the success of the project. In addition, a lighter rocket will enable a greater range of choices for motor selection.
- Design with modularity in mind can increase ease of assembly and preparation for launch. With multiple MQP teams working on systems on a single rocket, the separation of each system before assembly allows launch procedure steps to be completed concurrently.
- It is recommended that future teams do not rely on FLUENT as the primary analysis program unless team members have advanced competency in CFD.

- It is recommend that basic model rocketry software such as OpenRocket should be used early on as it provides a reasonably accurate estimate of basic aerodynamic stability.
- When constructing the rocket motors, care should be taken during assembly and storage to ensure the O-rings in the motor caps are under ideal conditions during launch.

7.4 HPRM Project and its Broader Impacts

The MSAT MQP team was one of three teams that constituted the HPMR Program with goal to design and test the HPMR. However, model rocketry in general has broad economic, environmental, and social impacts on society. On this section we address some of these broader impacts and summarize how model rocketry contributes to society beyond the engineering themes explored by the three MQP Teams.

7.4.1 Economic Impacts

The economics of model rocketry varies widely. Model rockets can vary in cost anywhere from under \$20 to well beyond \$1000, with individual motors costing more than \$250 (Stine, 1997). An economic impact analysis can be used to gain a more thorough understanding of the overall economics of the model rocket industry. Employment, value added to the economy, and total business output are all important impacts of the model rocket industry (Weisbrod & Weisbrod, 1997). The manufacturing and distribution of components for model rocketry creates a highly interpersonal network. Many companies employ fewer than 100 people, and ordering parts often involves direct contact with the company's CEO.

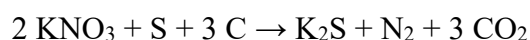
The relatively small size of the industry contributes to the high levels of demand for specific products. In many cases, components are manufactured in batches by a single company before

distribution to multiple separate sites. This system can lead to issues with supply and demand. For example, purchasing aft motor closures for the clustered HPMR configuration was delayed due to lack of supply. The manufacturer of these components, Aerotech, had not recently sent out another batch of supply, leaving every distributor without stock. Each distributor had to wait multiple weeks to receive new supply for these closures.

More broadly, it is important to note that the aerospace industry also impacts the model rocketry industry. Model rocket builders take inspiration from real-world orbital launch vehicles. At the test launch, for instance, a fellow rocket builder displayed his scale model of a Falcon 9 rocket. Other launches host scale models of famous launchers through history, from Apollo to STS. Further, some rocket builders are working to replicate SpaceX's powered landing maneuvers by using thrust vectoring within the airframe of the model rocket (Anon., n.d.). Replicating real rockets expands the economic reach of model rocketry beyond the niche component industry. The realistic models require access to high quality finishing products, as well as electronic components to control powered maneuvers.

7.4.2 Environmental Impacts

In addition to its economic impact, model rocketry has the potential for adverse environmental impacts. These are mainly caused by the use of chemicals throughout the launch process and production of components. The launch process has an impact to the environment due to the rocket engines and stage separation charges that are used. Ammonium perchlorate and the products of black powder combustion are both toxic and dangerous to human health (Scheer & Moss, 2013). The products resulting from the combustion process are shown below (Calvert, 2004):



Because model rocket launches typically take place on fields used for agriculture, the products and reactants can contaminate the soil. Depending on how often the field is used for launches, this

contamination may even reach toxic concentrations. Once the chemicals contaminate the launch site, they can join other chemicals contributing to farm runoff. Large amounts of runoff are environmentally concerning due to the concentration of toxic chemicals that they cause (Torno, et al., 2000). Periodically changing launch zones can work to reduce the contributions of rocket launches to farm runoff.

7.4.3 Social Impacts

Model rocketry has had a significant social impact on many communities across the country. As a hobby, it allows many people to explore their interests in STEM and it introduces them to others who share similar interests. It also provides an outlet for hobbyists to hone their design skills and showcase their creations.

The hobby as it is known today began in the 1950's, with the advent of the space race. As government interest in rocketry grew, so did public interest. Citizens were trying to build small amateur rockets in their backyards, often having little to no experience and injuring themselves in the process (Colburn, 2012). Orville Carlisle, who had developed a miniature rocket with a paper airframe and balsa fins for educational demonstration purposes, read an article in *Popular Mechanics* about these accidents and realized his creation could be sold and as a result, make the practice of hobby rocketry safer (Colburn, 2012). These kits grew in popularity and soon more companies such as Cesaroni and Aerotech expanded the market.

In education, model rocketry has served a multitude of purposes—primarily as a means to foster students' interest in STEM. The hobby serves as a great way to get students interested in physics, aerodynamics, electronics, and chemistry. Students can compete in competitions that allow them to practice engineering related design skills. These competitions encourage cooperation and teamwork, as building and launching a rocket is often a team effort. At the

university level, these competitions provide even more complex design challenges and goals. These give students the opportunity to apply engineering principles taught in classes to a real, hands-on project. Participation in model rocketry clubs and competitions can stand out to potential employers. Meanwhile, club launches can function as great networking opportunities, as the rocketry community is tight knit.

Model rocketry as a hobby is accessible to people of many different backgrounds. Many online retailers ship rocket kits and parts to anywhere in the country. A multitude of online resources can be used as reference for those looking to enter the hobby. Model rockets vary greatly in terms of building difficulty; some beginner kits are purchased almost fully assembled, whereas other designs can be completely custom (Anon., 2019). Cost scales with size, with smaller motors and kits costing less than larger, more powerful motors and parts. This creates a very low barrier to entry, allowing anyone interested to build small rockets before deciding to invest in larger models.

This accessibility is aided by the close-knit community that is associated with model rocketry. Rocketry clubs and associations hold day long rocket launches that people can attend to fly their rockets. More experienced hobbyists are willing to share their experience with people who are new to the hobby. These events are often a valuable source of design ideas and rocketry information (Anon., 2019).

8 References

Anon., 2008. *Moored balloons, Kites, Amateur Rockets, Unmanned Free Ballons, and Certain Model Aircraft*, s.l.: s.n.

Anon., 2016. *Aerotech Rocketry*. [Online]
Available at: http://www.aerotech-rocketry.com/uploads/55867411-cc96-4e24-9bd8-c009920eba92_RMS-38_120-360%20Plus%20%20pg%20Instr%205-12-16%20Small.pdf

Anon., 2017-2018. *NASA Student Launch College and University*, Annapolis: s.n.

Anon., 2018. *Flight Readiness Review*, s.l.: s.n.

Anon., 2019. *Aerotech 38mm Propellant Kit - H73J-10*. [Online]
Available at:
https://www.apogeerockets.com/Rocket_Motors/AeroTech_Motors/38mm_Propellant_Kits/38_240_Kits/Aerotech_38mm_Propellant_Kit_H73J-M
[Accessed 23 January 2019].

Anon., 2019. *Frequently Asked Questions*. [Online]
Available at: <https://www.alwaysreadyrocketry.com/blue-tube-2-0/>
[Accessed 2019].

Anon., 2019. *MODEL ROCKET INFORMATION*. [Online]
Available at: <https://www.nar.org/model-rocket-info/>
[Accessed 24 February 2019].

Anon., n.d. *Model Rocket Aerodynamics*, s.l.: s.n.

Anon., n.d. *SIGNAL R2*. [Online]
Available at: <https://bps.space/signal/>
[Accessed 2019].

Anon., n.d. *Vulcanized Fibre Specifications*, s.l.: s.n.

Barrowman, J. S., 1967. *The Practical Calculation of the Aerodynamic Characteristics of Slender Finned Vehicles*, s.l.: s.n.

Behlman, N., Caron, R., Dempsey, S., Niles, R., 2007. *WPI AIAA Research Rocket for the Investigation and Observation of Recovery and Staging II*, Worcester: Worcester Polytechnic Institute.

Belliss, M., Braun, T., Brayshaw, P., Matook, G., Moore, K., Otterman, A., 2006. *WPI AIAA Research Rocket for the Investigation and Observation of Recovery and Staging I*, Worcester: Worcester Polytechnic intitute.

- Bowman, S. et al., 2012. *Two-Stage, High-Altitude Rocket with Internal Skeleton Design Entered in Advance Category of 7TH ESRA IREC*, San Luis Obispo: Cal Poly.
- Buhler, J., Coverstone, T., Cummins, N., Fleming, S., Huleatt, T., McDonald, T., 2008. *WPI AIAA Research Rocket for the Investigation and Observation of Recovery and Staging III*, Worcester: Worcester Polytechnic Institute.
- Calcara, L. E., Fernandez, M., Green, C., Hosokawa, T., 2016. *High Power Rocket Design Report*, s.l.: Loyola Marymount University.
- Calvert, J. B., 2004. *Flash! Bang! Whiz!*. s.l., University of Denver.
- Cannon, B., 2004. *Model Rocket Simulation With Drag Analysis*, s.l.: s.n.
- Chang, S., Fedors, C. & Bryan, Z., 2017-2018. *Proposal for the NASA Student Launch Competition: Deployable Rover and Air Braking System Payloads*, Ithaca: s.n.
- Colburn, W., 2012. Where Did Model Rocketry Really Start. *Peak Of Flight*, 5 June, pp. 2-4.
- Exeler M, C. G. H. D. L. Y., 2017. *NASA Student Launch 2016-2017 Critical Design Review*, s.l.: s.n.
- Goss, W. P. & Miller, R. G., n.d. *Thermal Properties of Wood and Wood Products*, s.l.: s.n.
- International Fastener Institute, 2018. *Book of Fastener Standards*. s.l.:s.n.
- JB3-1901, Farias, N., Furter, J., Halfrey, S., Handy, M., Legere, V., Murphy, C., Songer, N., Tavares, J., 2019. *Design and Integration of a High-Powered Model Rocket-III*, Worcester: Worcester Polytechnic Institute.
- John, S. & Spyros, P., 2006. *Atmospheric Chemistry and Physics: From Air Pollution to Climate Change*. 2nd ed. Hoboken: John Wiley & Sons Inc.
- MAD-1901, Alvarez, A., Gerhardt, G., Kelly, E., O'Neil, J., Whitehouse, J., 2019. *Design and Integration of a High-Powered Model Rocket-II*, Worcester: Worcester Polytechnic Institute.
- Parker Hannifin, 2018. *Parker O-Ring Handbook*. Cleveland(Ohio): s.n.
- Powling, J. & Smith, W., 1965. *The surface temperature of burning ammonium perchlorate*. Essex, s.n., pp. 1373-1390.
- Scheer, R. & Moss, D., 2013. Perchlorate in Drinking Water Raises Health Concerns. *Scientific American*.
- Schilter, C., 2019. *The Swiss Wind Power Data Website*. [Online]
Available at: <https://wind-data.ch/tools/profile.php?lng=en>
[Accessed 23 January 2019].

Stine, G. H., 1997. *Fourty Year of Model Rocketry a Safety Report*, s.l.: The National Association of Rocketry.

Stine, G. H. & Stine, B., 2004. *Handbook of model rocketry*. Hoboken: John Wiley.

Torno, H. C., Marsalek, J. & Michel, D. eds., 2000. *Urban Runoff Pollution*. Berlin, Springer-Verlag.

Weisbrod, G. & Weisbrod, B., 1997. *Measuring Economic Impacts of Projects and Programs*, Boston: Economic Development Research Grou.

West System, 2014. *Technical Data Sheet*, Bay City: s.n.

Appendix A

HPMR Overall Project Budget				
	Total Budget	Order #	Description	Cost
MSAT	\$2000	1	AAR- Tubes	\$161.29
		2	West Systems	\$100.84
		3	McMaster Carr	\$23.45
		4	GiantLeap Rocketry	\$33.06
		5	Amazon - Cameras	\$69.30
		FDC 1	McMaster, with FDC team	\$36.68
		6	DigiKey	\$112.72
		7	DigiKey – Strain gauge parts	\$83.56
			Remainder:	\$1379.10
PSR	\$2000	1	Evike CO ₂ Magazine	\$27.00
		2	Apogee Rockets	\$144.67
		5	Apogee Rockets - Recovery	\$89.63
		6	McMaster Carr	\$32.69
		7	ServoCity	\$9.99
		MSAT 6	DigiKey - electromagnets	\$31.11
		9	Mouser - Transistors	\$9.90
		10a	MotoJoe – Motor Closures	\$159.77
		10b	OffWeGo – Aft Motor Closure	\$45.20
		11	DigiKey – Motor Drivers	\$7.50
		13	McMaster Carr - Garolite	\$45.20
		14	Sparkfun – Motors for CO ₂	\$43.84
		15	Apogee Rockets - Motors	\$232.39
			Remainder:	\$974.23
FDC	\$1250	1	McMaster Carr – Wire and Rod	\$26.03
		2	Sparkfun – RF Transmitter	\$4.95
		3	Adafruit – SD and IMU	\$62.35
		4	Copper Hill – Mega Core	\$40.95
		5	ServoCity – Fin Servos	\$166.99
			Remainder	\$948.73
			Total Remainder	\$3302.06
Total	\$5250.00		Total Spent	\$1947.94

Appendix B

Rotating Fins				
Provide Space Estimate	MSAT-M	100%	9/27/18	9/28/18
Mechanical Integration of fins into Rocket	MSAT-all	100%	11/26/18	12/5/18
Electrical Connections	MSAT-M	0%	1/19/19	2/2/19

Autorotation				
Determine where Blades Mount	MSAT-M	100%	9/29/18	9/29/18
Structural Analysis	MSAT-S	100%	1/9/19	2/14/19
Physical Integration	MSAT-All	0%	1/25/19	2/1/19

CO2 Stage Sep.				
Mechanical Integration of black powder separation system	MSAT-All	100%	11/19/18	12/1/18
Mechanical Integration into Rocket (Black Powder)	MSAT-All PSR	100%	12/1/18	12/10/18
Mechanical Integration into Rocket (CO2)	MSAT-All	50%	12/8/18	2/1/19

Nosecone & Side Cameras				
Choice of Camera	MSAT-All	100%	9/26/18	9/29/18
Camera Location / views	MSAT-All	100%	9/26/18	9/30/18
Side Camera mount & integration	MSAT-All	100%	11/12/18	12/1/18
Camera mount design & integration	MSAT-M	100%	11/2/18	11/20/18
Window selection & purchase	MSAT-All	100%	9/26/18	10/11/18
Subsection Physical & Optical Testing	MSAT-All	100%	11/14/18	11/20/18
Redesign Camera Gimbal	MSAT-M	100%	1/13/19	2/2/19
Replace Camera Gimbal in Rocket	MSAT-M	100%	2/2/19	2/16/19

Electronics Bay				
Share maximum dimensions	MSAT-M	100%	9/26/18	10/26/18
Physical Installation	MSAT-All	100%	12/2/18	12/5/18
Mount Arming Switch	MSAT-M	100%	1/13/19	1/19/19

Airframe & Bulkheads				
Determine dimensions	MSAT--M	100%	9/26/18	10/5/18
Full CAD Model	MSAT--M	100%	9/26/18	10/10/18
Structural Analysis: Parachute	MSAT--S	100%	10/29/18	11/7/18
Structural Analysis: Fins	MSAT--S	100%	11/15/18	11/20/18
Structural Analysis: Body Tube	MSAT--S	100%	10/29/18	11/12/18
Structural Analysis: Bulkheads	MSAT--S	100%	10/29/18	11/9/18
Body Material Choice	MSAT--S	100%	9/27/18	10/2/18
Purchase Bulkhead Material	MSAT--All	100%	10/7/18	10/7/18
Acquire Body Material	MSAT--All	100%	10/7/18	10/19/18
Acquire Nosecone	MSAT--All	100%	10/7/18	10/14/18
Cut materials to size	MSAT--All	100%	10/23/18	10/26/18
Rail buttons	MSAT--All	100%	12/3/18	12/7/18
Assemble Airframe	MSAT--All	100%	10/26/18	12/1/18
Strain Gauge development and integration	MSAT--S	100%	1/13/19	1/19/19
Stage Sep Bulkhead design and integration	MSAT--M	85%	1/13/19	2/16/19
Stage Sep Bulkhead Structural Analysis	MSAT--S	100%	1/13/19	2/16/19

Propulsion				
Acquire Motor Mount Material	MSAT--All	100%	10/5/18	10/17/18
Motor Retention Design & Construction	MSAT--All	100%	10/23/18	12/1/18
Thermal analysis (simple conductive)	MSAT - T	100%	11/5/18	12/8/18

Launch Procedure				
Develop Test launch 1 Procedure	All Teams	100%	1/13/19	1/19/19
Develop Test launch 2 Procedure	All Teams	0%	1/19/19	2/16/19

Final Paper and Presentation				
Title page	Nick	100%	1/9/19	1/18/19
Abstract	Kyle	100%	1/26/19	2/15/19
Acknowledgments	Eve	100%	1/26/19	2/15/19
Authorship page	All	100%	2/14/19	2/15/19
Table of Contents	Amanda	100%	2/14/19	2/15/19
Table of Figures	Amanda	100%	2/14/19	2/15/19
List of Tables	Amanda	100%	2/14/19	2/15/19
Ch.1 Introduction and Background	All	100%	1/9/19	2/15/19
Requirements and Constraints	Kyle	100%	2/5/19	2/15/19
Engineering Standards	Jake	100%	2/5/19	2/15/19
General Considerations	Colin	100%	2/5/19	2/15/19
Ch.2 Mechanical Design	Peter, Kyle, Amanda, Jake	100%	1/9/19	2/15/19
CH3 Structural Analysis	Ty, Nick, Amanda	100%	1/9/19	2/15/19
Ch.4 Aerodynamic Analysis	Eve, Colin	100%	1/9/19	2/15/19
Ch. 5 Thermal Analysis	Jake, Peter	100%	1/9/19	2/15/19
Ch. 6 Integration and Testing	All	100%	1/9/19	2/15/19
SEG Breakdown	Jake, Colin	100%	1/9/19	2/15/19
Project management and budget	Peter, Kyle	100%	1/9/19	2/15/19
Economic Impact	Ty, Kyle, Jake	100%	1/9/19	2/15/19
Social Impact	Jake	100%	1/9/19	2/15/19
Conclusions and Recommendations	All	100%	1/9/19	2/15/19
References	All	100%	1/9/19	2/15/19
Appendices	Nick	100%	1/9/19	2/15/19
Final Revision	All	100%	2/15/19	3/1/19
Complete Comprehensive PPT	All	100%	9/1/18	2/20/19
Cut down the comprehensive PPT to 30 min presentation	All	100%	2/20/19	2/28/19
Practice Presentation	All	100%	2/28/19	3/1/19
AIAA paper abstract	All	100%	2/10/19	2/17/19
AIAA Paper final	All	100%	2/10/19	3/17/19

Appendix C

Below are the list of action items and timetable for this project. (GANTT chart to be added later)

Assigning Group	Group Responsible (Who does the action)	Description	Due by
	Advisors	Upload copies of last year's three MQP project reports to the myWPI site (SEG folder)	
	MSAT	Provide mounting information to Controls regarding fins	6-Nov
Controls	MSAT	Provide lift and drag curves, moments to Controls (ASAP)	12-Nov
	MSAT	Determine passive stability of rocket (CP and CG)	9-Nov
	MSAT	Provide booster separation space allotments	6-Nov
	Each team	Create: Flight test objectives, success/failure case, method of	1-Dec
	Each team	Review RIMRA launch protocol for December launch	6-Nov
	PSR	Provide Controls with dimensions for staging capacitors to be incorporated into Ebay	9-Nov
	PSR	Provide MSAT with an estimate for the space needed to contain autorotation mechanism	9-Nov
	PSR	Create list of staging events for Controls (event and what characteristic triggers it)	9-Nov
MSAT	PSR	Deliver CO2 ejection CAD model to MSAT	16-Nov
MSAT	PSR	Deliver CO2 Pressure Values (Pressure inside the body tube) to MSAT	14-Nov
MSAT	PSR	Give motor tube heat flux to MSAT	26-Nov
All	MSAT	Provide final rocket weight to controls	16-Nov
MSAT	Controls	Provide MSAT with velocity vs altitude for no-wind launch conditions	13-Nov
MSAT	Controls	Demonstrate on-board computer control software	5-Dec
PSR	MSAT	Provide/develop integration plan for black powder backup system	1-Dec
PSR	Controls	Report amount of voltage being sent from on-board computer to switch to activate booster system	16-Dec
PSR	Controls	Report if other parts or considerations are needed for ejection charge integration to Ebay	26-Nov
MSAT	All	Develop Launch day procedures	11-Jan
Controls	MSAT	Develop and Deliver strain gauge system to be integrated with the flight controller	14-Jan
MSAT	Controls	Deliver Completed E-Bay	14-Jan
MSAT	All	Launch Materials check list	11-Jan
MSAT	PSR	Give CAD model for Autorotating Blades	8-Feb
MSAT	PSR	Determine alternative motor setup for a safe launch	1-Feb
MSAT	Controls	Deliver active control fin system for integration	15-Feb
Prof.	All	Develop tool list	15-Feb

Appendix D

Below are the list of action items and timetable for this project.

Task	Responsible
Write team constitution	All
Summarize previous MQPs (for Friday Presentation)	Eve, Nick
Collect slides for Presentation	Amanda
Demonstrate rocket parts	Peter
Summarize goals	Ty, Jake
Introduce software	Kyle, Colin
Email when2meet to Prof. Gatsonis	Kyle
Research past projects: BOR	Kyle, Peter,
Research past projects: MQP	Nick, Eve
Research past projects: auto rotation decent	Amanda
Research past projects: IREC and USLI	All
Create presentation overview of previous rockets	All
Design Proposal	All
Talk to Propulsion Team regarding fin design	Ty
Email other teams regarding design proposal	Peter
Break into groups	All
Complete Lit Review pt. 2	All
Create slide presenting design proposal	Ty
Create summary slide of proposal finalization	Peter
Create Lit Review pt. 2 slides	all
Summarize objective break up for SEG presentation	Amanda
Create preliminary rocket design	All/each
Slides	Eve
Slides: CO2 separation - Side Boosters	Nick
Slides: Camera - end	Kyle
Component research: blue tube, plastic	Peter
Component research: fiberglass	Ty
Find Camera	Collin
Provide component bay sizes to other SEG teams	Peter
Make nice table of tasks	Jake
Create slides of CAD model	Peter, Ty
Create slides of Gantt chart	Amanda
Talk to the FDC team about Rotating Fins	Eve
Buy given materials	Kyle
Fill in parts list with Epoxy, side camera	Peter, Collin
Summarize past rocket teams work for Mechanical, structure	All/each
Create bulleted list of objectives	Amanda
Outline summary: BOR	Peter
Outline summary: Warriors	Nick, Eve

Outline Summary: USLI	Ty
Outline summary: IREC	Jake
Outline summary: other	Kyle, Eve
Background: mechanical	Amanda
Background: structural analysis	Nick
Background: aerodynamic analysis	Eve
Background: Thermal analysis	Kyle
Introduction: Define the problem	Amanda
Introduction: approach	Peter
Slides for 10/5: Parts ordered	Peter
Slides for 10/5: Camera options	Eve, Collin
Slides for 10/5: Preliminary Stress Analysis	Ty
Slides for 10/5: Preliminary Aerodynamic Analysis	Collin
Order small side cameras (4x)	Kyle
Finish Preliminary CAD model	Peter
Ensure gimbal sizing to fit in nose cone	Eve
Submit introduction to Prof. Gatsonis	Amanda
Reach out to FDC Team about E-bay	Nick
Order motor retention hooks	Kyle
10/26 SEG presentation: Analysis	Eve, Collin
10/26 SEG presentation: Parts	Kyle
10/26 SEG presentation: Upcoming	Amanda
10/26 SEG presentation: Design	Peter
Cut tubes to length	Amanda
Reserve laser cutter time	Kyle
Become basic user	All/each
Ask PSR for autorotation models	Nick
Ask PSR for CO2 system layout	Nick
Assemble body tube	Eve, Ty, / All
Create entire rocket mesh	Eve, Colin
Determine parachute forces on the bulkhead	Nick, Ty
Determine CO2 separation forces on bulkheads	Nick, Ty
Find rocket vibration modes	Nick
Perform aft end thermal analysis research	Jake, Peter
Create Fins & Booster Schematic	Kyle, Amanda
Ask PSR about stage separation footprint	SEG meeting
Build Camera Mount	Peter (team lead)
Figure out how FDC are making their wooden parts	SEG meeting
Make sure FDC fins won't change between launches	SEG Meeting
Work on Project Comprehensive PowerPoint	All/each
Print 2D Blue Print of Rocket Model (With dimensions) To scale?	Ty
Make SEG meeting agenda	Peter
Find Coefficient of Lift, Drag, Moments, Lift-to-Drag Curves	Eve/Colin
Perform Aft end thermal analysis 1st pass	Jake, Peter
Update MSAT only Gantt chart	Peter

Perform OpenRocket CP and CG Estimation	Eve, Peter
Find Accurate CP and CG Numbers	Eve, Colin, Amanda, Kyle
Review Launch Protocol	All/each
Finish SEG presentation	All/each
Determine CO2 separation forces on body tube	Nick, Ty
Create external Camera mounting design	Peter
Email FDC team about progress on bulkhead and fins	Nick
Run COMSOL models of three motors	Jake
Complete structural Analysis of Fins mounts	Nick, Ty
Provide final rocket weight to FDC	Kyle
Find sensors for vibration and strain	Amanda
Update thermal analysis using PSR combustion data	Jake
Update Comprehensive PPT	All/each
Email Blue Tube maker for materials properties	Nick
Create rocket flight protocol checklist	Peter
"Mechanical flight test objectives, success/failure case, method of determining if success occurs, post-test analysis"	Peter, Kyle, Amanda, Jake
"Structural flight test objectives, success/failure case, method of determining if success occurs, post-test analysis"	Ty, Nick
"Aerodynamical flight test objectives, success/failure case, method of determining if success occurs, post-test analysis"	Eve, Colin
"Thermal flight test objectives, success/failure case, method of determining if success occurs, post-test analysis"	Jake, Peter
Develop a plan for installing strain gages	Amanda
Update Fin Mounting Brackets with thicker plastic	Kyle
Print final side camera mount	Kyle
Find Accurate CP for our Report	Kyle, Eve
Miniaturize Circuit	Amanda
Discuss Circuit Integration with control system/recorder	Nick
Write Paper: Mechanical (M) Outline	Peter, Kyle, Amanda, Jake
Write Paper: Structural Analysis (S) Outline	Ty, Nick, Amanda (Strain Gages?)
Write Paper: Aerodynamic Analysis (A) Outline	Eve, Colin
Write Paper: Thermal Analysis (T) Outline	Jake, Peter
Write up Tasks completed in B-Term	All/each
Update Comprehensive PPT	All/each
Develop C-term Gantt chart document	Peter, Amanda
Write rough drafts MSAT paper chapters	All/each
Put together booster trade selection preparation	Kyle
Start SEG presentation	Colin
Ask PSR their progress on Autorotation	Nick, Ty
Tell PSR about rearranging booster layout	Kyle
Finish Presentation for Gatsonis	Colin
Print OpenRocket simulation	Kyle
Write Project management and budget section outline	Peter, Kyle

Add AIAA paper write up to Gantt chart	All/each
Outline economic and social impacts	Jake, Ty
Create Booster Nosecone design	Ty, Amanda
Integrate MSAT Gantt chart to master Gantt chart	Nick
Write Integration and Testing Section	All/each
Design new camera gimbal	Kyle, Jake
Design stage separation bulkhead	Kyle
Incorporate Booster Mounting CAD	Kyle, Others
Design new camera fairings	Peter
Add appendices	Nick
Update mechanical section w/ new magnet and bulkhead designs	Kyle, peter
Put OpenRocket stuff into folders for appendix	Kyle
Laser Cut new bulkhead for construction	All/each
Integrate new magnet and bulkhead designs into full CAD model	Kyle
Add MATLAB wind code appendix	Eve
Add SolidWorks part drawing appendices	Kyle as lead team will assist
Add contributions to authorship page	All/each
Perform structural analysis of stage separation bulkhead	Ty
Complete literary review of launch failure (o-ring)	Jake
Finish nosecone design	Ty
Print Booster nosecones	Kyle
Design thrust rings	Nick
Booster hooks	Amanda
Design booster motor retention	Colin
Review 1st draft comments	All/each
Write "Requirements and Constraints" section	Kyle
Write "Engineering Standards" section	Jake
Write "General Considerations" section	Colin
3D Print: Camera Gimbal	Jake
3D Print: Booster nosecone	Kyle
3D Print: Thrust rings	Nick
3D Print: Booster Hooks	Kyle
3D Print: Camera Fairings	Peter
Perform Autorotation Hub Analysis	Ty, Nick
Perform Booster Hooks Analysis	Ty, Nick
Perform Thrust Ring Analysis (hand calculation)	Ty, Nick
Revisions: Introduction and Background, SEG Breakdown, Project Management, Chapter 7	Eve, Nick
Revisions: Mechanical Design	Amanda, Jake
Revisions: Structural Analysis	Peter, Eve
Revisions: Aerodynamic Analysis	Ty, Kyle
Revisions: Thermal Analysis	Colin, Amanda, Nick
Revisions: Integration & Testing	Peter, Jake
Add SEG Slides to Comprehensive PPT	Ty

Review: Conclusions and recommendations section	Peter, Eve, Nick, Jake
Create MAP Draft V2 Document	Amanda
Transfer sections for new draft document	all
Address comments and revisions and create new doc V3	All/each

Appendix E

Main body tube parachute forces MATLAB code:

```
clear;
clc;
rho = 1.225; %Density of air
C_d = 0.75; %Coefficeint of drag for the parachute that is going to be put on the nosecone
A = 1.19; %Area of the parachute that is going to be put on the nosecone
g = 9.81; %gravity
m = 4; %mass of the nosecone
F_g = m*g; %Force of gravity

t_steps = 0:0.01:2;
V_i = g*5; %Initial velocity of the mainbody when the parachute opens.

for i=1:201

    dt = .01;
    F_d(i) = 1/2*rho*C_d*A*V_i(i).^2;
    a(i) = (F_d(i)-F_g)./m;
    V_f(i) = V_i(i)-a(i)*dt;
    V_i(i+1)=V_f(i);

end

figure
plot(t_steps,F_d)
title('Force on Main Body Bulkhead vs Time');
xlabel('Time')
ylabel('Overall Force')
```

Nose cone parachute forces MATLAB code:

```
clear;
clc;
rho = 1.225; %Density of air
C_d = 0.75; %Coefficeint of drag for the parachute that is going to be put on the nosecone
A = 0.23; %Area of the parachute that is going to be put on the nosecone
g = 9.81; %gravity
m = 0.6; %mass of the nosecone
F_g = m*g; %Force of gravity

t_steps = 0:0.01:2;
V_i = g*5; %Initial velocity of the nosecone when the parachute opens.

for i=1:201

    dt = .01;
    F_d(i) = 1/2*rho*C_d*A*V_i(i).^2;
    a(i) = (F_d(i)-F_g)./m;
    V_f(i) = V_i(i)-a(i)*dt;
    V_i(i+1)=V_f(i);

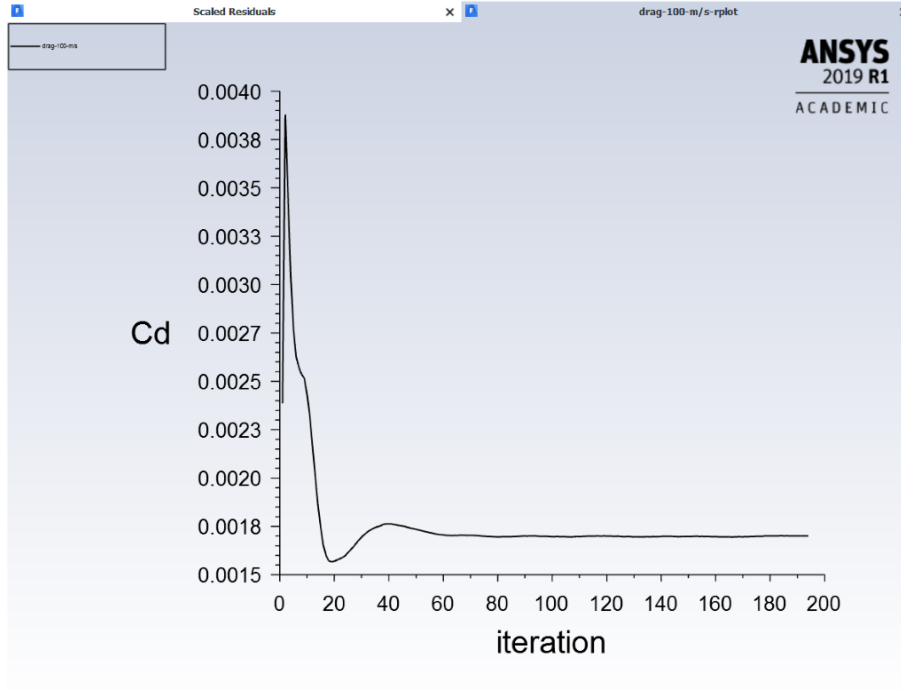
end

figure
plot(t_steps,F_d)
title('Force on Nosecone Bulkhead vs Time');
xlabel('Time')
ylabel('Overall Force')
```

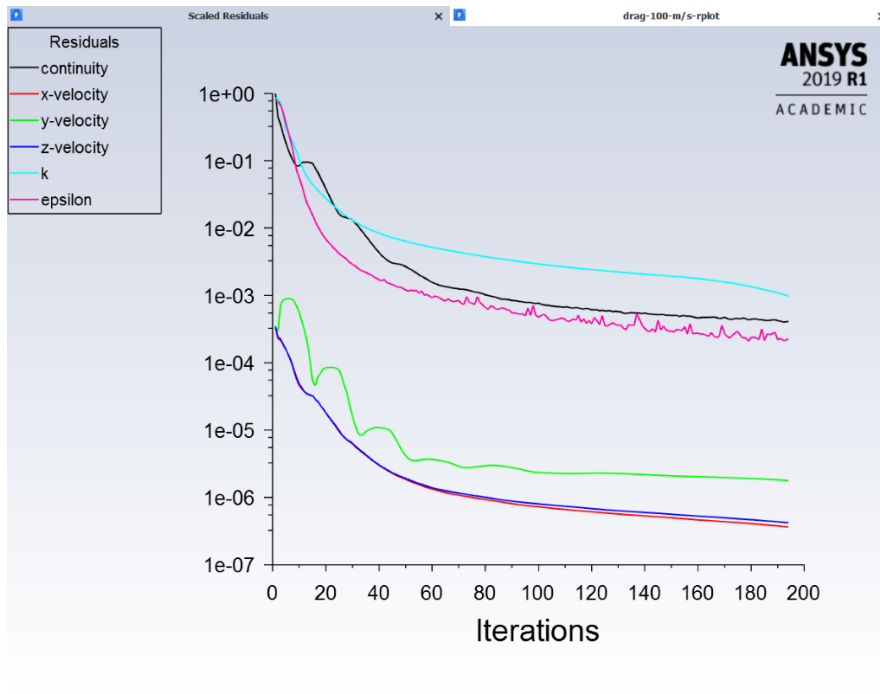
Appendix F

Steady Flow, 100 m/s:

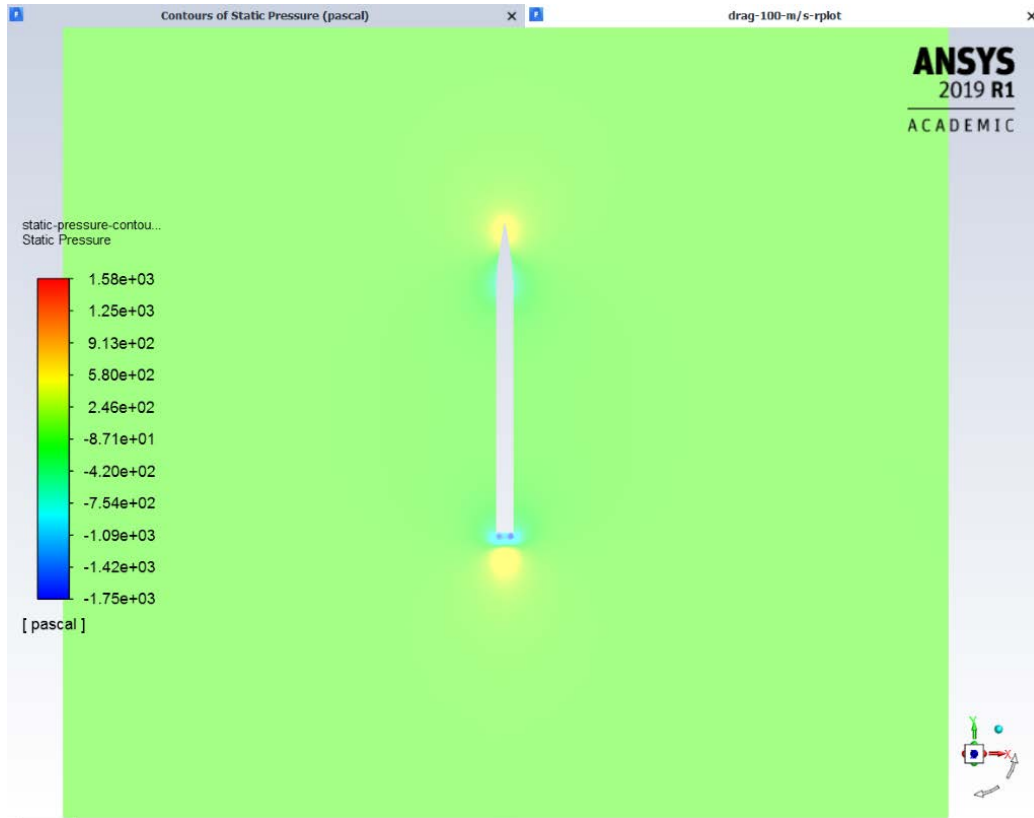
Coefficient of Drag Plot:



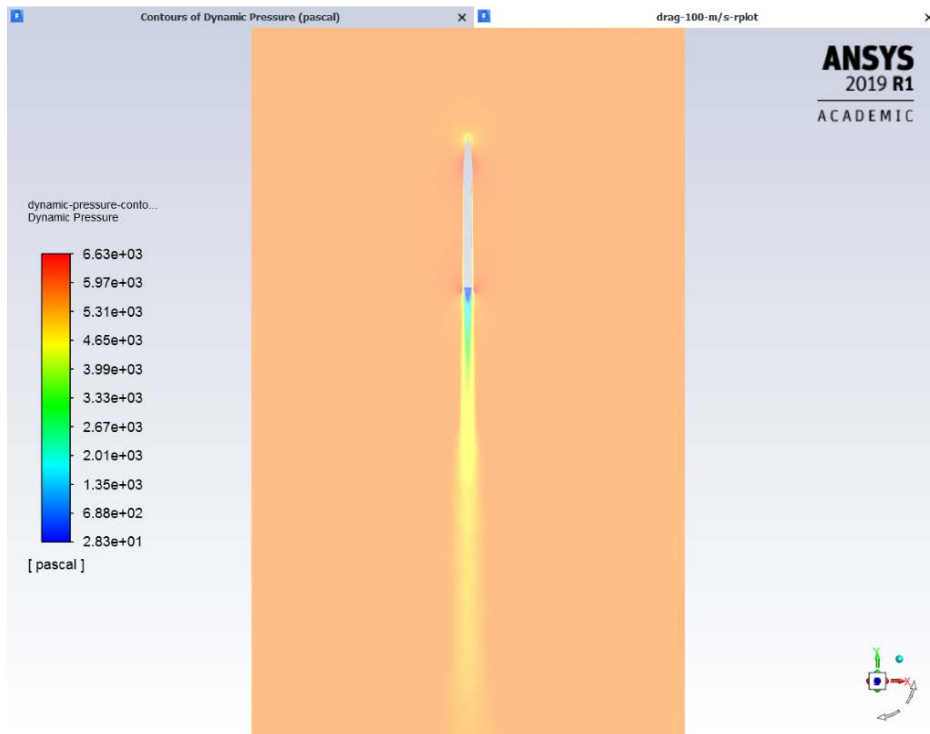
Scaled Residuals:



Static Pressure Contour:



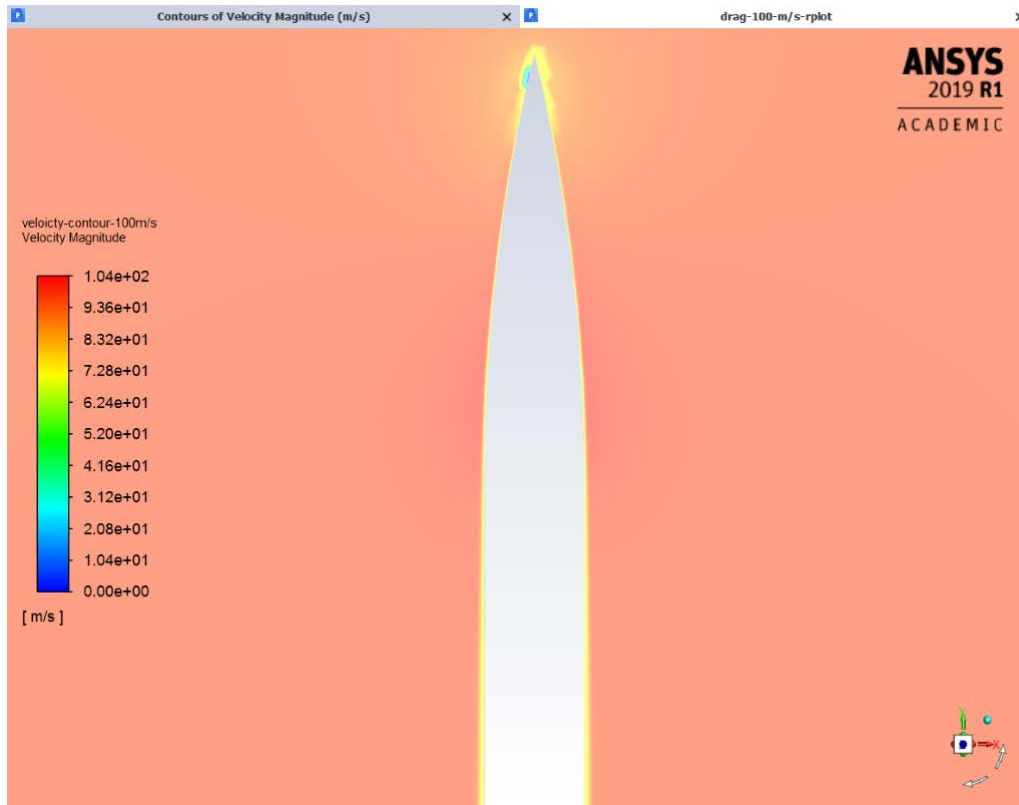
Dynamic Pressure Contour:



Velocity Contour:

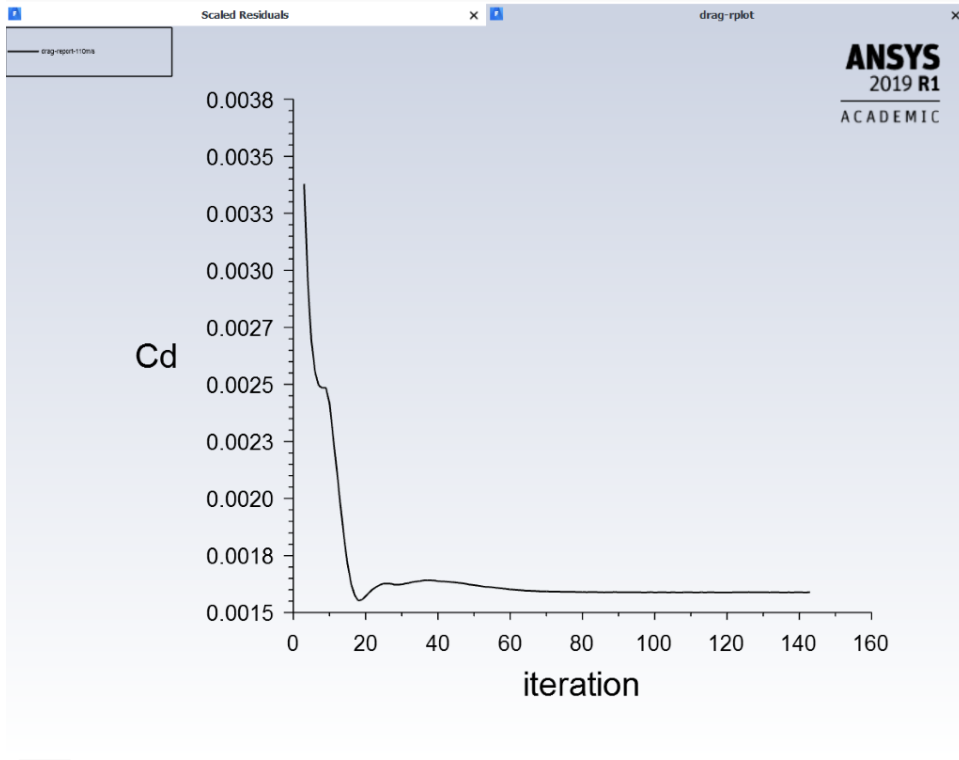


Velocity Contour Zoomed In:

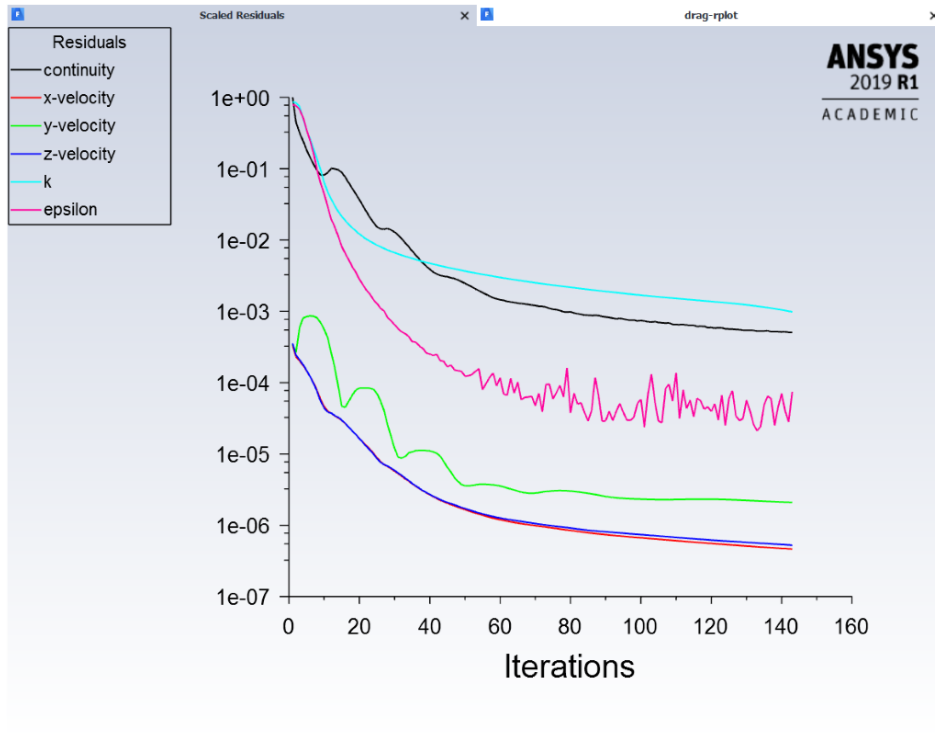


Steady Flow, 110 m/s

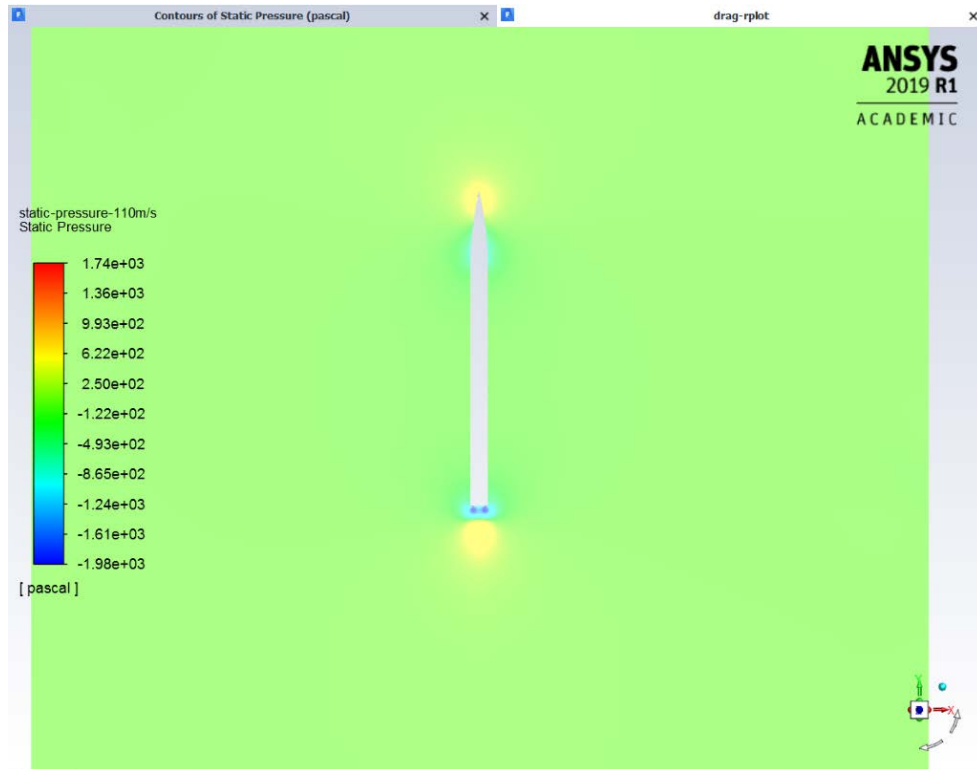
Coefficient of Drag:



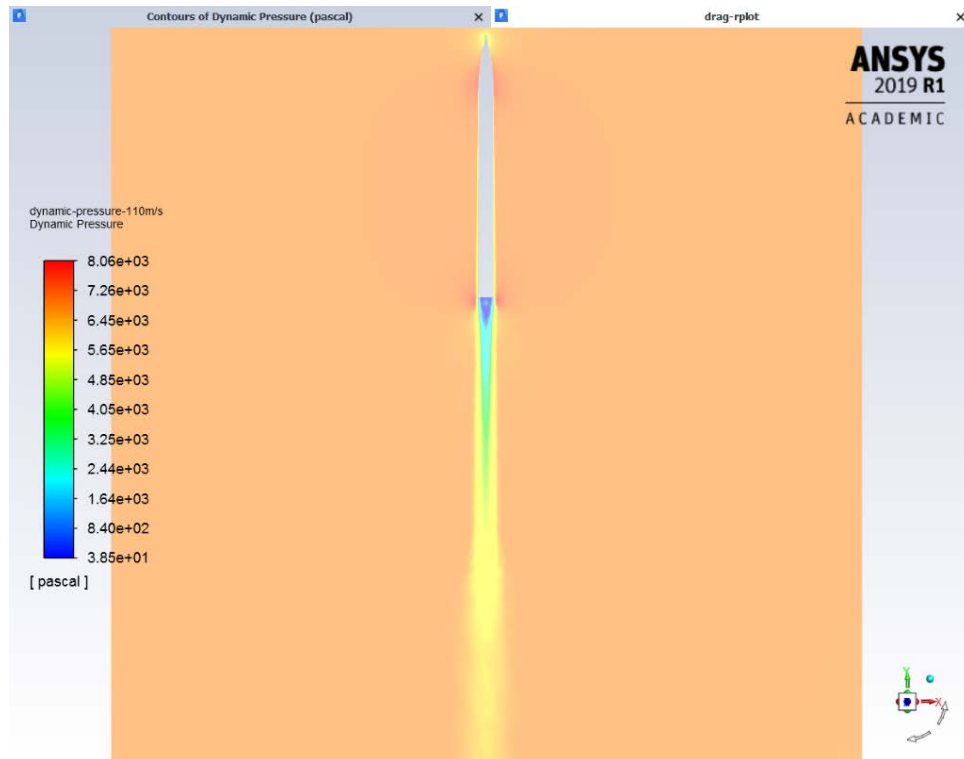
Scaled Residuals:



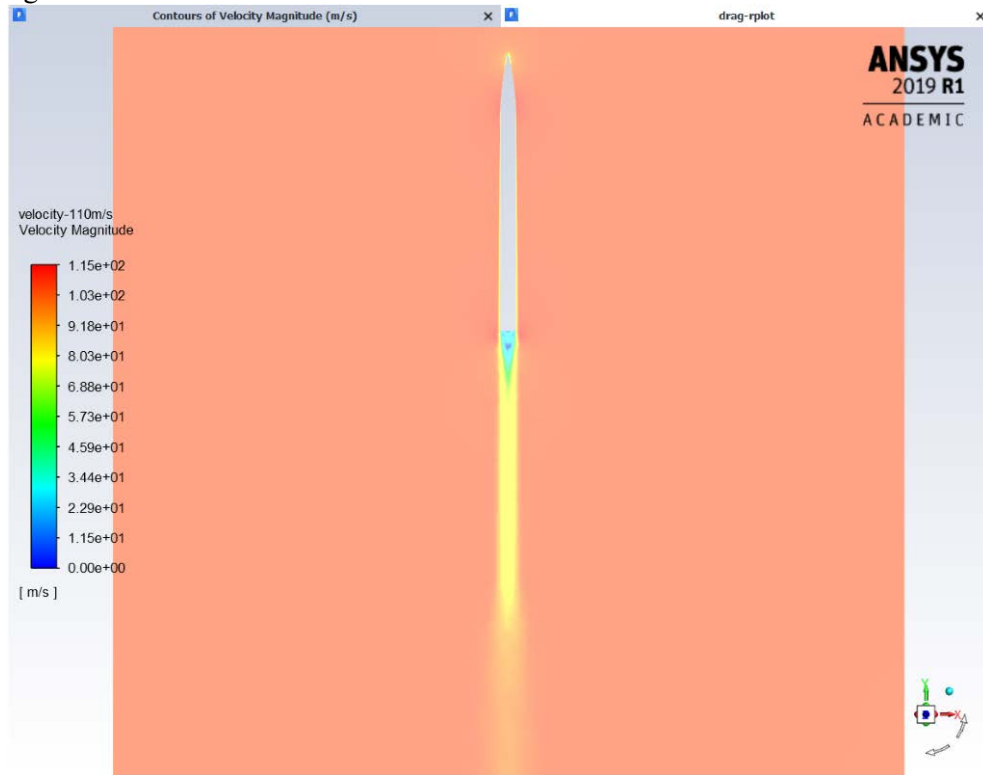
Static Pressure Contour:



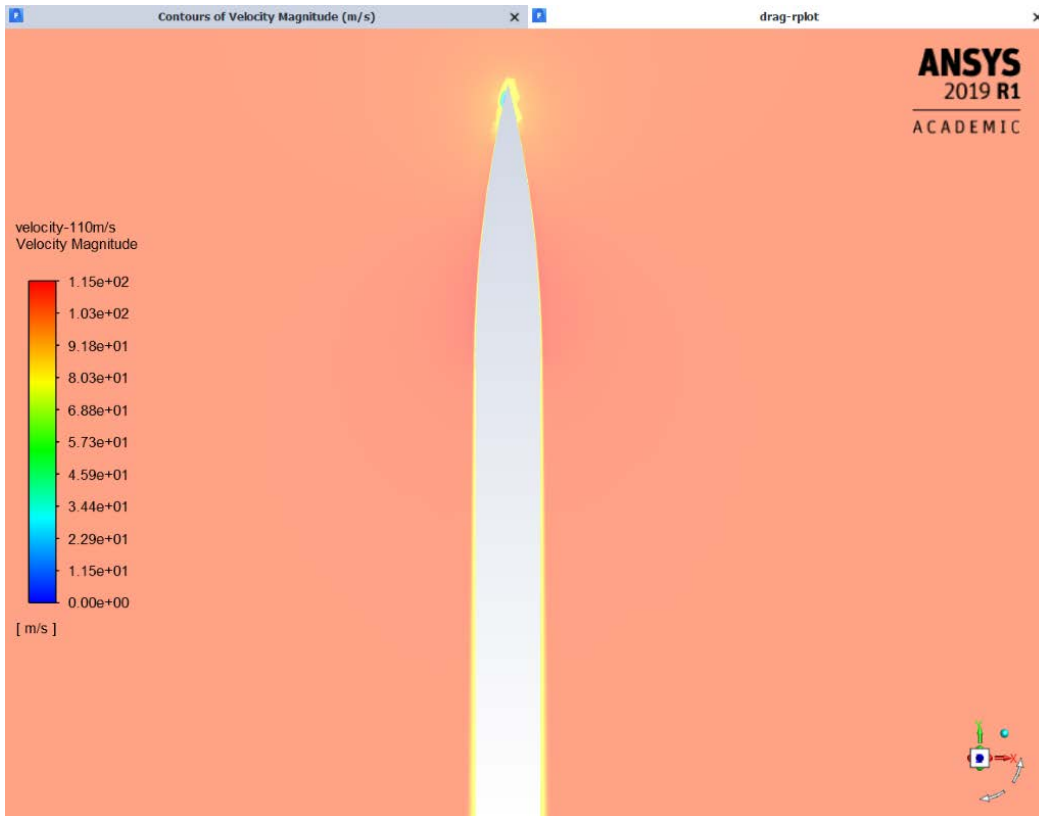
Dynamic Pressure Contour:



Velocity Magnitude Contour:

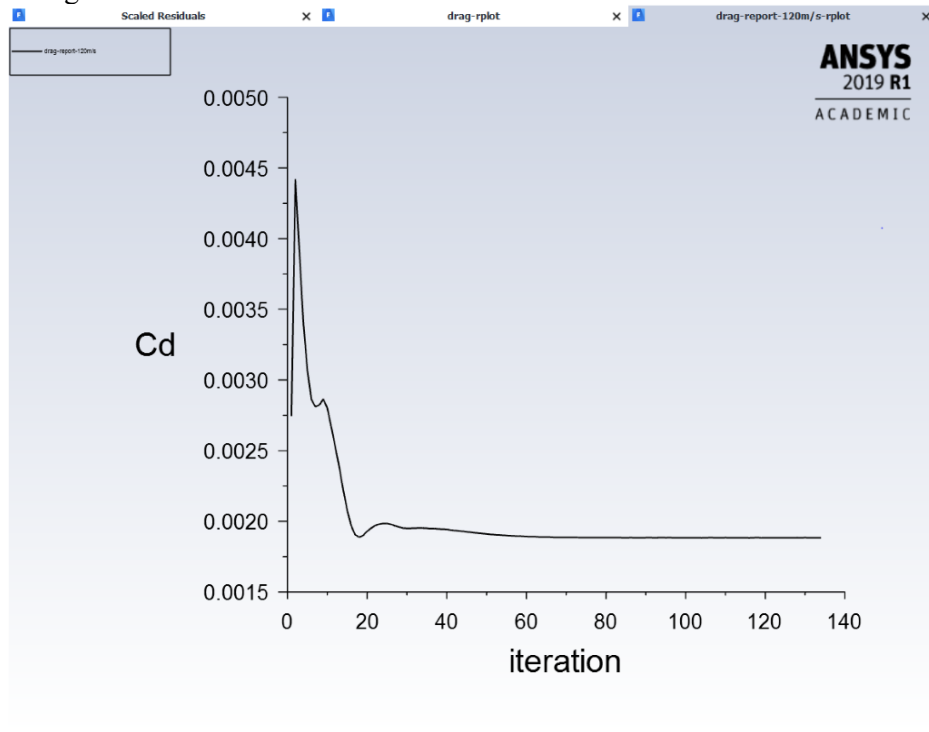


Velocity Contour Zoomed In:

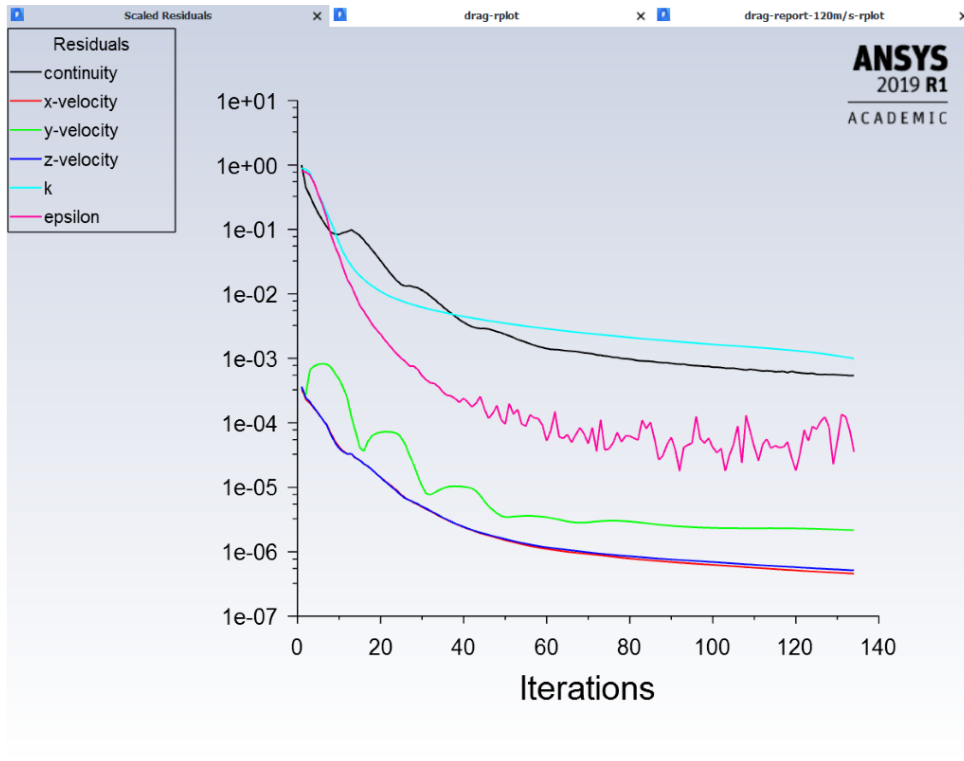


Steady Flow, 120 m/s:

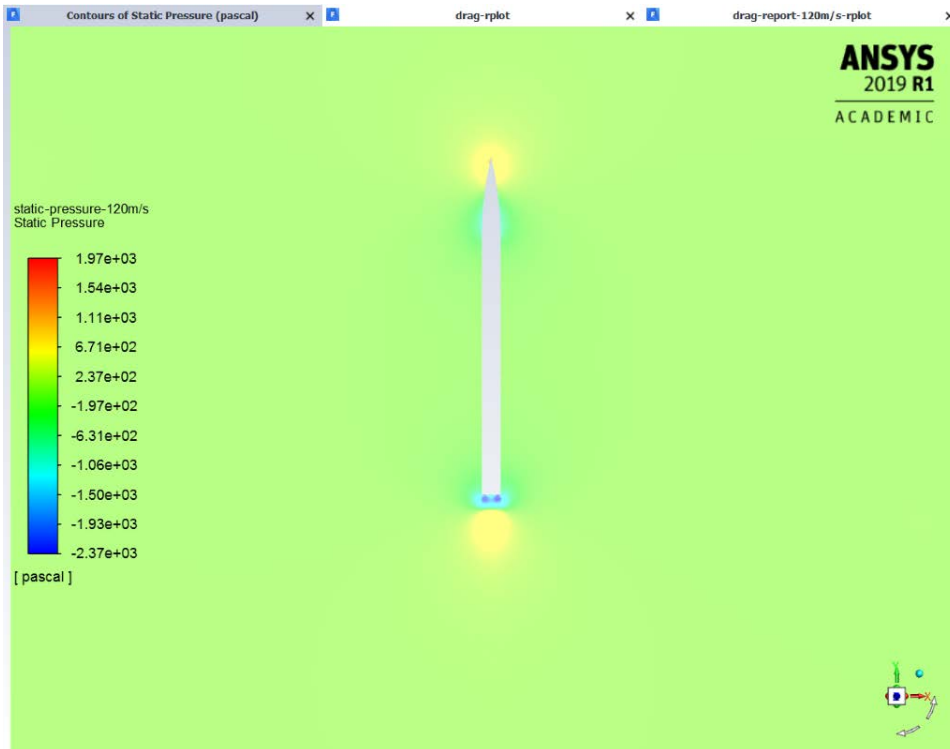
Coefficient of Drag:



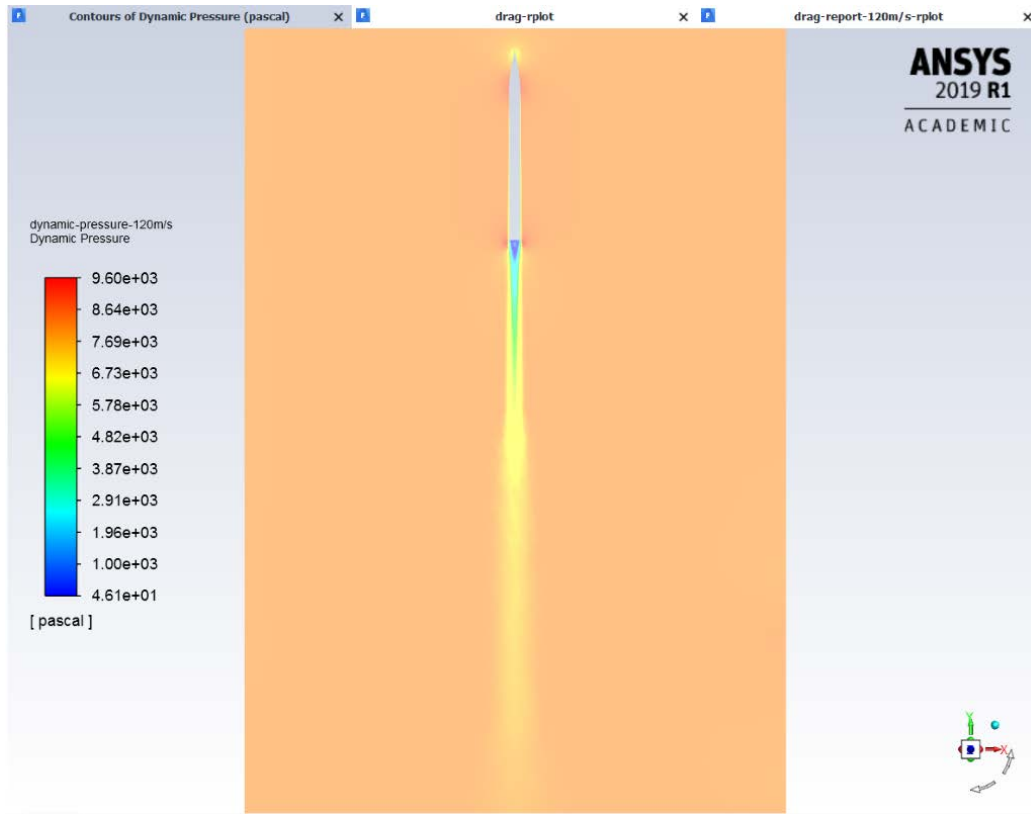
Scaled Residuals:



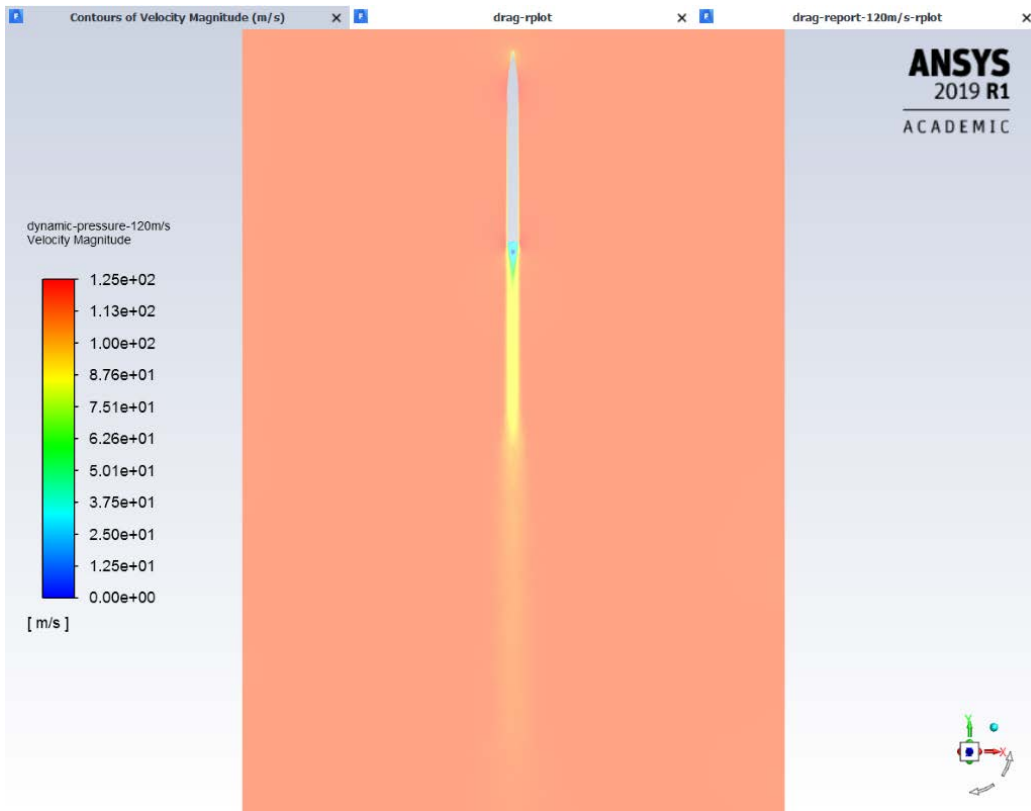
Static Pressure:



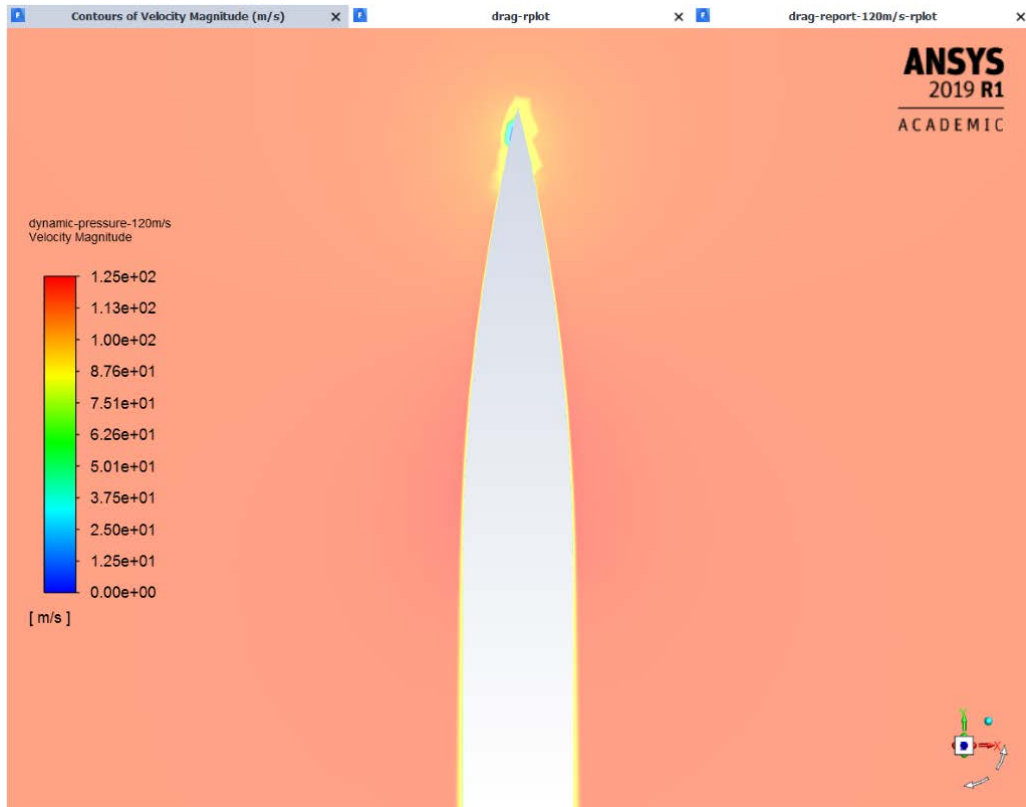
Dynamic Pressure:



Velocity Contour:

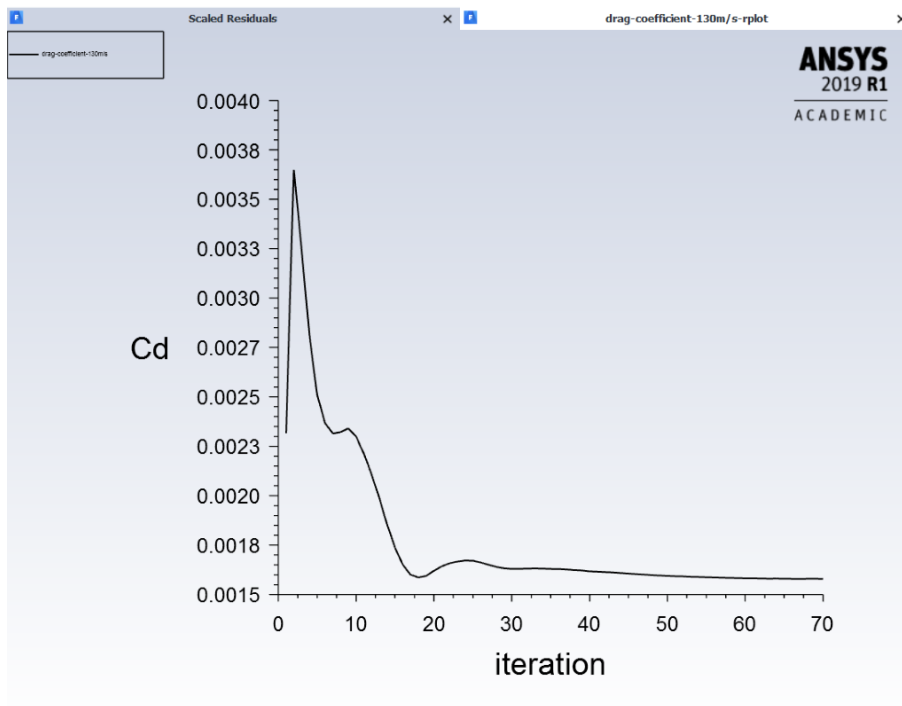


Velocity Contour Zoomed In:

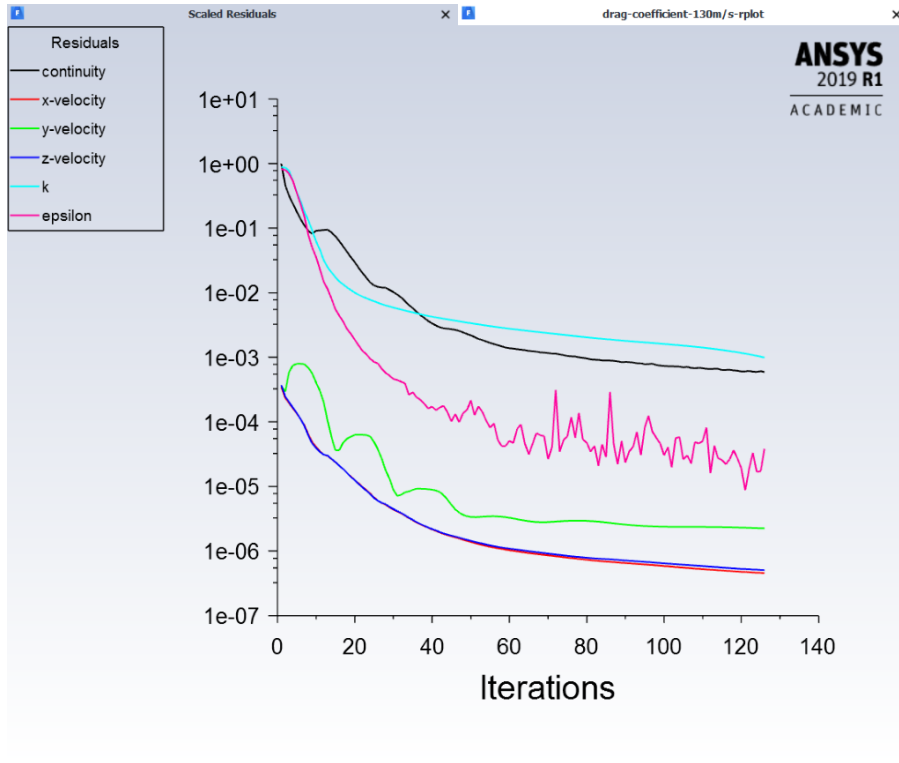


Steady Flow, 130 m/s:

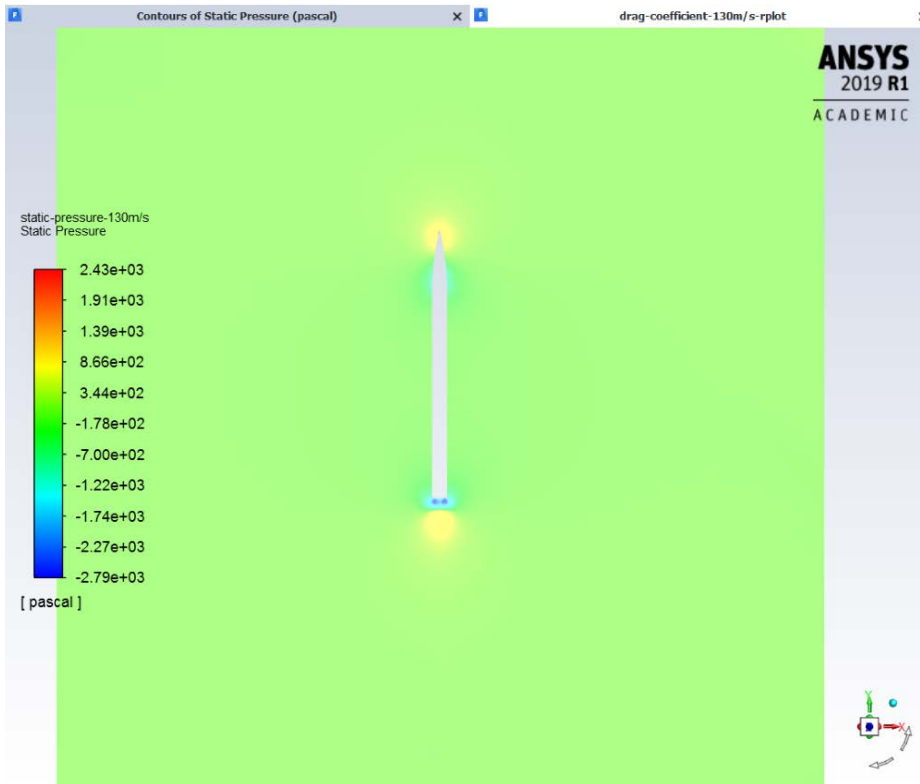
Drag Coefficient Graph:



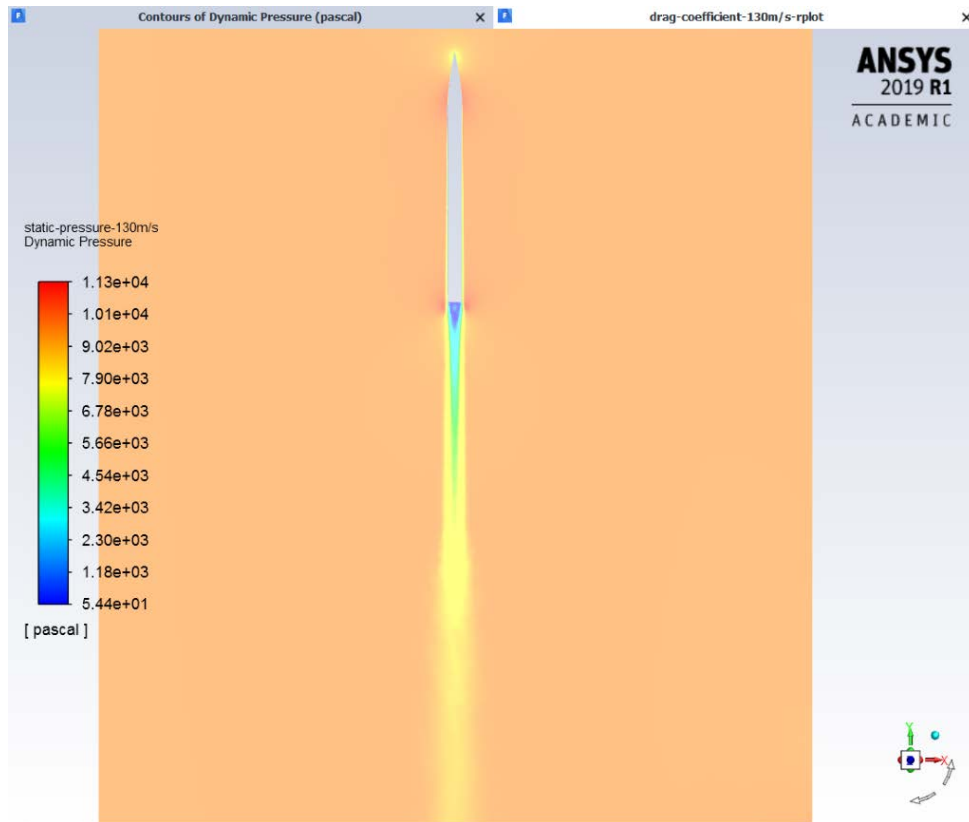
Scaled Residuals:



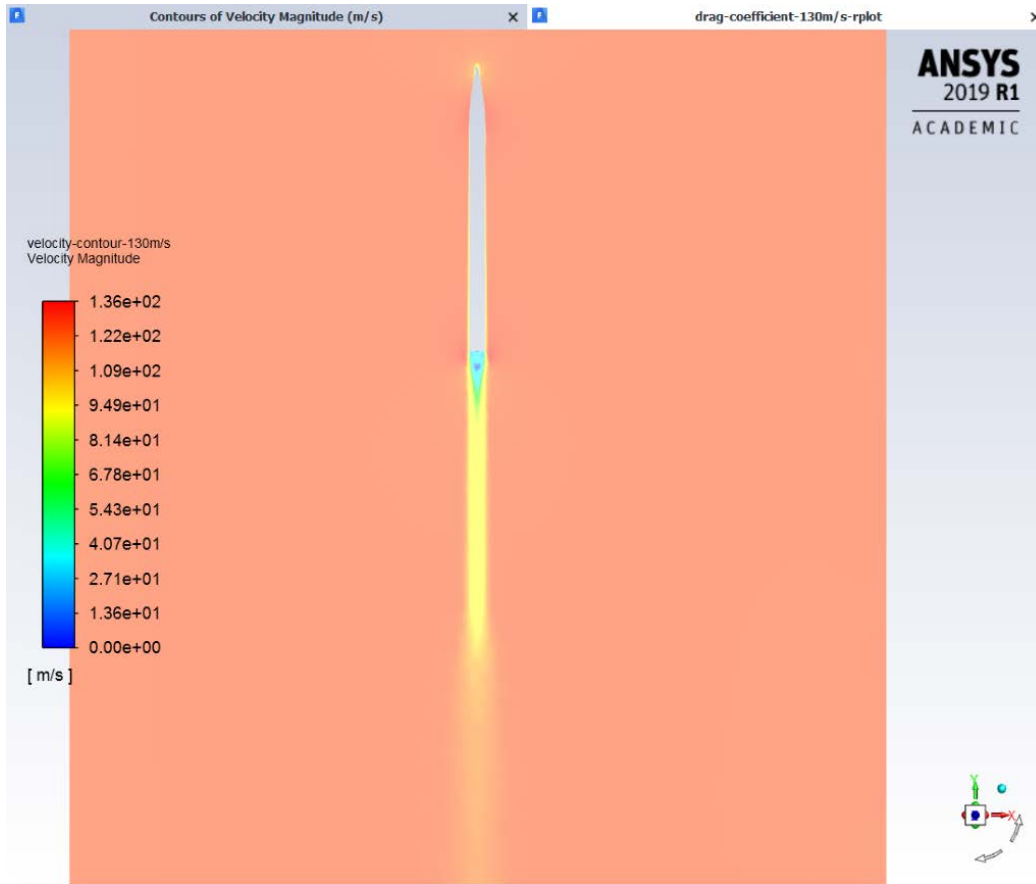
Static Pressure:



Dynamic Pressure:

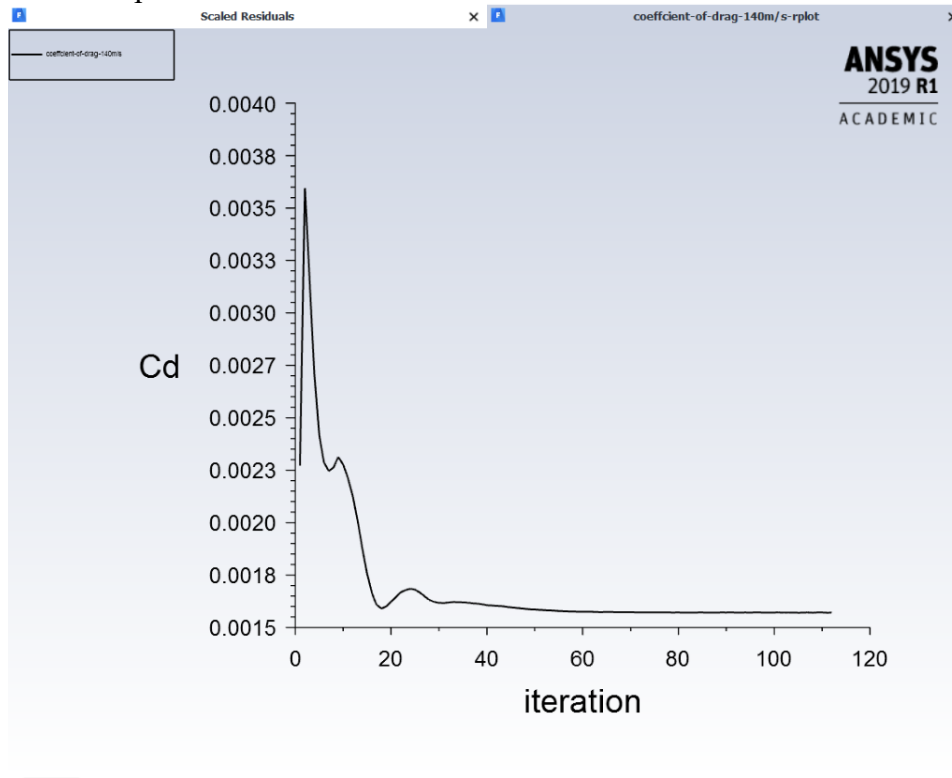


Velocity Contour:

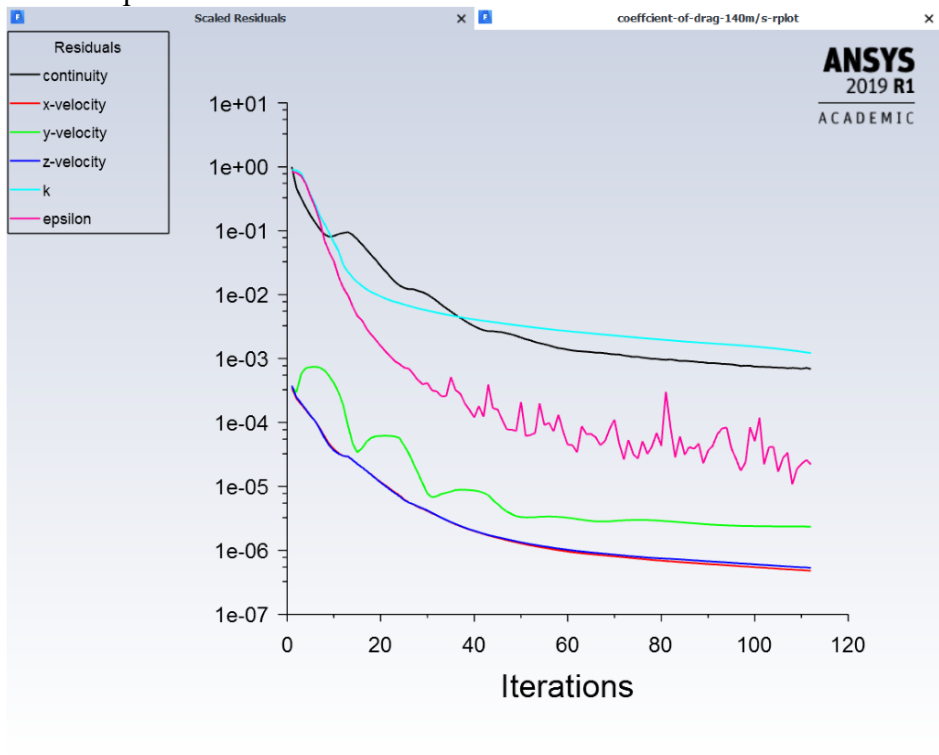


Steady Flow, 140 m/s:

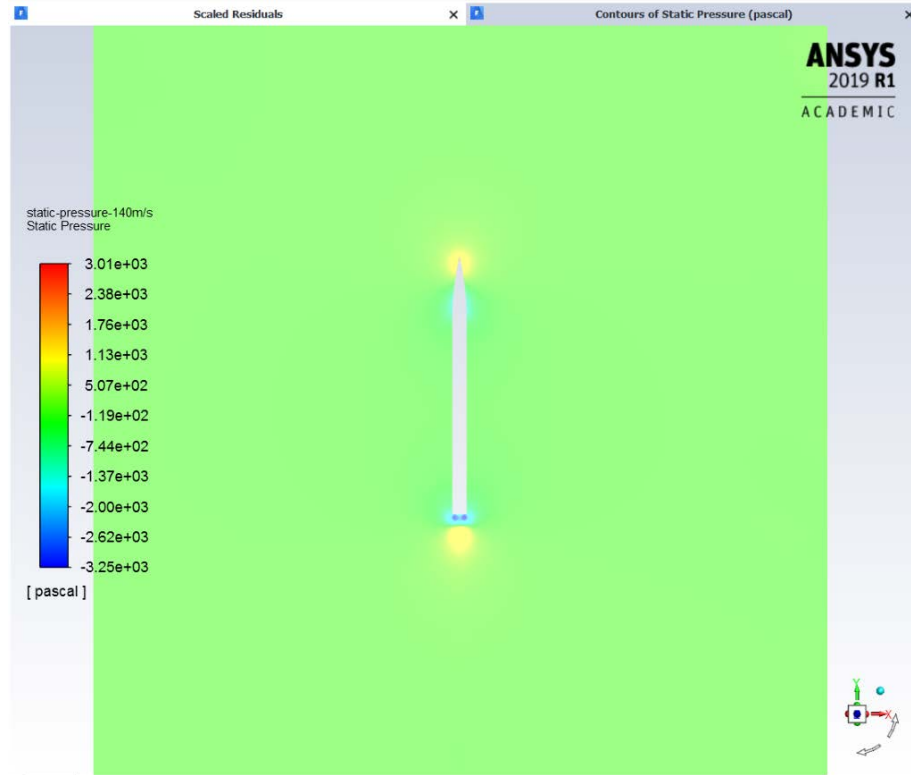
Drag Coefficient Graph:



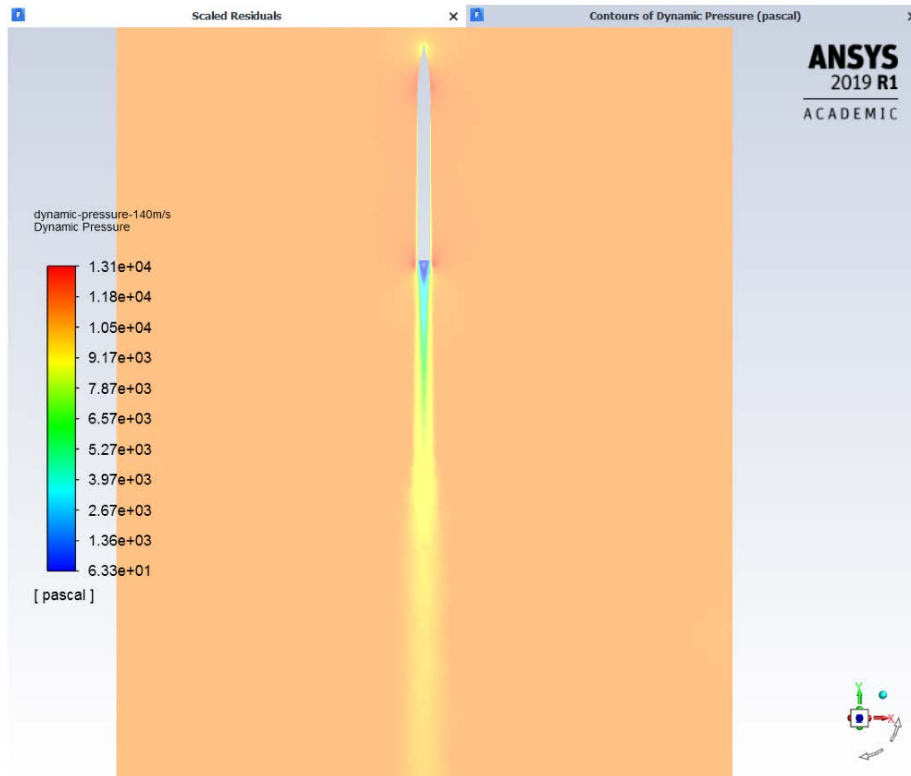
Scaled Residuals Graph:



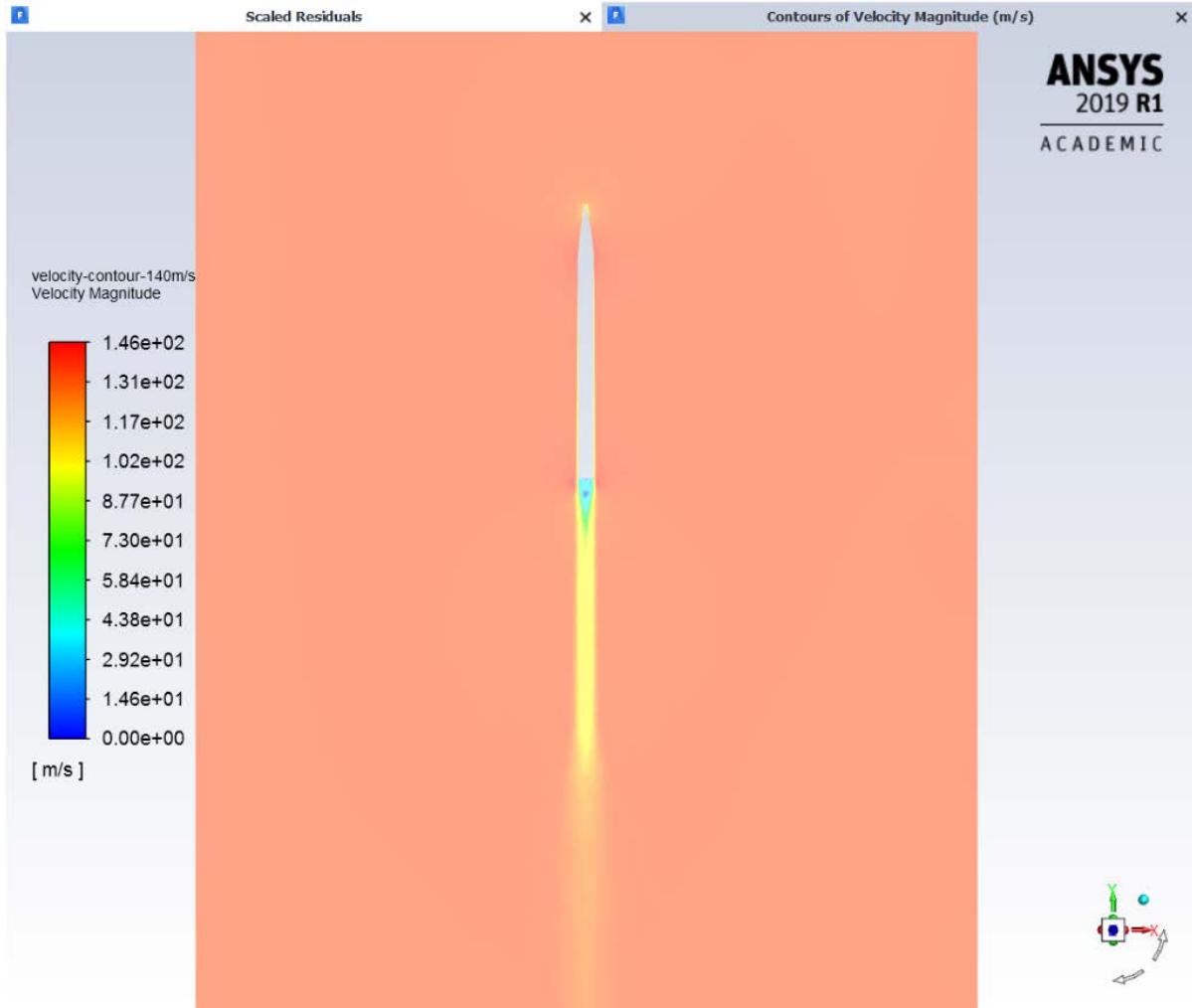
Static Pressure Contour:



Dynamic Pressure Contour:

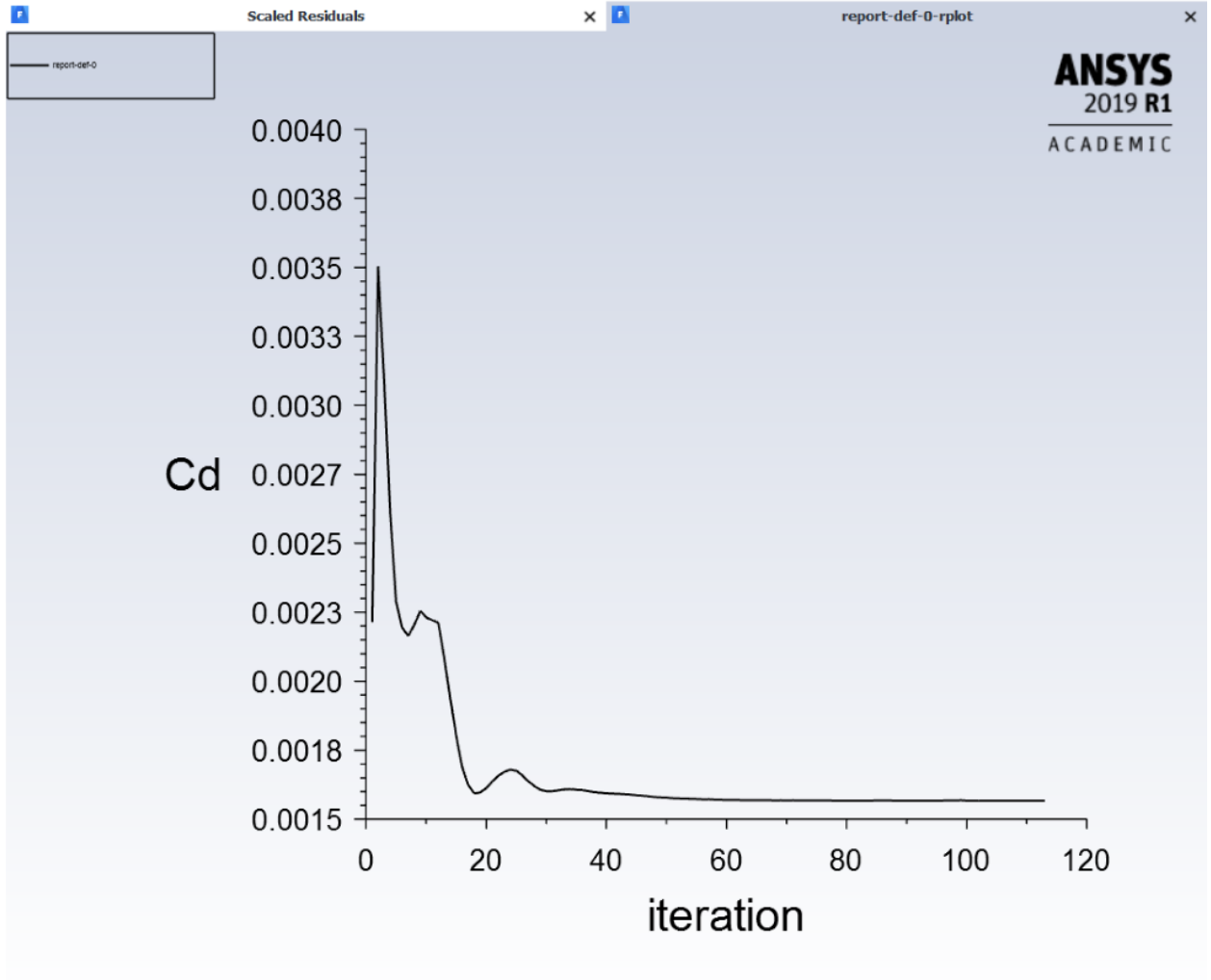


Velocity Contour:

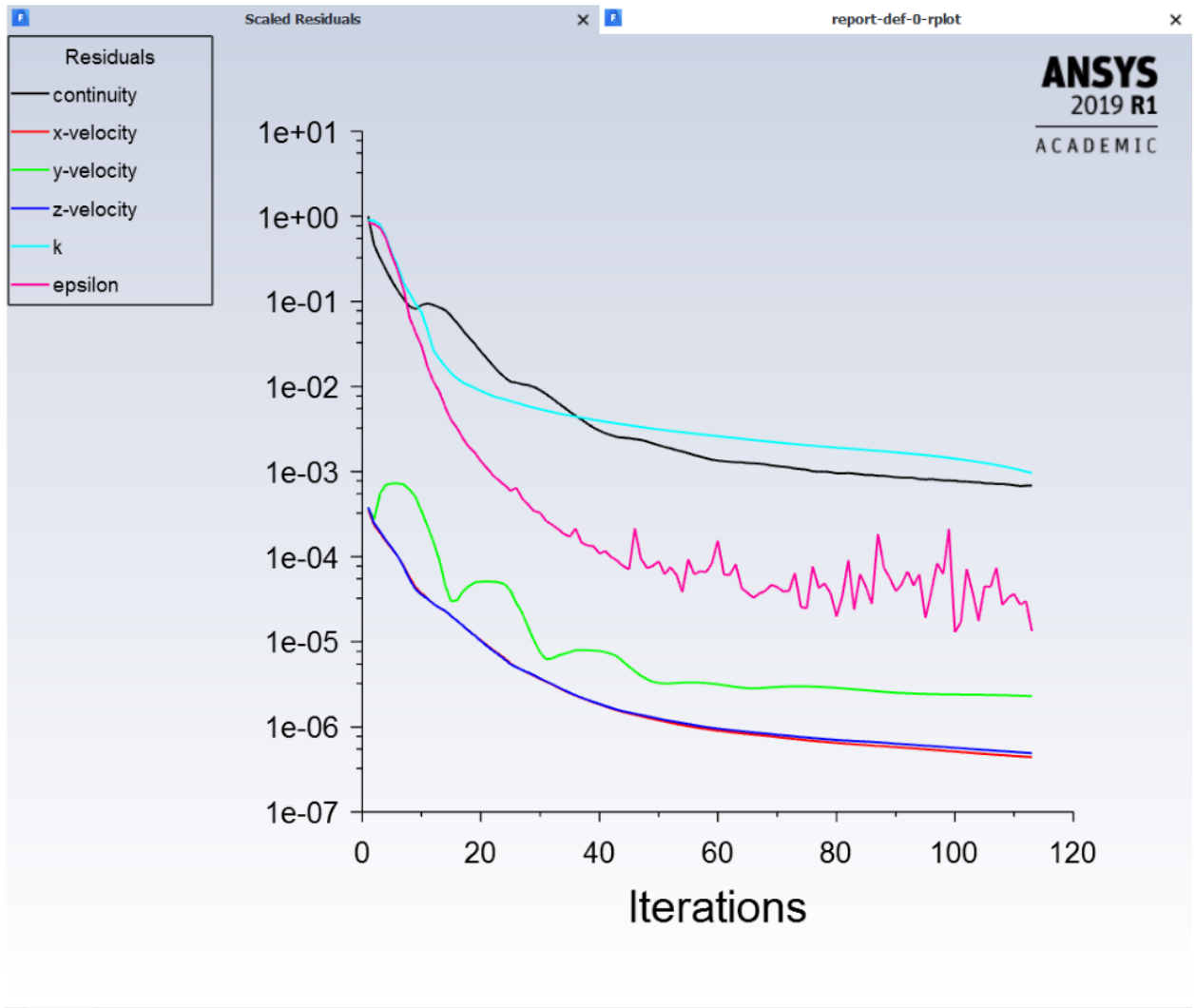


Steady Flow, 150 m/s:

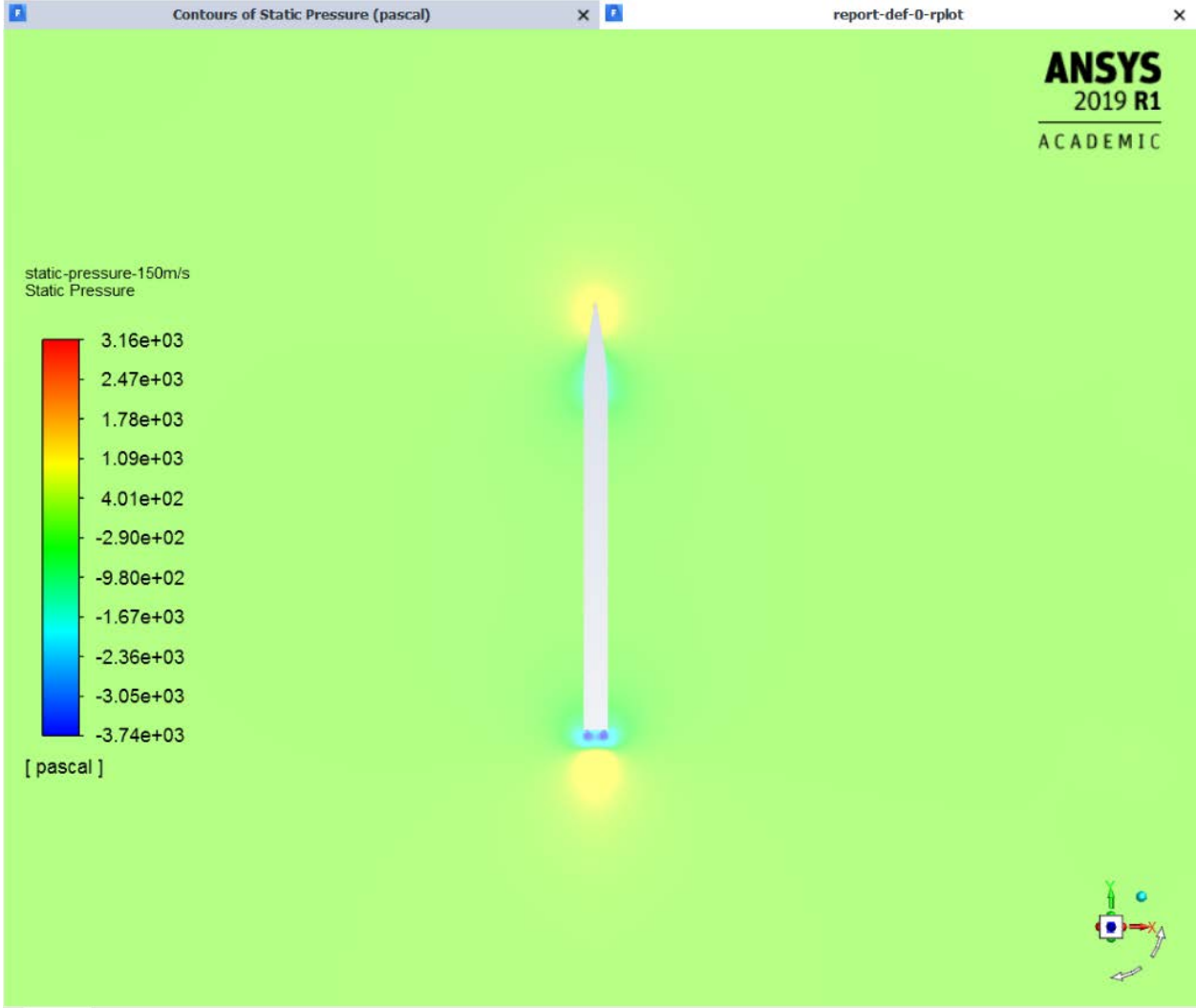
Coefficient of Drag:



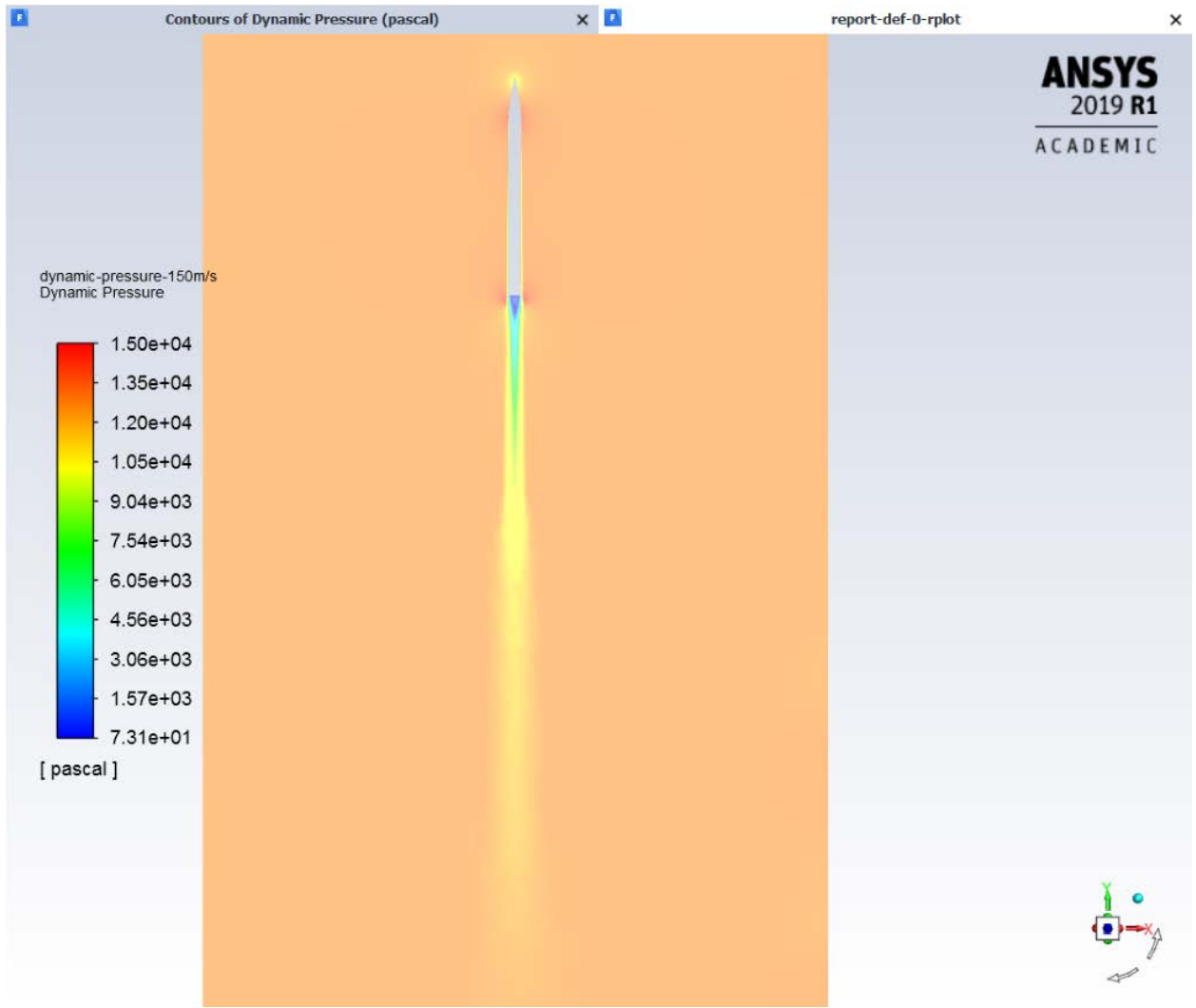
Scaled Residuals:



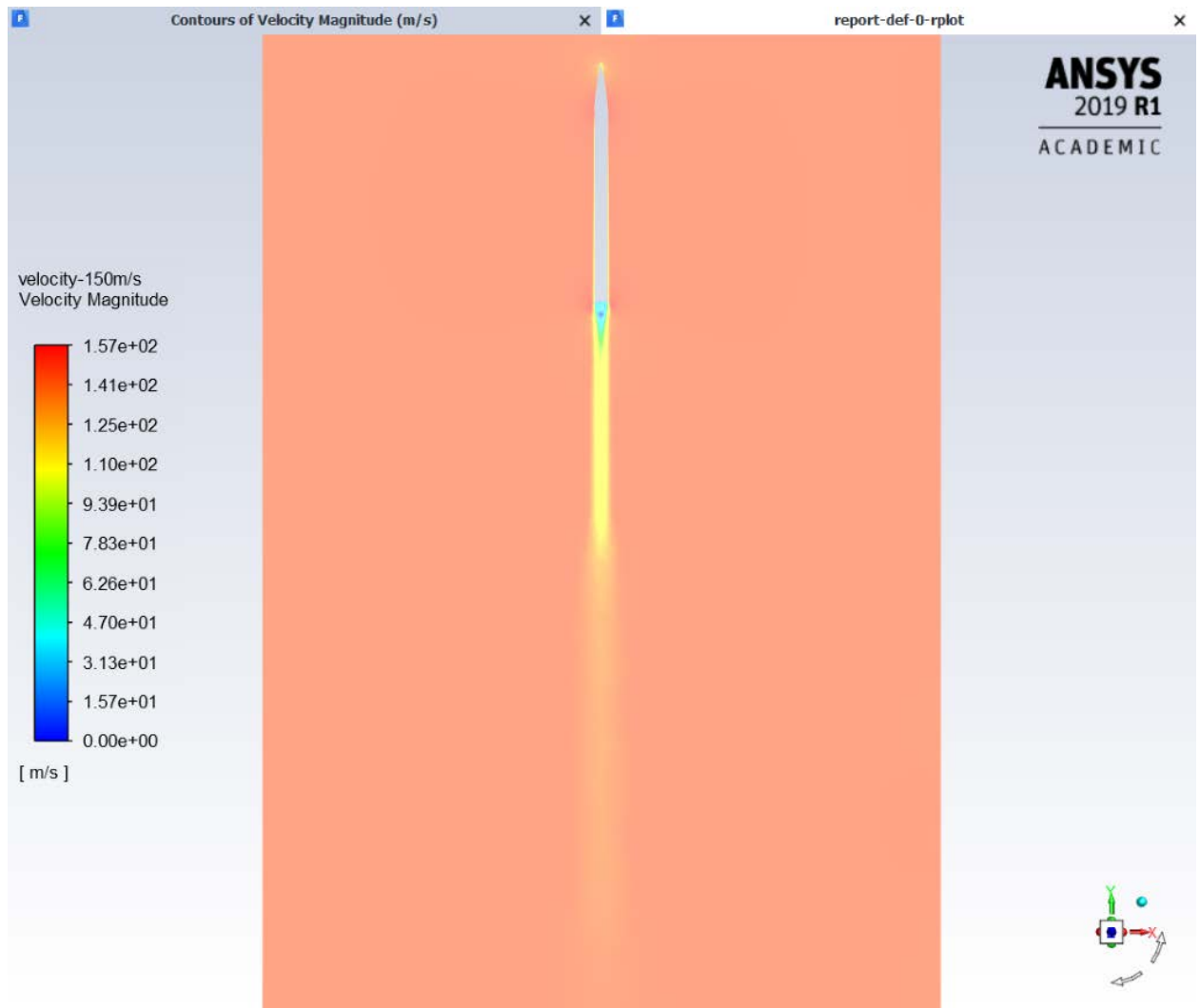
Static Pressure Contour:



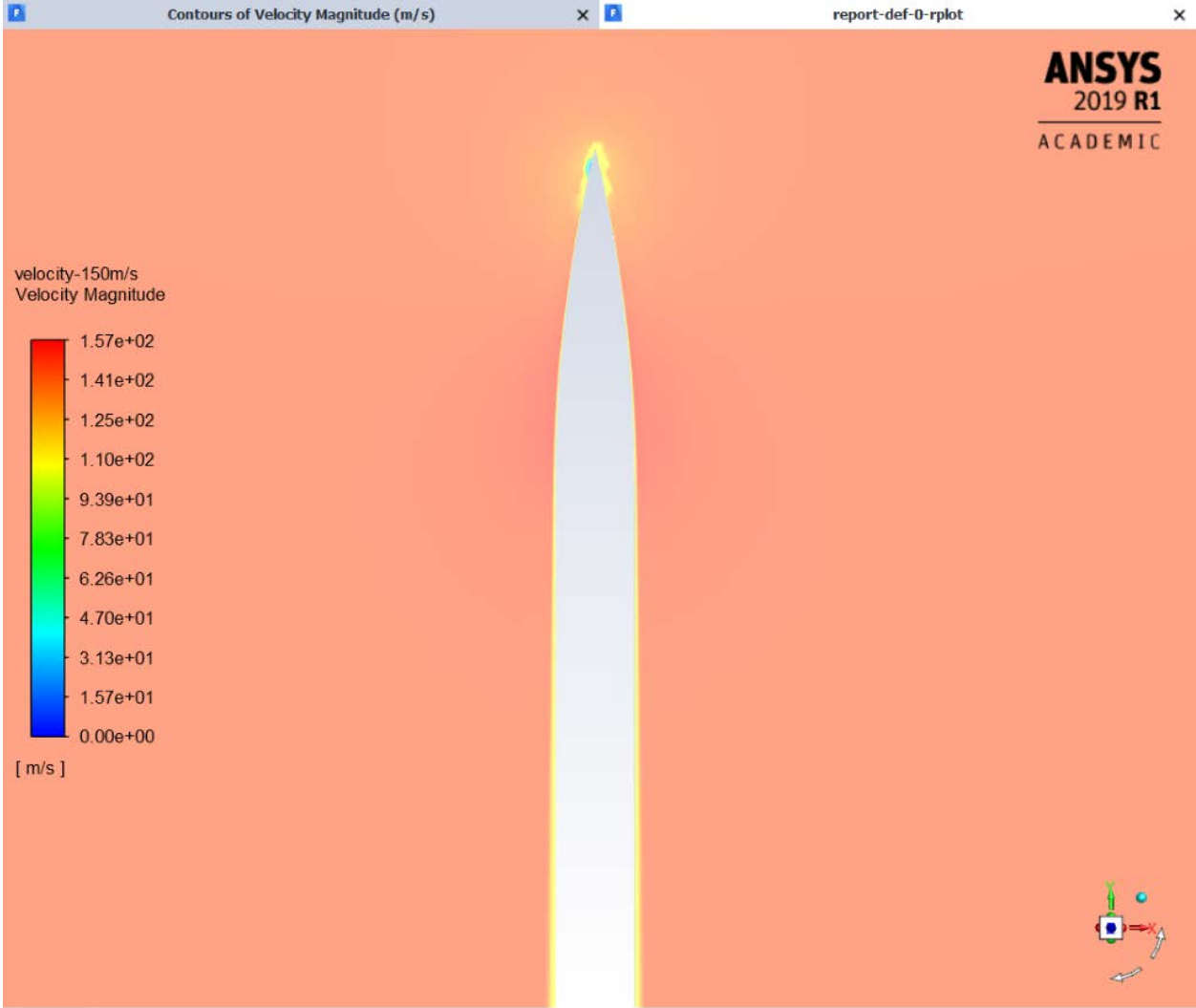
Dynamic Pressure Contour:



Velocity Contour:



Velocity Contour Zoomed In:



Appendix G

```
clc; clear all; close all;
%Inputs

V_ref = 5.75    % wind speed at reference height (m/s)
h_ref = 10     % reference height (m)
P = 0.143     % power law exponent for neutral stability conditions
z = 0:10:457.2 % changing height range (m) (we are getting up to 1500
               ft or 457.2 m)

V_x = V_ref*(z/h_ref).^P

plot (z, V_x)

xlim([0 460])
ylim([0 12])

xlabel ('Height (m)')
ylabel ('Wind Velocity (m/s)')
title ('Wind Velocity vs. Height')
```

Appendix H

Below is the launch day procedure for the test launch.

1	Examine all airframe components for travel induced damage
2	Hand off E-bay to FDC for component check out and installation
3	Hand off motor section to PSR for Motor installation
4	Install the three loaded motor casings into the motor section
5	Install and secure the motor retention system
6	Hand off E-bay to PSR for separation system installation
7	Hand off the motor section to MSAT for integration
8	Hand off E-bay to MSAT for integration
9	Bolt lower section of E-bay to top end of motor section
10	Secure shock cord to top E-bay bulkhead
11	Run shock cord through main body tube
12	Bolt upper section of E-bay to aft end of main body tube
13	Recovery system
13.1	Properly fold and pack recovery system
13.2	Secure recovery system to shock cord
13.3	Load recovery system
14	Internal camera
15.2	Secure internal camera to mount
15.3	Bolt nose cone and camera mount to camera housing
16	Attach nose cone parachute to camera housing
17	Shear pin the Camera mount section to the main body tube
18	External cameras
18.1	Secure external cameras to Velcro tabs
18.2	Secure external camera fairing to Velcro tabs

Appendix I

Subgroup	Item Being Tested	Test Objectives
Mechanical	Quality of footage from gimballled camera	Is the image quality from the gimballled camera clear and viewable?
	Quality of footage from the side cameras	Is the image quality from the side cameras clear and viewable?
	Nosecone shear pins	Do the shear pins shear when the separation charge fires?
	Motor Tubes Section	Does the removable motor tube module remain in place throughout the flight?
	Motor Retention	Does the motor retention system retain the motors through the entire flight?
Structural	Fin	Are the fins capable of performing without damage?
	Fin Bracket	Are the fin brackets capable of performing without sustaining damage?
	Vibrations	Do the attached strain gauges measure and record data correctly?
	Body Tube	Does the body tube survive launch? Can the body tube launch again?
	Parachute Mounting Bulkheads	Do the bulkheads survive parachute deployment?
Aerodynamics	Cd Values	Do the Cd Values obtained from altimeter "backtracking" match the pre-launch numbers?
	Stability	Does the rocket show signs of stability (Does it stay upright)?
Thermal	Motor Tubes	Do the motor tubes withstand the temperature of the motors?